Max Planck Institute for Molecular Genetics

Freie Universität Berlin

Genome-wide analysis of LXR-alpha regulated transcriptional networks in human atherosclerotic foam cell development

Dissertation to obtain the academic degree Doctor rerum naturalium (Dr. rer. nat.)

Submitted to the Department of Biology, Chemistry and Pharmacy of the Freie Universität Berlin

by

Radmila Feldmann

From Riga

February 2013

This thesis has been conducted in the period of September 2008 to August 2012 at the Max-Planck Institute for Molecular Genetics in the Nutrigenomics and Gene Regulation research group under the supervision of Dr. Sascha Sauer.

1st Reviewer: Dr. Sascha Sauer

Max-Planck Institute for Molecular Genetics

2nd Reviewer: Prof. Dr. Markus Wahl

Freie Universität Berlin

Date of defense: 09.01.2014

TO MY HUSBAND, TOBIAS.

"The only source of knowledge is experience."

Albert Einstein

Acknowledgements

I would like to express my very great appreciation to my advisor Dr. Sascha Sauer for giving me the opportunity to work in his lab and to freely develop my research study on LXRα. I am very grateful for his valuable and constructive suggestions, inspiring discussions and encouragement during this project and for reviewing this thesis. I am also very thankful to Prof. Dr. Markus Wahl for his support and for reviewing this work.

I would also like to extend my thanks to my colleagues Dr. Christopher Weidner, Claudia Quedenau, Dr. Vitam Kodelja, Anja Freiwald, Annabell Witzke, Magdalena Kliem and Beata Lukaszewska-McGreal for their technical support, scientific discussions and daily encouragements. I am very grateful to my former student and colleague Cornelius Fischer for his computational support, valuable discussions and substantial help in the laboratory. Especially his bioinformatics assistance was crucial for this study. I wish also to acknowledge the substantial help and commitment provided by my student Anne Geikowski who was essential for the STLX4 study.

A special thank should be given to my colleague Susanne Holzhauser for her encouragement and support through the last years.

I also thank all the other members of the Nutrigenomics and Gene Regulation group for their help and the good working atmosphere.

Finally, I wish to thank my family and in particular my husband Tobias, for his support, encouragement and patience during the last years.

Contents

1. Introduction

1.1 Cardiovascular disease - major cause of death

Cardiovascular diseases (CVD) are disorders of the heart and blood vessels, which are mainly caused by the chronic inflammatory disease atherosclerosis. CVD is the most important contributor to worldwide morbidity and caused in 2008 ~17.3 million deaths (30% of all global deaths (1)). Although a large proportion of CVD could be prevented they continue to rise and may affect in 2030 almost 25 million people (1). The most common CVD are coronary heart disease (CHD, heart attack) and cerebrovascular disease (stroke). Major risk factors for CVD include tobacco use, unhealthy diet, obesity, physical inactivity and raised blood pressure (hypertension) (2). These broad causes are responsible for the rise of CVD across countries at all stages of development. Notably, over 80% of CVD deaths occur in low and middle income countries (1). There is an emerging body of evidence claiming that these rapidly urbanizing countries undergo a nutritional transition with rapid changes in diet and amount of physical activity (3). Apart from evident increase in total kilocalorie intake per day there was also a remarkable raise in meat consumption and in unhealthy fats, oils, sodium and sugar (4). Therefore the global increase in CVD incidence and mortality seems to be evidently linked to rapid dietary changes along with decreased physical activity (3). Both factors can lead to high blood cholesterol, a major risk factor for CVD events (5), and an important target of medical treatment.

CVD are also enormous economic burdens. Currently the constantly escalating costs for CVD in Europe add up to more than 500 million euro per day (6). Clearly, successful approaches are urgently needed to protect our heart and blood vessel health.

1.2 Major risk factors for cardiovascular disease

Metabolic risk factors as well as unhealthy behavior lead to metabolic and physiological changes that result in increased CVD risk. CVD rarely develop from a single risk factor; they are mostly multifactorial with several, often related

risk factors that contribute to the development of the disease over a long period of time. Aging, inherited disposition, dyslipidemia, obesity, hypertension and diabetes are all risk factors that can cause atherosclerosis and damage coronary and cerebral blood vessels (2).

1.2.1 Aging

Throughout our life-course, beginning as early as our fetal life, we accumulate risks to develop CVD and other chronic diseases. In middle age individuals often have accumulated a significant risk (7). This accumulation is especially important, as life expectancies increased dramatically over the past 150 years and will continue to rise (8). Given the progressive increase of the aging population researchers are eager to find solutions to delay the onset of disability due to chronic and age-related diseases. This is not only important for improved individual life quality but also for the society to deal with health and economic implications. The increase of physical activity but also major changes in diet can help to prevent adverse cardiovascular outcomes (9, 10). To improve life quality of the aging population approaches including calorie restriction have been investigated (11, 12). It has been shown that the long term reduction of calorie intake per day reduced risk factors for atherosclerosis and other chronic inflammatory disease (13).

1.2.2 Blood lipids

Lipids in the blood comprise mainly fatty acids and cholesterol derived from dietary intake and secreted by cells from *de novo* synthesis. Cholesterol is fundamental for the normal function of animal cells. It is pivotal for the fluidity of cell membranes and a precursor of various critical substances such as steroid hormones and bile acids (14). These and other sterol metabolites are important signal molecules in metabolism, development and homeostasis of cellular processes. As cells cannot degrade cholesterol, it must be exported to extracellular acceptors for transport and catabolism. All hydrophobic lipid molecules are transported by various lipoprotein particles (15). These lipoproteins are subdivided into five major classes according to their hydrated density, relative content of lipids and type of protein: chylomicrons, very-low-

density lipoproteins (VLDL), intermediate-density lipoproteins (IDL), low-density lipoproteins (LDL), and high-density lipoproteins (HDL) (16).

1.2.2.1 Apolipoproteins

Lipoproteins are constituted from various apolipoproteins including APOA1, APOA2, APOA4, APOB, APOC1-APOC3 and APOE. They regulate lipoprotein metabolism through their involvement in transport and redistribution of lipids. Further, they act as co-factors (e.g. APOC2 for lipoprotein lipase (LPL) or APOA1 for Lecithin-Cholesterin-Acyltransferase (LCAT)) and maintain the lipoprotein structure (17, 18). The major component of several plasma lipoproteins is apolipoprotein E (APOE). *APOE* gene is located within a cluster of genes encoding APOC1, APOC2 and APOC4 on chromosome 19 in humans (19). These apolipoproteins are important regulators of lipid transport and catabolism. Single nucleotide polymorphisms (SNPs) within this cluster were associated with changed lipid profiles and an increased risk of CHD (19). One of the most common models for atherosclerosis is the $APOE^{-/-}$ mice. These mice show distinct elevation of lipids including triglyceride rich VLDL and IDL (20). APOE is also synthesized by macrophages and plays an important role in promoting cholesterol efflux from macrophages back to the liver known as reverse cholesterol transport (21).

1.2.2.2 Lipid metabolism

Lipids are metabolized in an exogenous (dietary) and an endogenous pathway (**Figure 1**). Intestinal cholesterol is derived from diet and bile (exogenous and endogenous cholesterol) (22). In the exogenous pathway, dietary fats are processed and packed to chylomicrons. Chylomicrons contain phospholipids, cholesterol and apolipoproteins. Chylomicrons circulate to peripheral tissues and deliver energy in form of fatty acids and cholesterol for muscle cells or for storage in adipose tissue. The APOC2 surface protein initiates the progressive hydrolysis of triglycerides by triggering the capillary endothelial enzyme LPL to convert chylomicrons in atherogenic remnants, which can be processed in the liver. Cholesterol in the liver can be stored as cholesterol esters (esterification by acyl coenzyme A: cholesterol acyltransferase 1 (ACAT1)), reused for lipoprotein synthesis, re-secreted to the plasma or excreted into the bile. Bilary cholesterol

and bile acids can be either excreted or reabsorbed from the intestine (enterohepatic cholesterol metabolism). Cholesterol can also be synthesized *de novo* in the endoplasmatic reticulum. Hepatic and other cells synthesize cholesterol from acetate, which is than reduced to mevalonate by the rate limiting enzyme in cholesterol biosynthesis, HMG-CoA reductase (15).

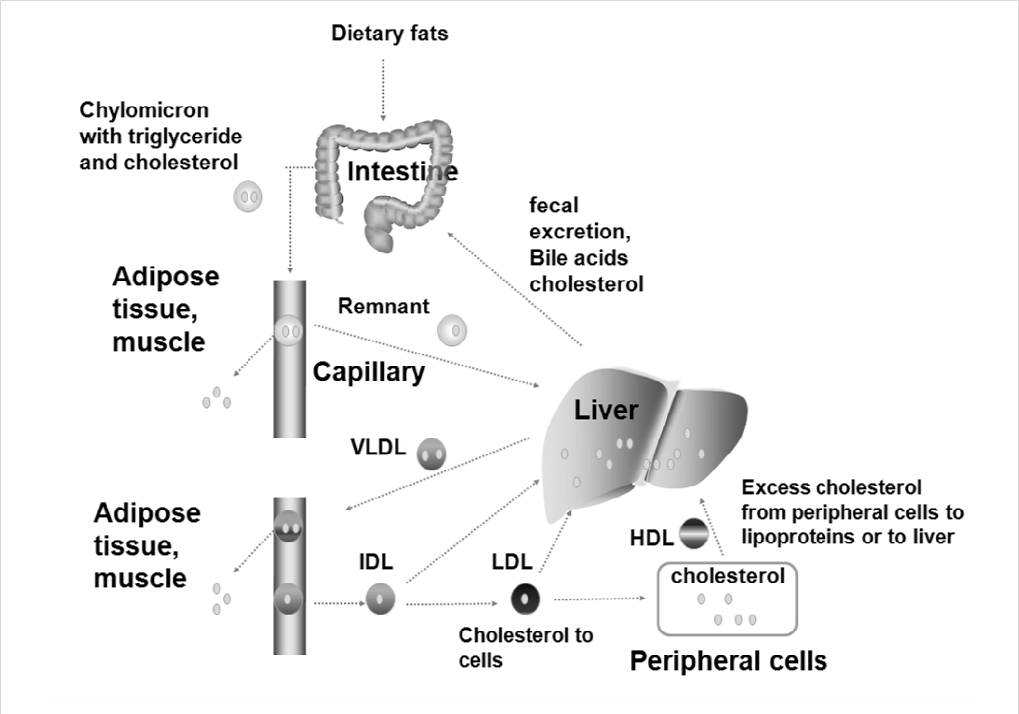

Figure 1: Exogenous and endogenous lipid metabolism. Exogenous lipids are derived from diet and bile. Packed in chylomicrons they deliver energy to adipose tissue and muscles. Chylomicron remnants are further processed in liver. In the endogenous lipid metabolism very low density lipoprotein (VLDL) is produced in the liver and transported through the capillary. When energy is delivered to adipose tissue and muscles VLDL becomes intermediate-density lipoprotein (IDL) and is further metabolized to low density lipoprotein (LDL). LDL transports cholesterol to liver and to peripheral cells. Excess cholesterol can be transported to the liver through high density lipoprotein (HDL). In the liver cholesterol can be either further processed or excreted to the intestine.

In the endogenous lipid metabolism, VLDL is produced in the liver and transported through the capillary. When triglycerides are hydrolyzed, free fatty acids and glycerol are transported to muscle cells or for storage to adipose tissue and LDL is metabolized from IDL. LDL is taken up in an endocytotic process that involves the LDL receptor. The number of LDL receptors is regulated by cholesterol content of hepatocytes. Downregulation of LDL receptor leads to

lowered LDL uptake and results in elevated plasma LDL cholesterol levels and accumulation of cholesterol in peripheral cells. Mutations in the LDL receptor in humans lead to hypercholesterolemia (23, 24). Increased LDL levels are associated with atherosclerosis and CHD (25). LDL can be used by cells or can be removed to the liver. Excess cholesterol in peripheral cells can be transferred to HDL and removed by liver via bile acids and fecal excretion.

Initially HDL is synthesized in liver and enterocytes as cholesterol free lipoprotein. Its overall responsibility is to obtain cholesterol from other lipoproteins and peripheral tissues and transport it to other cells, lipoproteins or to liver for clearance. HDL has overall anti-atherogenic functions (26). Further compensatory mechanisms in response to lipid overload include repression of endogenous cholesterol and lipid biosynthesis by inhibition of the sterol regulatory element-binding transcription factor 1 (SREBF1) pathway (27).

The condition of abnormally elevated lipid and lipoprotein levels in the blood is called hyperlipidemia. Abnormal blood lipids are globally the most important contributors to CVD (28). Already in the 1960s, researchers demonstrated that there is a link between hypercholesterolemia and increased risk of CHD. Especially elevated levels of LDL and triglycerides along with lower levels of HDL were linked to increased risk of CVD (29–31). Consequently, reduction of LDL cholesterol is associated with reduced coronary event rates and lowered stroke incidence (32).

1.2.3 Overweight and obesity

Obesity and overweight are major global contributors to CVD incidence and mortality. One of the key reasons to overweight and obesity is excess energy intake, especially from food enriched with salt, sugar, and saturated fat (33). The level of overweight and obesity increased steadily over the past decades, with growing prevalence also in children between the ages 5-17 (33). The distribution of body fat is of importance for association between overweight and CVD risk. Visceral but not peripheral obesity is associated with increased CVD risk, independent of body mass index and other cardiovascular risk factors (34). Further, obesity is also an independent risk factor for other cardiovascular outcomes (such as congestive heart failure and sudden cardiac death) and often

accompanied by other risk factors such as hypertension, high cholesterol and diabetes (35).

1.2.4 Genetics

Family history of CVD is associated with increased atherosclerotic risk and points towards a genetic component to CVD. There are certain forms of familial disease such as hypercholesterolemia, linked to a single gene mutation in the apolipoprotein B gene (36). In the past years many genome-wide association studies (GWAS) made efforts to identify genetic risk factors for CVD and related diseases. Frequently, the identified loci contain several genes in strong linkage disequilibrium (LD). Although, the identification of CVD relevant genetic loci advanced the understanding of CVD pathophysiology, it explains only a small fraction of the heritability and does not substantially help to functionally explain all underlying mechanisms or predict, diagnose and treat CVD (37). This is mainly due to the complexity of most common CVD as they involve interplay of various genes and gene networks rather that single gene events. Thus, functional studies are required to gain deeper understanding in the development of CVD. This approach includes the study of interaction of molecular networks and physiological outcomes or clinical traits (38). Application of the rapidly evolving high-throughput technologies will expand the scope of functional CVD research (39).

1.3 Pathology of heart attacks and strokes -Atherosclerosis

One of the main underlying pathologies to heart attacks and strokes is atherosclerosis, also known as atherosclerotic vascular disease (1). Narrowed and hardened arteries due to an excessive plaque accumulation characterize this condition. The major step for acute cardiovascular events is the atherosclerotic plaque rupture and subsequent thrombus formation in the lumen of medium and large sized blood vessels (arteries). In a coronary artery this can cause a heart attack and in the brain a stroke (40).

Atherosclerosis is a complex multifactorial pathological process that develops over many years. The atherogenic development starts in childhood and progresses over time to manifestations such as heart attack and stroke in middle

age mainly due to the overall effect of several risk factors (41), most mentioned in the section above. The hallmark of early atherosclerosis is the fatty streak formation, due to cholesterol and other lipid depositions in blood vessel walls. With continued irritation over time the atherosclerotic lesion results in a protruding lesion of lipids and necrotic cells, which gradually thickens the arterial wall leading to the ultimate major blockade of blood flow and possible plaque rupture (42).

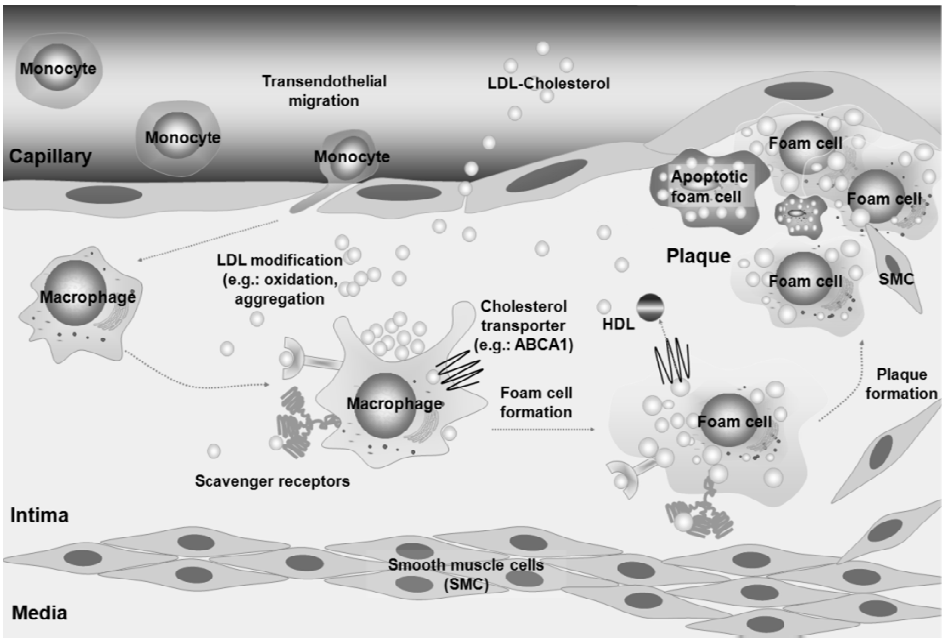

Figure 2: Monocytes/macrophages in the formation and progression of atherosclerotic plaque. Monocytes migrate into the subendothelial space and differentiate into macrophages. Uptake of modified low density lipoprotein (LDL) leads to foam cell formation. Cholesterol is subject to esterification and storage in lipid droplets or can be converted to forms that are more soluble and exported to extracellular HDL cholesterol acceptors via cholesterol transporters, such as ATP-binding cassette transporter A1 (ABCA1). Lipid overloaded foam cells progress into necrotic cells. Together with smooth muscle cells (SMC), they form the atherosclerotic plaque.

Atherosclerosis is a chronic inflammatory process in the walls of arteries. Macrophages and foam cells, which differentiate from blood monocytes, are the major leukocytes in the atherosclerotic plaque. Although it is not well defined how and whether monocytes migrate to healthy aortas, more is known about recruitment and accumulation of monocytes and lymphocytes at lesion prone

sites during atherogenesis (43–45). Activated monocytes roll over and become tethered by endothelial cells (46). Adherent monocytes migrate to the subendothelial space where they subsequently differentiate to macrophages. Through uptake of mostly modified lipids (mainly oxidized LDL (47)) macrophages transform to so called foam cells (**Figure 2**). Captured cholesterol can be either exported to extracellular HDL particles via cholesterol transporters (e.g. ATP-binding cassette transporter subfamily A and G member 1 (ABCA1, ABCG1)), or cholesterol can be stored as cholesterol ester in lipid droplets. Without adequate removal of lipids, macrophages transform to lipid-rich foam cells, the major constituents of fatty streaks, which accumulate in the arterial wall. In subsequent plaque progression, smooth muscle cells migrate to the lesion and form with collagen a fibrous cap. Simultaneously, foam cells begin to die and without effective clearance of apoptotic cells (impaired efferocytosis); they form a necrotic core, which is covered by the fibrous cap. Over time, the fibrous cap can thin out and the endothelial surface can fissure under the growing atheromatous plaque. In case of plaque rupture thrombogenic lipid fragments and cellular debris are released to the vessel lumen and can form a thrombus (48).

To date there is no efficient treatment for atherosclerosis available. Apart from surgical intervention, a low cholesterol diet combined with drugs that control cholesterol synthesis and absorption are recommended. Control and avoidance of predisposing risk factors is of central importance. In order to find successful therapeutic targets for clinical atherosclerosis treatment extensive investigation of underlying mechanisms that drive the disease are in the focus of current research.

1.3.1 Cause of atherosclerosis

Atherosclerosis is a complex process and to date its cause is still widely discussed. There have been several theories proposed to explain the initial steps of atherosclerosis. The two major hypotheses are the endothelial injury hypothesis and the lipid hypothesis.

1.3.1.1 Endothelial injury hypothesis

Already in 1856 Rudolph Virchow believed that atherosclerotic lesions result from an injury in the artery wall (49). In 1977 Russell Ross and others modified

this hypothesis and postulated the chronic endothelial injury hypothesis (50). According to this theory injuries of the endothelium, caused by factors such as chronic hyperlipidemia, mechanical factors (increased shear stress), hypertension or infectious microorganisms, lead to adherence, aggregation, and release of platelets at the sites of focal injury. Subsequently, platelets and other plasma constituents such as lipoproteins stimulate intimal smooth muscle cell proliferation and influence lipid deposition. In the case of a chronic injury of the endothelium, lipid deposition and smooth muscle cell proliferation continues and can lead to the development of a complicated atherosclerotic lesion. A modification to this theory describes the endothelial dysfunction as the first step in atherosclerosis (45). In this theory every change in the endothelium, including misbalance between vasodilating and vasoconstricting substances can cause atherosclerosis. Endothelial dysfunction leads to increased permeability, expression of adhesion molecules, growth factors, chemokines and reactive oxygen species (51). Infectious microorganisms can also cause such injuries. For example, in chickens infection of the arterial smooth muscle cells with Marek's diseases (herpes virus) leads to cholesterol ester accumulation, and also the cytomegalovirus was found to be associated with CVD (52–54). There is also evidence that bacteria from the mouth and the gut can contribute to the development of atherosclerosis. Once in the body they can either cause or contribute to inflammation and plaque rupture (55).

Taken together, all kind of biochemical and anatomical changes of the endothel can contribute to increased vascular damage and oxidative stress.

1.3.1.2 Lipid hypothesis

Goldstein and Brown reported at first the uptake of modified LDL by macrophages and their subsequent transformation to foam cells (56, 57). The lipid theory claims that accumulation of LDL in the subendothelial matrix is the initiating step in atherosclerosis. According to this hypothesis cholesterol deposition in the intima is proportional to the level of pro-atherogenic lipoprotein exposure in the artery (58–60). Thus, increased lipoprotein levels in the plasma are thought to explain elevated CVD risk (25). When LDL levels are raised, transport and retention of LDL particles are increased. Inside the vessel wall trapped LDL is likely to become modified (e.g. aggregation, oxidation). Modified

LDL can be recognized by scavenger receptors and can cause cholesterol accumulation in macrophages with subsequent foam cell transformation (57).

One of the main modifications to LDL, that promotes foam cell formation and inflammatory responses in macrophages, is oxidation (61). Oxidation of LDL can result from interaction with endothelial cells by mechanisms involving free radicals and the action of phospholipase (62, 63). Oxidized LDL (oxLDL) is cytotoxic (64) and exposition of the endothelium to oxLDL causes cell damage. Endothelial cells become permeable to T-lymphocytes and macrophages (65), which are recruited by chemotaxis towards oxLDL and to respond to artery wall damage. Over time, the triggered cascade of immune responses can produce an atheroma. This theory has been further precised during the last years. There is a growing body of evidence that a specific subset of lipoproteins is preferentially retained in the arterial wall, for example apolipoprotein B containing lipoproteins (58, 66). Further, it has been shown that plasma cholesterol lowering did not necessarily protect against CVD (67–69). In contrast to cholesterol, its oxidized form, oxLDL, is widely accepted as causal factor for atherosclerosis.

One of the recent hypotheses on the initial cause of atherosclerosis stated that cholesterol levels are correlated but not causative for CVD. Instead it was hypothesized that stimulation of mevalonate pathway in endothelial cells by inflammatory factors (e.g.: homocysteine), or indirectly by reduced intracellular cholesterol levels, may be an important causal factor for atherosclerosis (70). The mevalonate pathway controls numerous biological processes including the formation of the anti-oxidant coenzyme Q10, cholesterol formation and activation of NADPH oxidase, which produces superoxide radicals. Superoxide radicals can transform native LDL cholesterol to oxLDL and subsequently contribute to atherosclerosis. From the evolutionary perspective, the mevalonate pathway in endothelial cells was probably very important in protection against infectious invaders. Lipids appear to protect against infections as exemplified by LPS, derived from gram-negative bacteria, detoxification with LDL cholesterol. Superoxide radicals are also useful agents against invading bacteria (71). Notably, atherosclerosis is not exclusively a modern society disease. It did also affect our ancient ancestors as recently observed in mummified ancient Egyptians (72).

Taken together, the initial causes of atherosclerosis remain elusive. In order to determine the extent of arterial retention and inflammatory response it is pivotal to characterize lipoprotein size, density, lipid composition and amount of free radicals - rather than the overall amount of lipoproteins circulating in plasma (73).

1.3.2 Role of macrophages

Macrophage derived foam cell accumulation in the vascular intima is the hallmark of fatty streak formation in atherosclerosis, and thus one of the prime targets for therapeutic interventions. Macrophages appear at a very early stage of atherosclerotic lesion development and persist at that site as main components of atherosclerotic plaques (74). Apart from foam cell formation macrophages can contribute to disease pathogenesis through chemokine and cytokine production, stimulation of reactive oxygen species and the production of matrix degrading enzymes, which prolong the inflammatory response and majorly affect plaque progression and stability (75). Thus, understanding underlying mechanisms of inflammatory response and lipid metabolism in macrophages is critical for combating atherosclerosis.

1.3.2.1 Inflammatory response

Macrophages as dual modulators of lipid metabolism and immune response, play a central role in atherosclerosis (65, 76). When the endothelium is activated to secrete chemokines and adhesion molecules, monocytes roll on the inflamed aortic endothelium, adhere and enter the subendothelial space. Triggered by differentiation factors such as macrophage colony stimulating factor (M-CSF), monocytes differentiate into two major types of macrophages (M1 and M2). These both types play opposite roles during inflammation. Whereas M1 macrophages promote inflammation, M2 macrophages possess functional characteristics to suppress inflammation and clean up cellular debris (77). Differentiated macrophages ingest retained lipoproteins, which promotes foam cell formation and inflammatory response. This process includes pro- and anti-inflammatory factors such as scavenger receptors, toll like receptors, nuclear

factor kappa-light-chain-enhancer of activated B-cells (NFκB) signaling, endoplasmatic reticulum (ER) stress and cholesterol efflux via ATP-binding cassette (ABC) transporters, which are activated in macrophages. When resolution of inflammation fails, the inflammatory process continues and is amplified resulting in more retained lipoprotein and a persistent recruitment of inflammatory monocytes into atherosclerotic lesions (78). Various cytokines and transcription factors act as inflammation resolution mediators. Of central importance are interleukin 10 (IL10), transforming growth factor beta (TGFβ) and the transcription factor liver X receptor (LXR). IL10 receptor signaling induces several anti-inflammatory pathways including inhibition of NFκB pathway, which suppresses further activation of inflammatory T-cells and decreases the production of inflammatory cytokines such as interleukin 6 (IL6) and tumor necrosis factor alpha (TNFA) (79). Further, IL10 stimulates the conversion of M1 macrophages to M2 macrophages (80). TGFβ is an important factor for efferocytosis and triggers collagen production in fibroblasts, which resolves lesions (81, 82). The transcription factor LXR is also known to have anti-inflammatory properties such as inhibition of NFκB-mediated signaling in macrophages (83). Notably, LXR further regulates cholesterol efflux from macrophages and macrophage egress from atheroma (84).

1.3.2.2 Foam cell formation

Homeostasis of a healthy lipid metabolism relies on balanced cellular cholesterol levels regulated by uptake, -efflux, and endogenous synthesis. In macrophages normal cholesterol metabolism involves a balance between the uptake of native and modified LDL, cholesterol efflux by the reverse cholesterol transport and mechanisms for esterification, storage and traffic of cholesterol (85). Disturbance of this balance such as enhanced uptake of modified LDL or dampening of reverse cholesterol transport machinery leads to extensive accumulations of intracellular cholesterol esters with subsequent transformation from macrophages to lipid-rich foam cells (**Figure 3**) (75, 86). The uptake of modified LDL is accomplished by receptor-mediated endocytosis. As previously mentioned mainly modified LDL triggers foam cell formation. OxLDL can be formed in several sites including the vessel wall (87). Atherosclerosis is characterized by excessive oxidative stress, which leads to protein structural and lipid

modifications (88, 89). Macrophages and endothelial cells can promote oxidative damage in presence of high LDL levels by processes that involve myeloperoxidase (MPO), NADPH oxidase and the nitric oxide synthase (NOS). This mechanism, to provide antibacterial host defense, results in increased oxLDL formation, uptake and lesion progression (90–92). Native LDL uptake

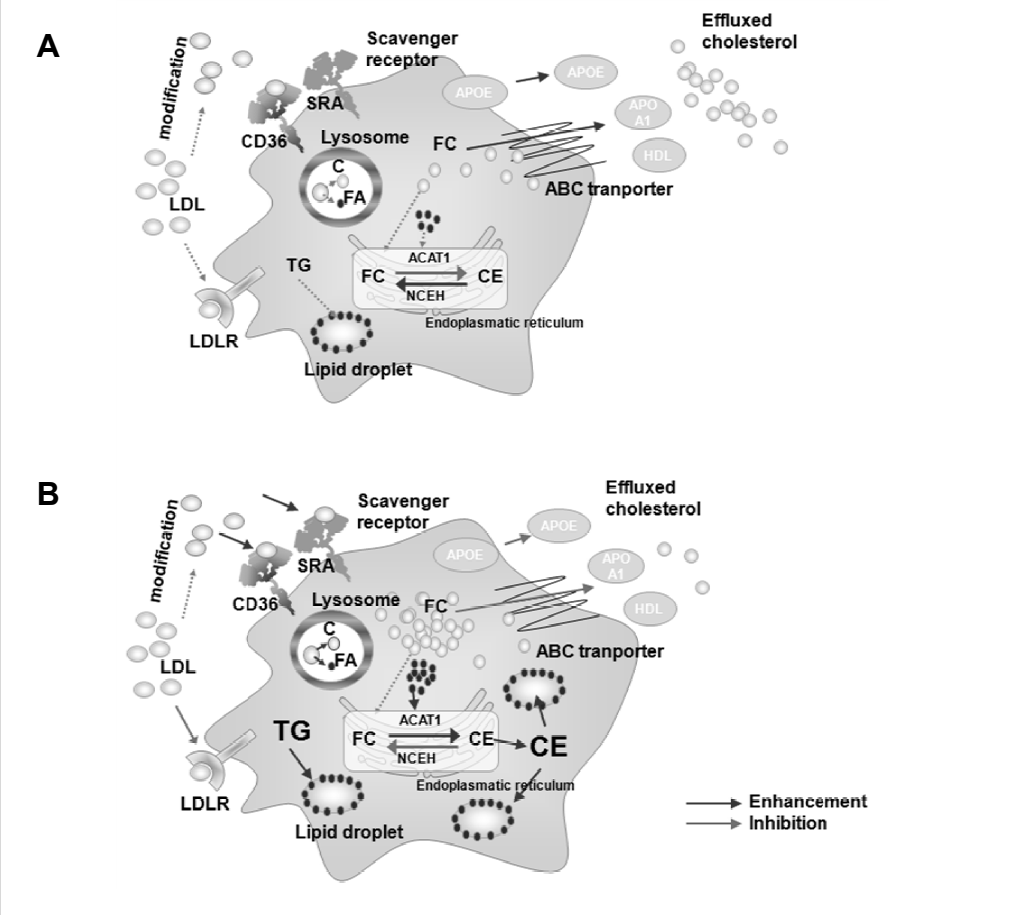

Figure 3: Macrophage transformation to foam cell. (**A**) Macrophage under homeostatic cholesterol metabolism. Native and modified LDL uptake by LDL receptor (LDLR) and scavenger receptor SRA, CD36. Modified LDL (mainly oxLDL) is hydrolyzed in the lysosome to free cholesterol (C/FC) and fatty acids (FA), which can be further processed in the endoplasmatic reticulum (ER) with Acyl-CoA:cholesterol acyltransferase-1 (ACAT1) to cholesterol esters (CE) for storage in lipid droplets. CEs can also be removed from cell in reverse cholesterol transport when CE are hydrolyzed by neutral cholesteryl ester hydrolase (NCEH) to FC and effluxed via ABC transporter and APO/HDL involvement. (**B**) Foam cell development under imbalanced cholesterol metabolism. Extensive accumulation of CE, triacylglycerols (TG) and increased intracellular cholesterol storage enables macrophages to transform into foam cells. Foam cell transformation is promoted by enhanced scavenger receptor mediated LDL uptake, inhibited cholesterol efflux and imbalance to favor of CE accumulation. Black arrow indicate enhancement, grey arrow indicate inhibition.

can be regulated by the decrease of LDL receptors (LDLR) on cell surface (57, 93). Modified LDL uptake is mainly mediated by scavenger receptors (SR) such as SR class A (SRA) and SR class B (CD36). Unlike the LDLR, SR are not regulated by cellular cholesterol content (94). SR are mainly expressed by cells of the innate immune defense, which are normally supposed to protect the organism against pathogens. Interestingly, oxLDL is also recognized by toll-like receptors 2 and 4 (TLR2, TLR4), pointing towards a similarity between pathogen epitope structure and oxLDL structure patterns (95, 96). Thus, atherosclerosis could also be considered an autoimmune disease (88). Although the clearance of oxLDL by macrophages can be considered as part of self- defense, it can also cause an extensive accumulation of lipids with subsequent foam cell formation and contribution to lesion development when misbalanced. Apart from cholesterol uptake, foam cell formation can be promoted by intracellular traffic, esterification and storage of cholesterol. Foam cells are characterized by extensive cytoplasmatic accumulation of cholesterol ester and triacylglycerol-rich lipid droplets (97). Once in the macrophage cytoplasm oxLDL is hydrolyzed in the lysosome to free cholesterol and fatty acids. High accumulations of free cholesterol within macrophages were recently proposed as originator of pro-inflammatory signaling response in early atherosclerotic lesions (98). Excess free cholesterol can be esterified in the ER by ACAT1 to fatty acid sterol esters for storage in cytoplasmatic lipid droplets. The actions of ACAT1 can be opposed by the neutral cholesterol ester hydrolase (NCEH), which converts fatty acid sterol esters to free cholesterol and fatty acids (97). In foam cells, this balance is disturbed in favor of fatty acid sterol ester storage and the storage of intracellular triacylglycerols is also enhanced. Further, in foam cells the cholesterol efflux mechanisms for hepatic removal are dampened. Mechanisms such as reverse cholesterol transport normally stimulate via HDL and apolipoprotein A-1 (APOA1) cholesterol efflux through ABC-transporters. Further APOE, secreted by macrophages, also contributes to cholesterol efflux (99, 100).

1.3.2.3 Apoptosis and necrosis of macrophages

When the atherosclerotic plaque progresses it accumulates cholesterol-rich, apoptotic/necrotic cores (101, 102). These cores arise due to apoptosis of foam cells and a dysfunctional efferocytosis, which leads to secondary necrosis in

advanced lesions. The effect of apoptosis on atherosclerosis progression is very complex. It involves multiple mechanisms including ER stress, which activates the unfolded protein response (UPR) pathway and subsequent activation of the pro-apoptotic C/EBP-homologous protein (CHOP) (78). CHOP and other ER stress proteins are correlated to apoptosis and plaque vulnerability (103). ER stress can be induced by high levels of intracellular oxysterols (oxLDL). Plaque necrosis is mainly due to ineffective efferocytosis, probably resulting from defective anti-inflammatory signaling (78). Normal efferocytosis prevents from necrosis through activation of anti-inflammatory pathways involving TGFβ and other cell survival pathways (104).

1.4 Ligand dependent nuclear receptor

As described above atherosclerosis is driven by a pathogenic interplay between metabolism and inflammation. Thus, for effective prevention and treatment there is a need for inducible targets that link control of metabolism and inflammation. Gene regulatory factors such as ligand-induced nuclear receptors are very promising targets for atherosclerosis therapy (105). Their mode of direct ligand regulation and interaction with the genome is in the focus of modern pharmacology and therapy. Nuclear receptors (NR) are a superfamily of phylogenetically ancient and mostly ligand-induced transcription regulators. The human genome contains 48 nuclear receptors (106). The largest subfamily of NRs is the NR1 family with members such as peroxisome proliferator-activated receptor (PPAR) and liver X receptor (LXR) (107). As cellular sensors, ligand-induced NR are activated by the presence of diverse endo- and exogenous substances (mostly small lipophilic compounds) and regulate various physiological processes of multicellular organisms such as metabolism, development and reproduction. Ancient NRs were probably independent from ligands and acted as monomers but with progressing evolution of higher organisms, the need for more functional complexity in gene regulation arose. This need was potentially addressed when NR acquired the ability to homo- or heterodimerize with other NRs and being regulated by ligands (108). One of the evolutionary oldest NRs is the retinoid X receptor (RXR). RXR can act as homodimer and regulate various fundamental biological processes. Further, RXR plays a pivotal role in regulating the activity of other NRs by acting as partner for

heterodimerization. Different binding partners render a diverse DNA binding site specificity and thereby influence the regulatory potential of NRs (109).

1.4.1 Nuclear receptor structure

The structural architecture is similar among all nuclear receptors. The canonical structure of nuclear receptors contains a poorly conserved N-terminal region with a ligand independent transactivation domain (AF1), a highly conserved DNA binding domain (DBD), a hinge region that links to the C-terminus and the discrete ligand binding domain (LBD) with an activation function 2 (AF2) domain for ligand-dependent interaction with co-factors (110). The LBD is a globular 11-13 α-helix protein with a hinged final helix. LBDs functions include ligand recognition and co-factor interaction (111). LBDs can interact with a great variety of natural and synthetic lipid soluble ligand molecules through binding to the 100 – 1400 Å pocket with a hydrophobic cavity in the core. The plastic nature of the LBD explains the promiscuity of some ligands to bind to multiple NRs (112). The function of LBDs is defined by the AF2 sub-domain, which is controlled by ligand-dependent positioning of the final helix resulting in differential binding to protein co-factors. Co-factors have various properties and can support activation or repression of target gene transcription. This classic receptor model is challenged by observations of tissue and cell-type specific biological effects upon NR stimulation with structurally similar ligands (113). Thus, it has been assumed that there may be additional cell-type specific partner proteins, which allow the efficient recruitment of a co-activator (114).

The DBD is composed of two highly conserved zink finger motifs that engage with definite DNA sequences, the so-called response elements (RE). For most NRs the recognition sequence is composed of a hexamer tandem repeat, which can be arranged in various bipartite configurations including direct repeat or inverted repeat separated by 0-8 nucleotides specific for each NR (115). Several *in vitro* studies and sequence comparisons of promoters, known to be bound by specific factors, allowed the definition of consensus binding motifs for several NRs (116, 117).

1.4.2 Interaction of response element and DNA binding domain

The ligand activated NR follows a very flexible and dynamic behavior. Some NRs constantly sample DNA until a high affinity binding site is reached and where they engage in a more stable interaction with their cognate RE (113). Base-specific sequence recognition is controlled via interactions between side chains and edges of base pairs including van der Waals interactions, hydrogen bonds and stabilizing backbone and electrostatic interactions (118). The occupancy time of NRs at the DNA site is comparably low (microseconds for RXR, (119)) and therefore does not compete with other transcription factors (TFs) that bind and collaborate at the same site (120, 121). Higher affinity of NR-DNA binding correlates mostly with stronger transcriptional activity. Nevertheless, the RE is supposed to be more than an anchor. REs showed properties of allosteric ligands and were able to influence NR structure (122, 123) leading to a selectivity in interaction with other proteins as well as cell and gene specific effects. However, the derived consensus motifs for NRs not necessarily specify binding, and their importance is a matter of discussion (114, 124–127). Recent genome-wide binding studies found that some NRs bind to DNA sequences much more promiscuous than expected from consensus motif studies. Further, a large number of NR-binding sites in these studies showed no resemblance with a specific NR-RE (124–126).

1.4.3 Gene regulation mechanisms

One of the main subjects of intense scientific investigation is the question how genomic information is translated to gene regulation. Single-gene studies revealed in the last decades general principles of gene regulation. According to these principles cis-regulatory elements such as promoters, enhancers, and proteins that bind to these elements control gene transcription (128).

Site-specific factor binding to proximal promoter regions and interaction with co-factors can either enhance or repress basal transcriptional activity. For the NR class that is permanently located in the nucleus (class II NR) the conventional concept describes constitutive binding to target DNA sites (RE) and association with co-repressors (e.g. nuclear receptor co-repressor (N-CoR) and HDAC3 histone deacetylase) in absence of a specific ligand. Upon ligand binding

conformational changes lead to dissociation of the co-repressor complex and recruitment of co-activators (e.g.: steroid receptor co-activator (SRC) and CBP/p300 histone acetyltransferase) to the NR, triggering transcriptional activation (**Figure 4A**) (129, 130). Some NRs such as PPAR and LXR are able to bind other TFs and deactivate the signal transduction by preventing the exchange of co-repressor for co-activator complex in a process called transrepression (**Figure 4B**). For example, the LXR can inhibit the signal dependent activation of proinflammatory TFs (e.g. NFκB, STATs, and AP1 family members) through transrepression. Essential for this process is the posttranslational modification of LXR by chromatin modifiers including the protein SUMO-2/3 (131).

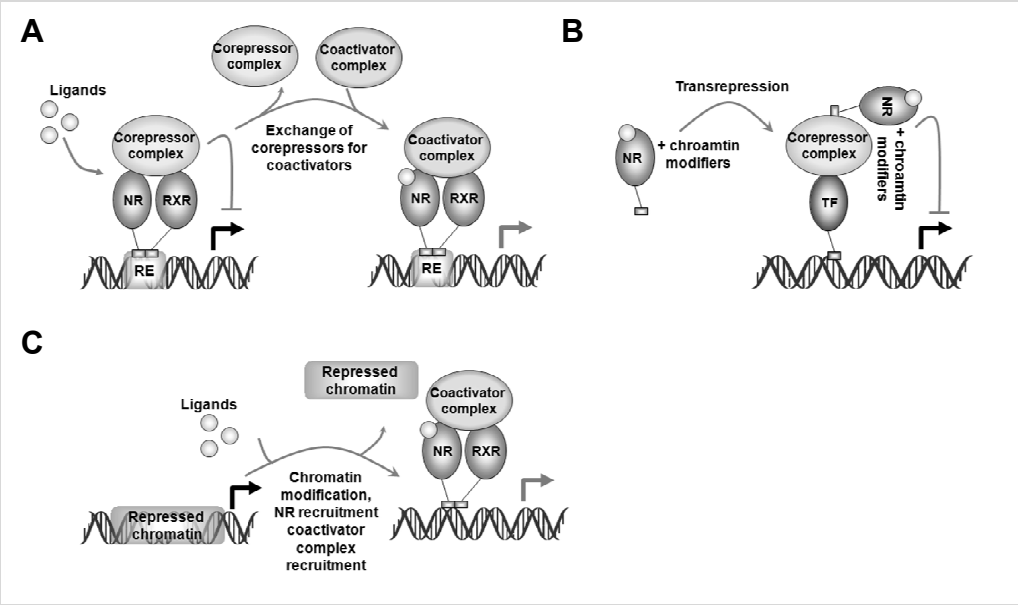

Figure 4: Molecular mechanism of nuclear receptor (NR) activation and transrepression. (**A**) Transactivation: In absence of a ligand NR-retinoid X receptor (RXR) heterodimer is bound to a response element (RE) of a target gene. Through interaction with the co-repressor complex gene expression is repressed (black arrow). Upon ligand binding the co-repressors are exchanged for co-activators triggering transcription of the target gene (green arrow). (**B**) Transrepression: Activation of the NR leads to posttranslational modification and subsequent inhibition of transcription factors (TF) by preventing the co-repressor complex exchange. (**C**) Alternative activation: Repressed chromatin excludes NR binding in absence of a ligand. Upon ligand stimulation, NRs in conjunction with co-regulators and chromatin modifiers can resolve the repressed chromatin state, bind to the specific DNA site and recruit co-regulators for target gene activation.

Recent genome-wide binding experiments challenged the classic model of transactivation suggesting for some NRs an alternative activation mode (**Figure 4C**). This mechanism includes ligand requirement, co-regulators and histone modifications (126, 125, 124). In absence of a ligand, the chromatin has a more closed structure and is less accessible for NR binding. Upon ligand activation the NR in conjunction with co-regulators and chromatin modifiers binds DNA and activates its target genes (132).

Clearly, recent and future studies generating genome-wide datasets of NR binding and global expression will provide a resource for more detailed re-examination of previous transcriptional regulation concepts.

1.4.4 Liver X receptor (LXR)

Two members of the NR family are the related oxysterol receptors liver X receptor alpha (LXRα, (133)) and liver X receptor beta (LXRβ, (134)). Loss of function studies clearly showed the requirement of LXRs for whole body cholesterol homeostasis and their impact on atherosclerosis development and progression (135–137). For example LXRα/β knockout mice display, even on a normal diet, increased cholesterol accumulation in macrophages at arterial walls (138). As permissive heterodimers LXRs function with RXR and bind to REs consisting of direct repeats with the consensus sequence 5'-AGGTCA-3' and half-sites separated by 4 nucleotides (DR4) (117). Human LXR subtypes LXRα and LXRβ share 77% sequence homology in their LBD and DBD (139). Evolutionary analyses of both LXR subtype sequences suggested a duplication of a single LXR during mammalian evolution (140). This duplication resulted in one more general and one specialized factor. The LXRβ subtype is ubiquitously but rather low expressed compared to LXRα, which is highly abundant in metabolically active tissues including liver, small intestine, kidney, spleen, brain, adipose tissue, and macrophages (141, 142). Additionally, in contrast to LXRβ, LXRα expression is controlled by an autoregulatory mechanism and highly induced by natural and synthetic LXR agonists (143, 144). This mechanism may be responsible for high expression levels of LXRα in foam cells, whereas resting macrophages contain more LXRβ subtype (145). Consequently, in the context of atherosclerosis, recent studies demonstrated that LXRβ activation was in general

low efficient in counteracting atherogenic processes compared to the LXRα subtype that efficiently induced anti-atherosclerotic gene expression profiles (146).

1.4.4.1 LXR physiology

LXRs are important in multiple physiological functions (**Figure 5**). The first discovered key functions, in particular of the LXRα subtype, comprised the control of cholesterol metabolism and lipogenesis in the liver (147–149). LXRs regulate hepatic lipogenesis through activation of key lipogenic factors including SREBF1, fatty acid synthase (FAS) and sterol CoA desaturase 1 (SCD1) (150). Further, LXRs promote excretion (142) and detoxification of bile acids (151) or lipids (152).

One of the central consequences of LXR activation in vivo consists of the increased rate of reverse cholesterol transport (RCT), mainly via induction of cholesterol transporters, cholesterol uptake through down regulation of Niemann-Pick C1-like protein 1 (NPC1L1) and activation of ABC transporter ABCA1, ABCG5 and ABCG8 (153). In macrophages, LXR activation leads to increased expression of ABCA1, ABCG1 and apolipoprotein APOE, which increases cholesterol efflux to lipid poor cholesterol acceptor proteins. In the intestine LXRs can limit APOA1-HDL and HDL particles (154). Through LXR dependent induction of the E3 ubiquitin ligase MYLIP (myosin regulatory light chain interacting protein) - also known as inducible degrader of LDL receptor (IDOL) - the LDLR is degraded. This degradation limits LDL cholesterol uptake in macrophages and other peripheral tissues (155). Additionally, LXRs are involved in *de novo* synthesis of cholesterol (156), regulation of carbohydrate (157) and energy metabolism. For example, LXRβ-knockdown increased the levels of uncoupling protein 1 (UCP1) in multiple tissues. Particularly in brown adipose tissue this effect lead to increased UCP1 expression and increased thermogenesis (158). In white adipose tissue LXR activation was associated with increased lipolysis and fatty acid oxidation (159).

It is also important to highlight the immune-related effects of LXRs. Both LXR subtypes were described as anti-inflammatory TFs that regulate the innate and adaptive immune responses, and are involved in apoptosis and phagocytosis.

Notably, during cell break down apoptotic cells generate cholesterol derivatives from cell membranes that serve as LXR ligands. This process stimulates

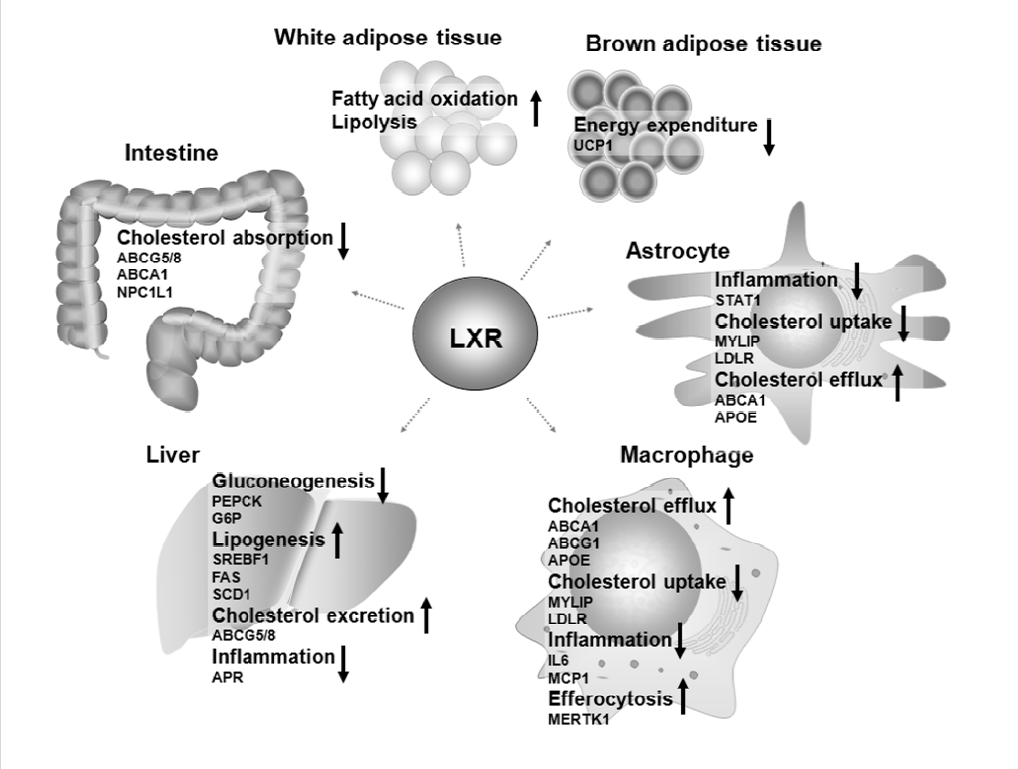

Figure 5: Physiology of liver X receptor (LXR). LXRs increase hepatic cholesterol excretion via ABC transporter (ABCG5/G8) and lipogenesis mainly via sterol response element binding transcription factor 1 (SREBF1), fatty acid synthase (FAS) and sterol CoA desaturase 1 (SCD1). Further LXR reduces hepatic gluconeogenesis and inflammation by decreasing the expression of phosphoenolpyruvat carboxykinase (PEPCK) and glucose 6 phosphatase (G6P) enzymes as well as mediate attenuation of hepatic acute phase response (APR). In intestine, LXRs decrease cholesterol absorption via upregulation of ABC transporters and downregulation of Niemann-Pick C1-like protein 1 (NPC1L1). In white adipose tissue fatty acid oxidation and lipolysis are increased. In brown adipose tissue energy expenditure is decreased via uncoupling protein 1(UCP1). In astrocytes and other brain and spinal cord cells LXR increases the expression of ABCA1 and apolipoprotein E (APOE) for elevated cholesterol efflux and decreases cholesterol uptake and inflammation with beneficial effects for neurodegenerative diseases such as Alzheimer's disease. In macrophages LXRs increase cholesterol efflux via induction of ABCA1, ABCG1, APOE and decrease uptake via reduction of low density lipoprotein receptor (LDLR) via myosin regulatory light chain interacting protein (MYLIP). Further, LXR have immune-regulatory roles in many cell types. In macrophages LXRs decrease inflammation and activate efferocytosis for increased engulfment of apoptotic cells via mer receptor tyrosine kinase 1 (MERTK1).

apoptotic cell clearance by macrophages supported by the LXR target gene mer receptor tyrosine kinase 1 (*MERTK1*) (160). Immune regulatory effects of LXR were observed in various cell types including hepatocytes, where LXRs inhibit the expression of acute phase proteins via transrepression pathways (131, 161). Moreover, LXR effects on inflammatory pathway were described as beneficial in several neurodegenerative diseases such as Alzheimer's disease (162, 163). LXRs can reduce plaque formation and increase plaque clearance through reduced inflammatory response (e.g. by inhibiting STAT1 inflammatory signaling) and activation of ABCA1 and APOE in astrocytes (164, 165).

So far, most studies applied single gene approaches and only a subset of all potential LXR target genes is known. With the advent of genome-wide binding and expression studies, the full potential of LXR in the human body will be elucidated.

Taken together, LXRs broad involvement in various metabolic and inflammatory signaling pathways clearly displays its anti-atherogenic potential for prevention and treatment of major health issues.

1.4.4.2 LXR dependent reverse cholesterol transport (RCT)

LXRs are cholesterol sensors. Excess cholesterol levels trigger several adaptive mechanisms that protect the cell from cholesterol overload. LXR activation leads to protection from atherosclerosis by inducing RCT (137). This multi-step process results in cholesterol transfer from various cells such as macrophages back to the liver for further procession, storage or bilary excretion (166). In the macrophage, LXR agonists increase RCT. As one of the natural strategies to maintain a net cholesterol balance, LXRs are activated by oxysterols, predominantly monooxygenated derivatives of cholesterol, and subsequently regulate LXR responsive macrophage genes (e.g. *ABCA1*, *ABCG1*, *APOE* and *NPC1/2*) that promote cholesterol efflux to APOA1, APOE and HDL (167) (**Figure 6**). The expression of the carrier proteins Niemann-Pick 1 and 2 (NPC1, NPC2) stimulates the post lysosomal mobilization of cholesterol from endosomal compartment to outer cell surface (168). At the plasma membrane, cholesterol becomes available for efflux via cholesterol efflux transporter ABCA1 and ABCG1, which facilitate the movement of free cholesterol from plasma

membrane to extracellular acceptors including lipid-free apolipoproteins and HDL. *ABCA1* was one of the first identified LXR target genes and is highly induced by LXR ligands in macrophages and many other peripheral tissues (169, 170). ABCA1 deficiency leads to Tangier disease an inherited disorder that is associated with very low HDL levels, increased accumulation of cholesterol in peripheral tissues and premature atherosclerosis (154, 171). For storage in the macrophage, free cholesterol is converted to cholesterol esters and stored in lipid

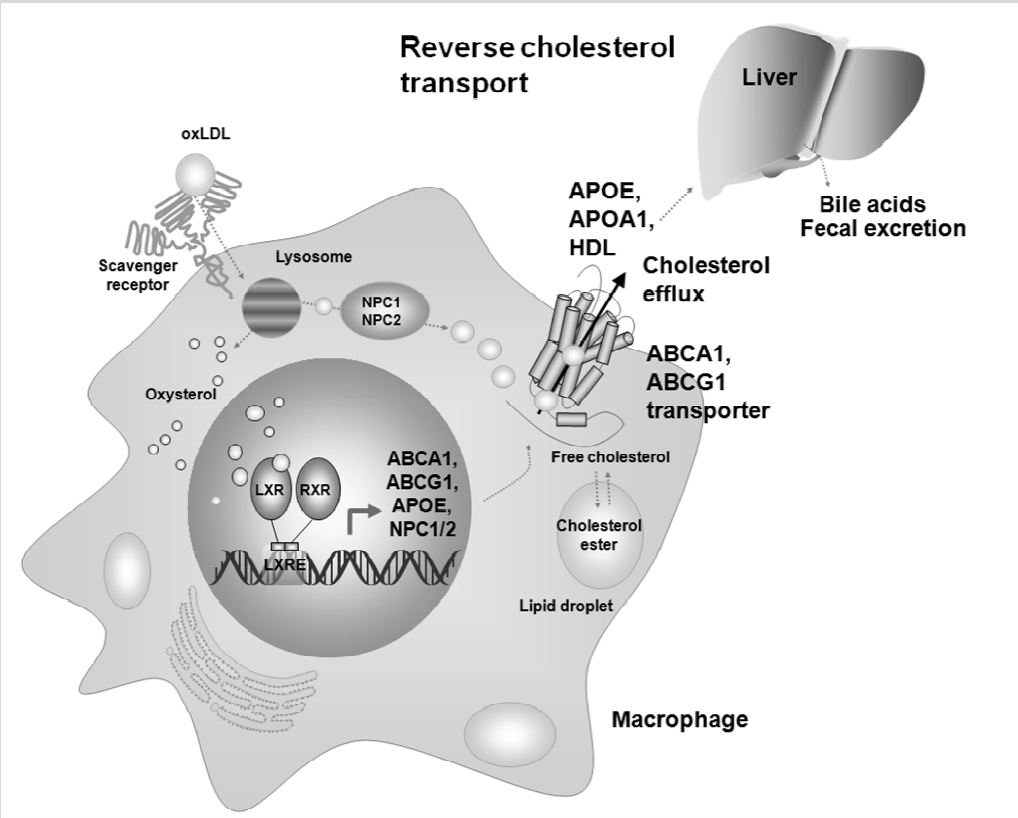

Figure 6: Liver X receptor (LXR)-dependent reverse cholesterol transport in macrophages. Oxidized low density lipoprotein (oxLDL) enters the cell via scavenger receptors and is processed in the lysosome. Oxysterols activate LXR. LXR regulates responsive macrophage genes including cholesterol efflux ABC transporter *ABCA1*, *ABCG1* as well as aplolipoprotein E (*APOE*) *or Niemann-Pick C1 and C2 (NPC1/2)*. NPC1/2 trigger post lysosomal mobilization of free cholesterol to the outer cell surface. At outer cell surface cholesterol can be further transported via ABC-transporter to lipid-free apolipoproteins and high density lipoprotein (HDL) and subsequently to the liver for bilary excretion. Excess cholesterol is stored in the cell as cholesterol ester in lipid droplets.

droplets. Most of the effluxed cholesterol is also esterified in HDL and can be either transferred to other lipoproteins (such as LDL or VLDL) or directly

transported back to the liver (172). Efficient RCT from periphery to the liver requires also other LXR responsive genes including lipid remodeling phospholipid transfer protein (PLTP), cholesterol ester transfer protein (CETP) and LPL for triglyceride lipolysis (173–175).

Taken together, LXR mediated target gene expression protects cells from cholesterol accumulation by promoting RCT. The subsequent reduction of foam cell formation, lesion cholesterol content and lesion regression makes RCT the main strategy for treating atherosclerosis and CVD treatment. The attempt to increase ABC-transporter or HDL is in the major focus of cardiovascular drug discovery (176).

1.4.4.3 LXR ligands

Initially, both LXR subtypes were designated as orphan receptors because no naturally occurring ligands were identified. Later, LXRs were de-orphanized by the discovery of cholesterol metabolites, which activated the receptors at physiological concentrations (177). Since then, various oxidized or hydroxylated cholesterol metabolites (oxysterols) have been recognized as endogenous LXR agonists. Oxysterols can be produced endogenously through enzymatic or chemical synthesis as well as enter the body through nutritional supply (177). These metabolic intermediates are found at high concentrations in plasma and tissue and the EC_{50} range for most oxysterols is within micromolar range. Interestingly, cholesterol has no affinity to LXRs (178). Position specific monooxidation of the sterol side chain is necessary for LXR activation (179). Most efficient oxysterols include 22-(R)-Hydroxycholesterol, 20-(S)–Hydroxycholesterol and other metabolites from steroid hormone synthesis (180, 181). Many structurally diverse natural and synthetic compounds were found as modulators of LXR transcriptional activity due to the highly flexible ligand binding pocket (182, 183). These LXR ligands include bile acid pathway derived molecules, plant sterols and stanols, fungal derivatives and synthetic non-steroidal agonists such as GW3965 or T0901317 (183). Although the synthetic ligand T0901317 is not completely selective for LXR it is still the most commonly used ligand in basic research.

1.4.4.4 LXR drugs

Efficient strategies for prevention and treatment of severe disease such as atherosclerosis are needed. One of the strategies with an estimated market of 50 billion Euro per year (184) is targeting NRs. Both LXR subtypes are significant drug targets among the NR family due to their dual role as physiological regulator of lipid/cholesterol metabolism and inflammatory response. The linkage of lipid metabolism and inflammation control in one drug is highly relevant for metabolic disorders (185). Targeting LXR with strong agonists such as GW3965 or T0901317 (138, 186) showed anti-atherosclerotic effects including plaque composition altering and regression, reduced inflammation and changes in fibrous cap thickness (138, 187, 188). Further, a substantial improvement of glucose metabolism was observed in mice fed with a high fat diet supplemented with GW3965 (189). One of the key limitations in pharmacological therapy targeting LXR consists of the increase in triglycerides (hypertriglyceridemia in mice), mainly contributed from LXRα in hepatocytes (190, 191). A major function of LXR activation in the liver is promotion of de novo lipogenesis (fatty acid biosynthesis) through the induction of SREBF1, SCD1 and FAS (147, 148, 190).

For future drug development it is important to develop selective LXR modulators to prevent deleterious side effects (183). Enhanced basic knowledge on drug-specific activation pathways and triggered networks will be substantial for future drug design.

1.5 Genome-wide transcription factor binding studies

Regulation of gene transcription is controlled by the dynamic interplay between TFs, chromatin modifiers and target DNA sequence. TFs are important gene regulators but the underlying mechanisms of their action and functional location within different cell types or treatments remain poorly understood.

In order to decipher gene regulatory networks that drive various biological processes it is pivotal to investigate the spatio-temporal binding pattern as well as the genomic environment (epigenetic marks) of TFs (114). For example, specific histone modifications were associated with closed versus open chromatin

conformation, which influences gene repression or activation, respectively (192). Our current understanding of transcriptional regulation is still based on the limited single gene studies and must be re-evaluated by genome-wide approaches. The first step is to identify genome-wide *in vivo* binding sites of TFs. There are several techniques to study DNA-Protein interaction including DNAse I footprinting, X-ray crystallography and chromatin immunoprecipitation (ChIP) (193).

1.5.1 Chromatin immunoprecipitation (ChIP)

ChIP is the current technique of choice to investigate protein-DNA interactions in living cells. This technique allows the isolation and identification of genomic DNA fragments that were *in vivo* occupied by proteins or nucleosome classes of

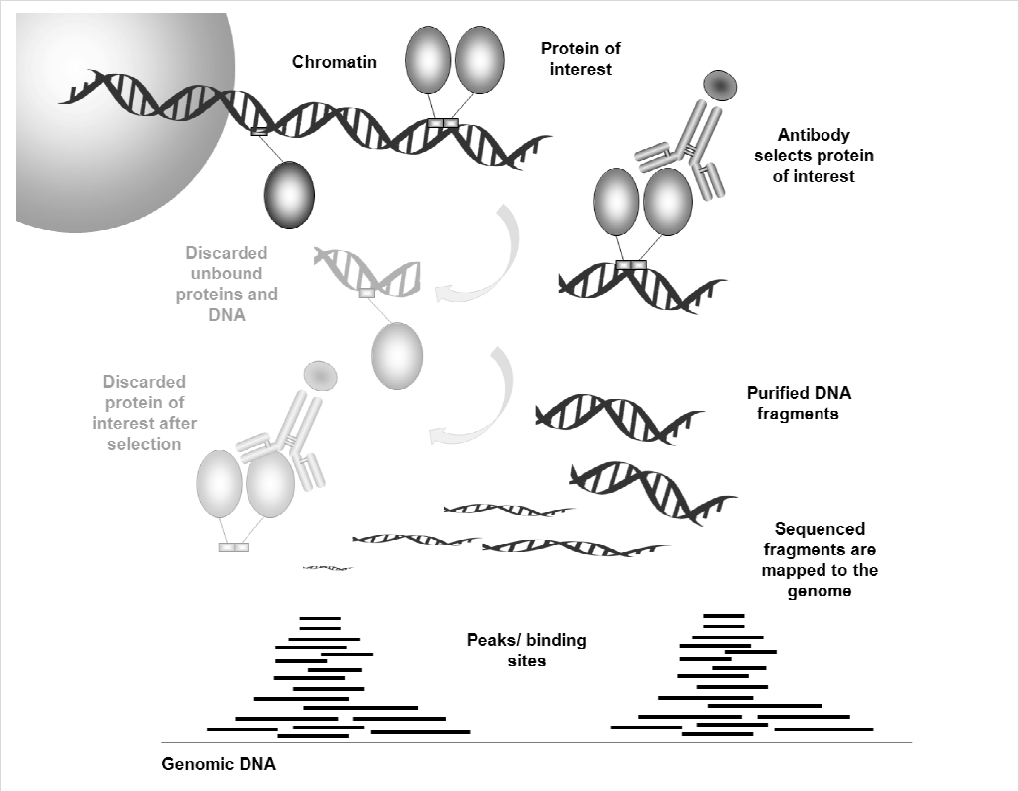

Figure 7: ChIP followed by sequencing identifies binding sites of proteins across the entire genome. Proteins are crosslinked to DNA, cells are split open and DNA is fragmented. A specific antibody against the protein of interest enriches protein-DNA complexes. The isolated complexes are reverse-crosslinked and DNA fragments that were bound by the protein of interest are purified. DNA fragments are sequenced and mapped to the genome. Protein binding is visualized as enrichment of isolated, sequenced and mapped fragments at genomic DNA sites (2 peaks at the bottom of this figure).

interest (194) (**Figure 7**). With the quickly evolving next generation sequencing (NGS) technology the genome-wide scale view of DNA-protein interactions became possible. In a ChIP experiment, cellular proteins associated with DNA are covalently bound to the DNA by chemical reversible crosslinking. In the next step, cells are split open and the crosslinked DNA is sheared into small fragments (often by sonication to 200-600 bp fragments). For immunoprecipitation, a specific antibody against the protein of interest is used to enrich the protein-DNA-complexes of interest. As immunoprecipitation control, unspecific IgG can be used. Unspecific DNA-protein complexes are discarded. After the reversal of crosslink, DNA of interest is released and can be further assayed. Putative binding sites of candidate target genes can be analyzed by PCR using flanking primers (ChIP-qPCR). For hypothesis-free genome-wide analysis, enriched DNA fragments can be sequenced in high-throughput using NGS techniques (195).

1.5.2 ChIP-sequencing

The first step in uncovering transcription regulation networks that underlie development, physiology and disease, consists of the genome-wide detection of TFs and modified histone occupancy. ChIP coupled with ultra-high-throughput parallel DNA sequencing (ChIP-seq) can provide an accurate and high-resolution map of the protein-DNA binding. For ChIP-seq, enriched DNA fragments from ChIP experiments are used to generate a library for high-throughput NGS platforms such as Illumina's genome analyzer. The sample preparation in Illumina's process includes linear amplification, hybridization to a flowcell, cluster generation and subsequent sequencing by synthesis using fluorescently labeled reversible terminators. Using this technique millions of DNA fragments can be analyzed simultaneously (196, 197). Short DNA reads (36bp) from one or both DNA fragment ends can be sequenced. Typically, a ChIP-seq experiment generates tens of millions of short reads, which can be mapped to the genome by a read alignment algorithm (198). DNA fragments that were bound to protein of interest are in general the most frequently sequenced fragments, which can be mapped back to the genome and displayed as peaks in a genome browser (**Figure 7**, bottom). During this process the genome is scanned with a sliding window and regions with significantly enriched read counts compared to control and according to a definite cutoff are defined as binding sites (194). ChIP- seq data

can be used for several analyses including motif analysis, identification of candidate regulatory regions, finding interacting factors that mediate a common regulatory action and integrative data analyses with multiple data sets (199).

1.5.2.1 Limitations of ChIP-sequencing

A central limitation of this still evolving technique consists in the false enrichment of sites resulting from bias towards highly accessible (open) chromatin, PCR preferences, unspecific immunoprecipitation due to antibody quality or other background noise (197). Therefore, it is important to include a control library (e.g. IgG ChIP), carefully remove false positives and validate the obtained binding sites by ChIP-qPCR and sequencing replicates (194). However, especially highly flexible and low abundant TFs are still difficult targets for ChIP-seq analysis. Additionally, ChIP-seq experiments can be subject to low reproducibility (200).

In summary, to generate a robust and significant data set careful filtering and stringent cutoffs are needed (201).

1.5.2.2 Data analyses

With the maturity of the NGS technology, the challenge shifted towards comprehensive computational analysis of terabytes of generated sequencing data. To support the analysis many statistical and computational methods have been developed (202). The derived sequence reads need to be aligned to the genome and analyzed for significant enrichment of potential TF binding sites (peak calling). Further downstream applications include visualization, binding motif discovery and relationship to gene structure.

To elucidate the functional impact of TF binding and implicated biological processes the ChIP-seq approach must be multi-pronged and combined with other data sets including global expression profiling (195).

1.6 Gene regulatory networks

Traditional genetic and biochemical approaches must be complemented with system-based strategies that integrate numerous genomic molecular and physiological data in order to fully address complex biological mechanisms (38).

There is a growing body of evidence that broad networks of interacting genes and proteins rather than single proteins or simple linear molecular pathways drive complex biological processes and disease (203). Consequently, instead of focusing research on few genes or proteins, it is essential to analyze numerous genes simultaneously to elucidate gene regulatory networks and their interplay in healthy and diseased states. For a full system overview it is required to know how individual components interact with each other and how for example genetic or environmental factors can influence molecular networks (204). Often such interactions, described in nodes (system components) with edges (connections/interactions), are based on previously known literature and new experimental data. The network concept was already successfully applied in studies of metabolic traits and novel drug targets (205, 206).

Integration of multiple datasets and identification of networks that comprehensibly respond to genetic, environmental and pharmacological intervention will provide a powerful approach in investigation of complex biological systems and perturbations during disease.

1.7 Aims of the thesis

Considering atherosclerosis as the leading cause of CVD, it is in the focus of current research to understand the underlying mechanisms and to find successful therapeutic targets for clinical atherosclerosis treatment. In this context the impact of macrophage`s dynamic regulatory molecular networks triggered by ligand dependent nuclear receptor LXRα in atherosclerotic lesion development and progression is of fundamental interest.

Hence, the objective of this thesis was to elucidate LXRα contribution to gene regulatory networks in macrophages, atherosclerotic foam cells and changes upon modulation with the anti-atherosclerotic LXRα ligand T0901317 by applying an integrative and genome-wide analysis. Further, it was also aim of this thesis to discover selective LXRα modulators without deleterious side effects.

Therefore, it was analyzed how small and highly active molecule agonists modulate LXRα actions in a well-validated human macrophage and foam cell model. The global LXRα binding and expression data was integrated and

compared in order to find new avenues for treating systematically atherosclerosis and related diseases. Analysis of histone modifications and chromatin accessibility at LXRα binding sites aimed to elucidate the interplay between the transcriptome and the epigenome.

In addition, a natural compound library was screened and promising candidate structures were analyzed for their LXRα activation potential and physiological impact in macrophages and foam cells.

Finally, the derived data of drug-specific activation pathways and triggered networks should enhance our understanding of LXRα gene regulatory mechanisms, which is substantial for future drug design.

2. Materials and Methods

2.1 LXRα ligands

The synthetic LXR ligand T0901317 and the natural ligand 22-R-Hydroxycholesterol were purchased from Sigma-Aldrich. LXRα ligand screening was performed with a very diverse natural compound library (207) applying the LXR alpha coactivator kit (Invitrogen) according to manufacturer's instructions. The promising stilbenoid backbone structure was chemically optimized by the addition of an epoxide. The resulting structure, named STLX4, was kindly synthesized and provided by Professor Thomas Erker (Department of Medicinal Chemistry, University of Vienna).

2.2 Cell culture experiments

All presented experiments were performed in human cell culture models.

2.2.1 THP1 cells

For most experiments, the well-validated human monocytic leukaemia THP1 cell line was used. THP1 cells were obtained from American Type Culture Collection (ATCC) and maintained at a density of $3x10^5$ cells/ml in RPMI 1640 medium (Sigma-Aldrich) supplemented with 10% fetal bovine serum (FBS, Biochrom) under a humidified atmosphere of 5% CO_2 and 95% air at 37°C. Medium was renewed every two to three days and cells were split two times per week for maximal 12 weeks. For experiments, THP1 cells were plated at a density of $2x10^5$ cells/ml and differentiated for 48h using 10^{-8} M phorbol 12-myristate 13-acetate (PMA, Sigma-Aldrich). Differentiated THP1 macrophages were treated either with vehicle control (0.01% dimethylsulfoxide (DMSO), Merck), or with 1μM T0901317 (Sigma-Aldrich) or with 1μM STLX4 for 24h.

2.2.2 Primary human macrophages

Experimental validation was performed with human primary macrophages, isolated from at least four individual buffy coats donated by healthy volunteers and kindly provided by DRK-Blutspendedienst Ost gemeinnützige GmbH Institut

Berlin. Peripheral blood mononuclear cells (PBMC) were isolated from buffy coats by density centrifugation (400 x g for 40 minutes) with Ficoll Paque (GE healthcare) and subsequent washing steps with saline phosphate buffer (PBS, Gibco) supplemented with 0.5% Bovine serum albumin (BSA, Sigma-Aldrich) and 2mM EDTA (Merck). Monocyte enrichment from PBMC was obtained using MACS Monocyte Isolation Kit II and MACS LS columns (Miltenyi Biotec) following manufacturer's protocol, yielding >95% purity. For differentiation $5x10^5$ cells/ml were plated in RPMI 1640 medium (Sigma-Aldrich) supplemented with 10% human AB serum (First Link UK LTD) and 1% Penicillin/Streptomycin (Gibco) mix and incubated for 7 days. Differentiated primary macrophages were treated either with vehicle control (0.01% DMSO, Merck) or with 1μM T0901317 (Sigma-Aldrich) for 24h.

2.2.3 HEK cells

For reporter gene assays human embryonic kidney (HEK293) cells were obtained from ATCC and maintained at a density of $2x10^5$ cells/ml in Dulbecco's modified Eagle's medium (DMEM, Invitrogen) supplemented with 10% FBS (Biochrom). The viability of treated cells was quantified by applying the CellTiter-Glo Luminescent Cell Viability Assay (Promega) according to manufacturer's protocol.

2.2.4 Foam cell formation

Foam cell formation in differentiated THP1 cells or primary blood derived macrophages was induced with 100μg/ml oxidized LDL (oxLDL, Autogen Bioclear UK Ltd) for 48h. Foam cells were treated either with vehicle control (DMSO) or with ligands (T0901317 or STLX4) for 48h. Cholesterol loading and treatment was controlled with Oil Red O staining (Alfa Aesar) according to manufacturer's instructions and for detailed cholesterol composition with the fluorometric method of Amplex Red Cholesterol Assay Kit (Invitrogen) according to manufacturer's instructions.

2.2.5 Cholesterol and triglyceride analyses

THP1 derived macrophages and foam cells were plated out into 24-well plates (Nunc) at a density of 2 x 10^5 cells/well. After differentiation and treatment cells were lysed with 100 µL lysis buffer (PBS, 0.25 M NaCl, 1% Triton X-100). Total and free cholesterol were determined using the colorimetric enzymatic Amplex Red Cholesterol Assay Kit (Invitrogen). Triglycerides were quantified by Triglyceride Assay Kit (BioVision). For normalization protein content was determined with Pierce 660 nm Protein Assay Reagent (Thermo Scientific).

2.2.6 LXR knockdown macrophages

Target specificity of gene expression effects was tested with siRNA-mediated LXRα/β knockdown in macrophages and foam cells with subsequent qPCR or microarray analysis. Therefore, THP1 cells (2x10^5 cells/ml) were seeded in 24-well-plates and differentiated for 48h as described above. For foam cell formation, differentiated cells were incubated with oxLDL for 48h prior to knockdown. Differentiated cells were transfected with transfection reagent (Mirus) and 15nM LXRα Silencer Validated siRNA (ID5458) and 15nM LXRβ Silencer Select Validated siRNA (ID s14684) or 30 nM Silencer Select Negative Control #1 (all Ambion), respectively. Transfection was carried out for 48h followed by treatment of LXRα/β knockdown macrophages with 10µM ligand or vehicle control (DMSO) for 24h.

2.3 Immunoblotting

For protein amount assessment in the THP1-derived cell models cells were harvested and nuclear extracts were prepared with the NE-PER Nuclear and Cytoplasmic Extraction Kit (Pierce). Protein contents were determined with the Pierce 660nm protein assay (Pierce). Protein concentrations were adjusted to 23 µg per sample and were analyzed by western blotting using the NuPage Bis-Tris Electrophoresis System (Invitrogen). SDS-PAGE was carried out using NuPage 15 well Novex 4-12% Bis-Tris gels (1.0 mm) and separated proteins were plotted on nitrocellulose membranes for 75 minutes at 400mA. After blotting membranes were stained with Ponceau S solution (Applichem) to confirm equal protein loading and de-stained using tab-water. After blocking of membranes (1X TBS,

0.1% Tween-20 with 5% w/v nonfat dry milk), membranes were incubated with 1:1000 anti-LXRα antibody (Abcam, ab 41902, (208, 209)) in milk powder solution at 4°C over night. After washing the membranes with TBS-Tween solution, membranes were incubated with 1:2000 goat anti-mouse IgG-HRP antibody (Santa Cruz Biotechnology, sc-2005) for 1 hour at room temperature. After washing steps, luminescence was detected with Western Lightning ECL solution (Perkin Elmer) on a Fujifilm LAS-1000 camera system using the Image Reader LAS-1000 Pro V2.61 software. Membranes were stripped with Restore Plus Western Blot Stripping Buffer (Thermo Scientific) for 10 minutes and incubated with β-Actin (C4) antibody (Santa Cruz Biotechnology, sc-47778) for 20 minutes at room temperature. After washing, the membrane was incubated with 1:2000 goat anti-mouse IgG-HRP antibody (Santa Cruz Biotechnology, sc-2005) for 20 minutes at room temperature. Similar procedures were applied for anti-LXRβ (Abcam, ab56237,(210)) and anti-RXRα antibodies (Santa Cruz Biotechnology, sc-774 X) with 1:1000 goat anti-rabbit IgG-HRP antibody (Santa Cruz Biotechnology, sc2004). For ABCA1 and APOE protein amount detection whole cell extracts were used. In this experiment LXRα protein detection was also repeated with whole cell extracts. Therefore anti-APOE antibody (Abcam ab1906), anti-ABCA1 antibody (Abcam, ab18180), anti-LXRα antibody (Abcam, ab 41902) and as housekeeping protein control anti-β-Actin (Santa Cruz Biotechnology, sc-47778, C4) were used. Secondary antibodies were HRP labeled anti-mouse and anti-rabbit (Santa Cruz Biotechnology). After detection with Western Lightning Plus-ECL solution membranes were stripped with Restore Plus Western Blot Stripping Buffer. Densitometry for all western blots was performed in ImageQuant TL (GE Healthcare). This tool measures quantitatively the optical density and provides more accurate data than simple eye-observations. The calculation of log (protein of interest/β-Actin) corrects data for loading imbalances.

2.4 Chromatin immunoprecipitation (ChIP)

ChIP was performed using the Transcription factor ChIP Kit (Diagenode) according to manufacturer's instructions. Briefly, at least six biological replicates of each experiment were crosslinked with a final concentration of 1% formaldehyde (Sigma-Aldrich) for 10 minutes. Fixation was stopped with

0.125M glycine and washed twice with ice-cold PBS. Collected cells were lysed with the provided buffers and dissolved in shearing buffer to a final concentration of $1x10^6$ cells per ChIP reaction. Shearing was performed using the Bioruptor^{TM} (Diagenode) at 4°C and 35-50 sonication cycles (30s on/ 30s off). Shearing conditions were optimized for differentiated THP1 cells and tested for shearing efficiency by agarose gel electrophoresis. The following antibodies were used: anti-LXRα (Abcam, ab 41902), anti-H3K4me3 (Diagenode, pAB-003-050), anti-H4K20me1 (Abcam, ab9051) and negative control anti-IgG (Diagenode, kch-819-015). For each ChIP 2 – 4 µg antibody were used. After washing and reverse crosslinking of precipitated samples, DNA purification was performed with the QIAquick PCR purification kit (Qiagen) according to the manufacturer's instructions. Each LXRα ChIP reaction was performed at least in quadruplicates and pooled at the DNA purification step. H3K4me3 and H4K20me1 ChIP reactions were processed in duplicates. DNA quantification was performed with Quant-it Picogreen dsDNA Kit (Invitrogen) according to the manual. Enrichment was measured as described above by quantitative real-time PCR with primers flanking new or known response elements and non target control regions (primers are listed in **Table M1**) applying at least 20pg sample/PCR. The relative occupancy of the immunoprecipitated factor at a locus was estimated using following equation $2^{(Ct\ input - Ct\ ChIP)}$. Ct input and ChIP are the threshold cycles of PCR done in triplicates on DNA samples from input and ChIP. LXRα ChIP qPCR was normalized against IgG ChIP qPCR of the same locus.

Name	**Forward primer**	**Reverse primer**	**LXRα binding position in genome**
ABCA1_1	CCCAGCTTCCCCATCTGCGC	CCGGAGGTGGGGTGCCCAAT	chr9:107689048-107689163
ABCA1_2	CTCACTCTCGCTCGCAATTA	ACGTGCTTTCTGCTGAGTGA	chr9:107690416-107690582
ABCA1_3	CGGGCTCATGCTCCACTCGG	GCCGATTGCCCCACATCCCT	chr9:107753699-107753804
LXRα_1	CATCTGTTTCGGTCTCTTTGG	GCAGATGCTCCAGTCCAGAT	chr11:47276460-47276651
ACCA1_1	CGCCCCTGTCTCCCACCTCA	TCGGAGGTGAACGGCCTGGA	chr17:35716119-35716190
FASN	CGGGGTTACTGCCGGTCATCG	GTGGGTGGACGTCCGTCTCG	chr17:80056847-80056934
SREBF1	CCGCCTTTAACCCGCTCGGTG	CCCTTTAACGAAGGGGGCGGG	chr17:17727207-17727290
ABCA1_4 negative control site	AGAGCGGACCCCAAAGCTGGT	GGCAGTGTGTCCAGGGCTTCC	chr9:107699191-107699307
LXRα_2 negative control site	GGATTACAGACCCGCATCAC	CCAGCAATGGTGTGTTGAAA	chr11:47277726-47277919
ACCA1_2 negative control site	TGCCACTGATCCACGATGTTGCC	AGTGGTCTTGGGAAAGAGCAGGC	chr17:35766683-35766761
ABCG1_ Prom	TGCTTTACGCCCAGTGACTT	CTGTGTAATGCTACAGGGAGGA	chr21:43619644-43619800
ABCG1_ Enh.	CCAGCTGGTAATGGCTTGTAG	CTGTCTGTCAACCCCTCTGG	chr21:43648221-43648419

COL4A1	ACTTGCACCACACTCACACA	CTCCGGCTAAGTGTGTGTGT	chr13:110969598-110969764
IGFBP4	TAGGGAAGCGGCTTTTCCTC	CACCTCAAGGGATCACTGCA	chr17:38486701-38486831
MYLIP	GCCCGATAGTAACCTCTGCC	AGGCTGAAGAAACTGACCAAGT	chr6:16131327-16131442
PBX4	AAGGAGTTCAAGGCCATGCTT	GAAAGTGGATGCGGCATTGT	chr19:19719349-19719526
PARP1	TCATTTGAGTCCCTGTGCAGT	TAATCGCATAGTCCCCCAGC	chr1:226637802-226637924
APOC1_1	GCCAGCCAACCTAGAGTCTG	ATCACTACATCCGTCCCCCA	chr19:45416303-45416430
APOC1_2	GCCGAACTAGAGTCTGAGGC	AATTCCTTCCCCACCAGCTG	chr19:45428862-45428953
H19	CTGGTCTGTGCTGGCCACGG	GCACCTTGGCTGGGGCTCTG	chr11:2026314-2026413
ACTB	CCATTGGCAAGAGCCCGGCT	GACACCCCACGCCAGTTCGG	chr7:5569866-5569984

Table M1: ChIP-qPCR primer list

2.4.1 ChIP-sequencing

For deep sequencing ChIP samples (10-15ng) were first amplified using the ChIP-Seq Sample Prep Kit (Illumina) according to the manufacturer's instructions. Sequence reads of 36bp were obtained using the second generation Genome Analyzer IIx and the Solexa Analysis Pipeline (Illumina). Unfiltered 36bp sequence reads were uniquely mapped to the human genome assembly (February 2009, GRCh37/hg19) using Bowtie (211) allowing for two mismatches along each tag. Sequencing data was submitted to EBI and can be accessed via www.ebi.ac.uk/ena/data/view/ERP001502. Data analysis after sequencing was

kindly performed by Cornelius Fisher (MPI for Molecular Genetics). 25bp resolution LXRα binding profiles were generated genome-wide using the MACS tool (212) with the option –wig. Resulting wiggle files (.wig) were converted to the bigWig format using the program wigToBigWig (213). Normalized signal profiles were generated using makeUCSCfile using the Hypergeometric Optimization of Motif EnRichment (HOMER) software (124). Resulting bedGraph files (.bg) were converted to the bigWig format using the program bedGraphToBigWig (213). BigWig files were uploaded to a web server and visualized as custom track in the UCSC Genome Browser (214). The program bigWigSummary (213) was used to retrieve signals from wiggle or bedGraph files based on genomic coordinates of LXRα peak intervals or intervals of open chromatin. The exact command used for this step is:bigWigSummary density.bigwig <chr> <start> <end> 1 type=mean. Where the density.bigwig is a bigwig file generated from filtered sequence alignments, <chr> is the chromosome, and <start> and <end> are the starting and ending positions of the interval, respectively. For visualization of selected loci the UCSC browser (http://genome.ucsc.edu) was used. Alternatively, tags for selected loci were extracted from UCSC and normalized against average of background tags of the same loci. Final visualization was performed with GraphPad Prism 5.0.

2.4.2 Peak calling and filtering

Peak identification was performed using the model based-analysis of ChIP-sequencing algorithm (MACS, (212)) with aligned sequencing tags in BED format from LXRα-ChIP and IgG-ChIP experiments. The MACS version 1.0.1 was accessed via Galaxy (main.g2.bx.psu.edu). The following peak calling parameters were used: p-value cut-off = 10^{-5}, effective genome size = 2.7^{9}, bandwidth = 300 and m-fold = 5. Additionally, three levels (1 kb, 5 kb, 10 kb) of regions around the peak regions were used to calculate the maximum lambda as local lambda. To estimate the false discovery rate (FDR) for each peak interval the traditional default method was used. The method considers the peak location, 1 kb, 5 kb, and 10 kb regions in the control data to calculate local bias. Due to imbalance between ChIP and control sample it was not possible to rank and filter the LXRα peaks according to FDR (215). To determine a stringent peak set for downstream analyses of LXRα ChIP-sequencing lanes, another filtering method

was applied. In this process, all peaks with a tag/length enrichment ratio <0.07 and peaks with less or equal number of tags as in the IgG control lane were discarded. This analysis was visualized in GraphPad Prism 5.0 with a box plot and median tag number of all raw tags of each lane analyzed (**Figure S1A**). For improved quality assessment k-means clustering of the LXRα ChIP-sequencing data was performed in SeqMiner (216, 217) and all clusters with control data mean density >0.25 of maximal LXRα enrichment were discarded (exemplified in **Figure S1B**). Additionally, cluster were manually removed after individual genome browser observation (201). Macrophages treated with T0901317 and vehicle control (DMSO), respectively were LXRα ChIPed and sequenced twice as independent biological replicates. For correlation analysis peaks for each biological replicate were called as described above, tag counts under the peak intervals were plotted and Pearson correlation analysis was performed. For final data assessment, all tags were combined and the peak calling and filtering procedure was repeated as described above.

2.4.3 Comparative ChIP-sequencing analysis

For better comparison between different ChIP-sequencing lanes and to detect differential LXRα binding across investigated cell models LXRα peak enrichment normalization was performed by Cornelius Fischer (MPI for Molecular Genetics) according the description of Bardet et al. 2012 (218) for all cell models. In brief, all independently MACS called and filtered LXRα peaks from all cell models were compiled and the union genomic regions of all peak coordinates with significant LXRα enrichment were computed (2652 genomic regions). Each region for each sample was scored and the LXRα peak heights were normalized with quintile normalization. After computing the $\log_2$ fold change between the peak heights three different LXRα peak sets could be categorized based on a change of 1.5 fold. For visualization SeqMiner (216, 217) was applied.

2.5 Formaldehyde assisted isolation of regulatory elements (FAIRE)

Chromatin accessibility has been described as dramatically predetermining for TF binding (127). To assess the relative openness of chromatin at LXRα binding

sites and at transcriptional start sites (TSS) of potential target genes, formaldehyde assisted isolation of regulatory elements (FAIRE) (219) was applied followed by sequencing and qPCR validation. FAIRE-seq and data analysis were kindly performed by Cornelius Fischer (MPI for Molecular Genetics). In brief, cells were cross-linked and chromatin was fragmented as described above for the ChIP assay. The input control sample of FAIRE was reverse-crosslinked over night at 65°C and 600rpm followed by incubation for 2h at 55°C and 500 rpm in the presence of 20 µg proteinase K (Invitrogen). The FAIRE-sample stayed crosslinked and was diluted with water. Chromatin of both samples was extracted from the aqueous phase by the phenol/chloroform procedure. DNA in nucleosome depleted regions is less likely crosslinked with proteins. Thus, active chromatin regions are preferably enriched in the aqueous phase. Total chromatin was used as control and the enrichment ratio of open chromatin compared to total chromatin was calculated.

2.5.1 FAIRE-sequencing

Sequencing and mapping of FAIRE enriched chromatin was processed as described for ChIP-sequencing above. Aligned sequencing tags were converted using F-Seq (220) and further processed with the Unix command 'sed' and the program wigToBigWig (213). Further visualization was done as described for ChIP-seq above. For relative openness analysis of the three defined LXRα peak sets (2652 genomic regions), the individual cell model enrichment intensities were extracted from BigWig files, quintile normalized and averaged for each genomic region. For visualization SeqMiner (216, 217) was used.

2.6 Transcription factor binding site enrichment

Regulatory elements, such as TFs, often bind DNA in cooperative manner in so-called hotspots that often also correlate with pattern of open chromatin (221–223). To determine the presence and number of co-localized TFs at LXRα binding sites, TFBS data was extracted from Encode consortium (Transcription Factor ChIP-seq from ENCODE, data contribution from the Myers labaratory at the Hudson Alpha Institute for Biotechnology and labaratory of Michael Snyder, Mark Gerstein and Sherman Weissman at Yale University; Peggy Farnham at UC Davis; and Kevin Struhl at Harvard; Kevin White at The University of Chicago;

Vishy Iyer at The University of Texas Austin, last update 04/28/2011,(224)). For visualization SeqMiner (216, 217) was used.

2.7 LXRα motif analyses

To analyze specific DNA motif occurrences at LXRα binding regions *de novo* motif search was performed with top 100 bound sequences for each defined peak set individually applying the MEME-ChIP tool from MEME suite (225) with default settings. Derived motifs were scanned using available position weight matrices (PWMs) from the Transfac database (226). Found motifs were aligned and visualized with STAMP tool (227). Motif distribution in all LXRα peak set sequences was determined by FIMO (Findmotif), a MEME suite tool with motif match display threshold: p-value 10^{-4}.

2.8 Reporter-gene assays

For more detailed analysis of detected LXRα/RXRα motifs, reporter-gene assays were performed with natural and mutated LXREs. All used clones were kindly provided by Claudia Quendenau and Dr. Vitam Kodelja (MPI for Molecular Genetics). In brief, for the mutated LXREs five copies of the designed LXREs (ordered as DNA-oligonucleotides from BioTEZ, **Table M2**) were cloned into pGL4.31 [luc2P/Hygro] vector (Promega) with the In-Fusion HD EcoDry cloning system (Clontech Takara Bio Europe). LXRα and RXRα, each were cloned into pBIND [Renilla/Amp] vector (Promega). Selection and Amplification was performed in *E. coli* cells. Purification of the plasmids was performed with a plasmid purification kit (Qiagen) according to manufacturer's instruction.

Name	**DNA ologonucleotide 5 x sequence**	**LXRα binding position in genome**
1 ABCA1	GCGCAGAGGTTACTATCGGTCAAAGC	chr9: 107690167-107690793
2 SREBF1	GCTGCGGGGTTACTGGCGGTCATTCA	chr17: 17727085-17727637
3 FASN	GCTGCGGGGTTACTGCCGGTCATTCA	chr17: 80056521-80057329
4 MYLIP	GCTGAGAGGTTACTATCGGGCATTCA	chr6: 16131062-16131653

5 DR4 motif set 2	GCTGCGGGGTTACTGCAGGTCATTCA	
6 DR4 motif set 1	GCTGCGAGGTTACTCCAGGTCATTCA	
7 Mutated DR4	GCTGCGGGGTTACGGCCGGTCATTCA	
8 Mutated DR4	GCTGCGGGGTTAGAGCCGGTCATTCA	
9 Mutated DR4	GCTGCGGGGTTACAGCCGGTCATTCA	
10 Mutated DR4	GCTGCGGGGTTAGTGCCGGTCATTCA	
11 Mutated DR4	GCTGCGGGATCACTGCAGGTCATTCA	
12 Mutated DR4	GCTGCGGGATTACTGCCGGTCATTCA	
13 Mutated DR4	GCTGCGAAAATACTGCAGGTCATTCA	
14 Mutated DR4	GCTGCGGGGTTCCTGCCGGTCATTCA	

Table M2: Mutated and natural sequences of LXR response elements.

Name	**Forward primer**	**Reverse primer**
LXRE primer Pr1099- Pr1050	TGGCCTAACTGGCCGGTACCGAGTTTCTAGATGAA	TTTTATAGCCCCCCGCTAGCGTCTTGCTGCGGGG
pGL4.31 vector primers	TACGGGAGGTATTGGACAGG	TCGATATGTGCGTCGGTAAA
Full length LXR/RXR primer 669-670	ATAGGCTAGCCAGCTTGAAGCAAGCCTCCTGAAAGATGGACACCAAACATTTCCTG	GCGGCCGCTCTAGACTAAGTCATTTGGTGCGGC
Full length LXR/RXR primer 669-670659-660	ATAGGCTAGCCAGCTTGAAGCAAGCCTCCTGAAAGATGCCCCACTCTGCTGG	AGTCGACGGATCCTCATTCGTGCACATCCCA

Table M3: Primers for cloning

For reporter gene analysis HEK293 cells were plated on a white, clear bottom 384 well plate (Greiner) at a density of $1x10^5$ cells/ml and cultivated in DMEM

media (Invitrogen) supplemented with 10% FBS for 24h prior to transfection. Transfection was carried out with 0.25% Lipofectamine (Invitrogen) in Optimem media (Invitrogen). HEK293 cells were co-transfected with the pGL4.31- LXRE-Luc (100ng), pBIND-LXRα and pBIND-RXRα (each 20ng) for 4h under a humidified atmosphere of 5% CO_2 and 95% air at 37°C. Afterwards transient transfected HEK293 cells were treated with 10µM T0901317 in DMEM media supplemented with 10% FBS for 24h. After the incubation period, cells were washed twice with PBS and harvested for luciferase reporter gene assay applying the Dual Luciferase Reporter System (Promega) according to provided instructions. Measurement of bioluminescence was carried out with the POLARstar Omega Microplate reader (BMG Labtech). Activity was expressed as relative luciferase unit (RLU) and finally visualized as fold change of T0901317 treatment versus vehicle control.

2.9 Functional annotation of LXRα binding sites

For a biological interpretation of our data, it was important to functionally annotate the LXRα binding sites to genomic position and nearby genes. Gene ontology analysis and association of LXRα bound target genes with genome-wide association studies (GWAS) data revealed new insights in LXRα activation.

2.9.1 Genomic distribution

Genomic distributions were determined using the Cis-regulatory Element Annotation System (CEAS 1.0.2, (228)). The derived percentual distribution was compared to normal genomic distribution and visualized in Excel (Microsoft) and GraphPAd Prism 5.0. (GraphPad Software Inc.) Average tag counts were calculated using the SitePro tool from Galaxy/Cistrome (228) and data was visualized in Excel (Microsoft).

2.9.2 Annotation of genes controlled by nearby peaks

Assuming that one LXRα binding site can regulate multiple surrounding target genes (229, 125), all potential LXRα target genes were annotated using a maximal distance of 200kb from peak center. Therefore, the Peak Center Annotation script (peak2gene) from the Cistrome Analysis Pipeline (AP) Module

(cistrome.org) was used. Gene definitions were taken from the UCSC Genome Browser's RefGene table (230). Peaks that did not have any annotated genes within 200 kb from peak center were termed as non- annotated or located in gene deserts.

2.10 Gene expression study

In order to understand the functional impact of TF binding and implicated gene regulatory networks, it is essential to perform integrative analysis with other data types including global expression data (194).

2.10.1 RNA purification, cDNA synthesis and qPCR

Total RNA was isolated from four biological replicates using RNeasy mini kit (Qiagen) following the manufacturer's instructions. An additional on-column DNAse digestion step (DNase-Set, Qiagen) was included. RNA quantity and integrity was checked by Nanodrop (ND-100 Spectrophotometer) and agarose gel electrophoresis, respectively. High quality RNA was utilized for whole genome microarray analysis and quantitative PCR analysis of selected LXR target genes. For quantitative PCR, 1µg total RNA was reversely transcribed to cDNA using the High Capacity Reverse Transcription Kit (Applied Biosystems) according to manufacturer's instructions. cDNA was amplified with specific primers (**Table M4**) by real-time PCR using an ABI Prism 7900HT Sequence Detection System and 2x SYBR Green PCR Master Mix (Applied Biosystems). PCR amplification was performed in a volume of 10µl containing 3-5ng cDNA, 0.5µM of each primer and 1x SYBR Green PCR Master Mix. The conditions were 95°C for 1 minute, followed by 40 cycles of amplification (95°C for 15s; 60°C for 60s). Product purity for PCR reactions was confirmed by examination of melting curves for the presence of a single peak. Relative gene expression levels were normalized using β-actin gene and quantified by the $2^{-\Delta\Delta Ct}$ method (231). Individual samples were analyzed in triplicates and data are presented as mean with ±standard error of mean (SEM). Statistical analysis was performed by using a two-tailed Students-T-test. Significance refers to compound treatment versus vehicle control. If not otherwise denoted, primers were designed with the Primer3 software (232), following specificity check with NCBI BLAST search (233).

Symbol	Forward primer	Reverse primer
ACTB	CAGCCATGTACGTTGCTATCCAGG	AGGTCCAGACGCAGGATGGCATG
LPL	ACAGAATTACTGGCCTCGATCC	CTGCATCATCAGGAGAAAGACG
CD36	GTTGATTTGTGAATAAGAACCAGAGC	TGTTAAGCACCTGTTTCTTGCAA
FABP4	GGTGGTGGAATGCGTCATG	CAACGTCCCTTGGCTTATGC
LXRα	CACCTACATGCGTCGCAAGT	GACAGGACACACTCCTCCCG
PLTP	GACACCGTGCCTGTGCG	GGTGGAAGCCACAGGATCCT
PPARG	CATGGCAATTGAATGTCGTGTC	CCGGAAGAAACCCTTGCAT
PPIB	ACGACAGTCAAGACAGCCTGG	CTTCCGCACCACCTCCAT
LXRβ	GGTGTGTCAGGGGCTAAAGA	CCTCTCGCGGAGTGAACTA
SREBF1	CCGCCTTTAACCCGCTCGGTG	CCCTTTAACGAAGGGGGCGGG
ABCA1	CTTCTCCGGAAGGCTTGTC	GGCCAGAGCTCACAGCAG
APOE	GGATCCTTGAGTCCTACTCAGC	CAGCCCACAGAACCTTCATC
IL6	CTGTCAGCTCACCCCTGCGCTC	GTGTGGGGCGGCTACATCTTTGG
TLR4	AGAACTGCAGGTGCTGGATT	ATGCCCCATCTTCAATTGTC
FASN	CGGGGTTACTGCCGGTCATCG	GTGGGTGGACGTCCGTCTCG
MMP9	CTGAGTCAGCACTTGCCTGTCAA	GCAGAGGTGTCTGACTGCAGCTG
TLR2	CTCCCAGTGTTTGGTGTTGCAAGC	GCACAATGAGCCCCACAGGTACC
CD68	GGTGAGGCGGTTCAGCCATGAG	GTTGTTCCAGTGCTCTCTGCCAG
IL10	ACCAAGACCCAGACATCAAGG	AGAAATCGATGACAGCGCC
TNFα	CCCAGGCAGTCAGATCATCTTC	CTGCCCCTCAGCTTGAGG
Cd163	TGGAATGGAAAAGGAGGCCATTCTG	GGTATCTTAAAGGCTGAACTCACTGGG
CD11b	TGTTAACAGCCTTGACCTTATG	ATCCCTGAAGCTGGACCAC
CD14	CTAAAGGACTGCCAGCCAAG	CCCGTCCAGTGTCAGGTTAT

Table M4: qPCR primer list

2.10.2 Genome-wide gene expression analysis

Microarray analyses were performed according to instructions of Illumina‘s TotalPrep RNA Amplification Kit, followed by hybridization on HumanHT-12 v3/v4 Expression BeadChips (Illumina). Scanning was performed with Illumina‘s BeadStation 50 (Illumina) platform and reagents. Samples were processed in biological quadruplicates. Basic expression data analysis was carried out using BeadStudio 3.1 (Illumina Software). Raw data were background-subtracted and normalized using the cubic spline algorithm. Processed data were then filtered for significant detection (P-value <0.01) and differential expression vs. vehicle treatment according to the Illumina T-test error model and were corrected according to the Benjamini-Hochberg procedure (P-values <0.05) in BeadStudio 3.1 (Illumina Software). For LXRα/β knockdown analysis only genes with significant detection (P-value <0.01) in control siRNA samples were chosen. Normalized T0901317 treated knockdown and control siRNA samples were compared to vehicle control (DMSO) or to foam cells. Statistical analysis of knockdown was performed by using a two-tailed Students-T-test. Significance refers to LXRα/β siRNA versus control siRNA with correction according to the Benjamini-Hochberg procedure (234) (P-values <0.05). Bead array data were validated by using quantitative real-time PCR. Gene expression data were submitted in MIAME-compliant form to the ArrayExpress database under accession number E-MTAB-1106 (www.ebi.ac.uk/arrayexpress). For overall gene expression comparison, we applied Gene distance matrix (GDM) analyses that include all gene expression data of a model, without restriction to a set of genes. Data reduction is achieved by collapsing the expression data of every gene to a vector sum in Euclidean space. The Euclidean distance between the vector sums of different compounds is therefore a measure of the similarity between the expression profiles. GDM comparison was performed in Multiexpression Viewer (MeV 4.3., (235)). Functional annotation enrichment of genes was processed with Gene Set Enrichment Analysis (GSEA) (236), which tests for enrichment of whole sets of genes (e.g. pathways) instead of single genes. GSEA was performed using the following parameters: 1000 gene set permutations, weighted enrichment statistic, and signal-to-noise metric. Alternatively the database for annotation, visualization, and integrated discovery (DAVID) (237)) was used.

After functional annotation clustering enrichment scores > 1.0 were considered as significant. Heatmaps were carried out with Mayday 2.8. (238).

2.11 Correlation of LXRα binding and gene expression

To analyze the correlation between LXRα binding and gene expression in each cellular model differentially expressed genes (vs. vehicle treated macrophages) were compared with binding site-associated genes. This analysis was kindly performed by Cornelius Fischer (MPI for Molecular Genetics). For visualization, the normalized LXRα peak enrichment and differential gene expression sorted in 4 up- and 4 down- quintiles according to the expression fold-change were plotted in GraphPad Prism 5.0 (GraphPad Software Inc.). Further, percentage of knockdown sensitive LXRα target genes with a nearby binding site was assessed. To additionally expand the view to potential LXRα target genes, not presented in the microarray data, promoter specific changes of H3K4me3, H4K20me1 and chromatin accessibility were determined at genes with a nearby binding site to predict potential gene expression regulation (239). To validate this approach differential gene expression data was sorted according to m-fold expression of treated vs. untreated macrophages (DMSO). For visualization with SeqMiner (216, 217) FAIRE-seq, H3K4me3 and H4K20me1 reads +/- 5kb from center of the TSS of the differentially expressed gene were extracted. Furher, a relative histone and FAIRE-seq signal of the cell models vs. untreated macrophage was generated and the mean signal +/- 1.5 kb of the target gene TSS was built. Finally, the mean signal and differentially expressed genes were plotted in quintiles for each cell model (240). Statistical analysis was performed by using a two-tailed Students-T-test. Significance refers to quintile 1 versus quintile 4 p-value < 0.05. For prediction, the mean signal fold-change of expression quintile 4 was chosen.

2.12 Functional description and network analyses

For further characterization of LXRα binding site-associated genes found to be differentially expressed and LXR knockdown sensitive in tested macrophage and foam cell models, following analyses were performed:

2.12.1 Gene ontology analysis

To classify functions for the genes targeted by LXRα, gene ontology (GO) enrichment analysis was performed using DAVID (237). Therefore, model specific and knockdown validated LXRα target genes with a binding site were analyzed. For this analysis functional annotation clustering for GO term Bioprocess_FAT with highest classification stringency was applied. Only enrichment scores >1.0 were considered as significant. Further, only terms with FDR <15% and maximal top 3 bioprocess were selected.

2.12.2 Pathway analysis

Pathway analysis was also performed with DAVID (237) analyzing the Kyoto Encyclopedia of Genes and Genomes (KEGG) and BIOCARTA pathways with the functional annotation chart option. Information on regulation of lipid metabolism by peroxisome proliferators activated receptor alpha (PPARα) were extracted from Reactome pathway database (www.reactome.org, (241)). Pathway analysis for T0901317 specific LXRα target genes in foam cells was performed with Ingenuity Pathways Analysis, a web-delivered application that helps to discover, visualize and explore therapeutically relevant networks (IPA, www.Ingenuity.com, (242)). Core analysis was performed using the Ingenuity Knowledge Base as reference set under consideration of only direct and indirect relationships with high or experimentally observed confidence.

2.12.3 Association of LXRα binding sites with GWAS

Correlation of LXRα binding data with (GWAS) was processed by overlapping the NHGRI GWAS catalogue (243) SNPs positions with the defined LXRα binding sites. A threshold of p-value $<10^{-5}$ was set. Additionally, the LXRα binding sites of interest were within the LD block (*DistiLD* Database, (244)) of the SNP. Further, only LXRα peak associated genes that were also reported in the GWAS were considered.

2.12.4 Functional network analysis

Interaction networks were derived from the FANTOM4-EdgeExpress Database (245) and STRING (246). Networks were visualized using Cytoscape (247).

2.12.5 Database search for known LXRα target genes

To differentiate between already known LXRα target genes, interactors and discovered new genes in this study, BIOGRID, NEXTBIO, Nuclear Receptor Resource ((248, 249), http://nrresource.org) databases were searched as well as most recent publications on LXRα (125, 126).

2.13 Figures, equipment and reagents

2.13.1 Figures

All figures presented in this thesis were designed and compiled with PowerPoint (Microsoft) and Science Slides (VisiScience Inc.). Figures presented in the Introduction section are based on information derived from literature cited in the according text passages.

2.13.2 Reagents

Reagent	**Manufacturer/Provider**
T0901317 (C17H12NSO3F9)	Sigma-Aldrich (Taufkirchen, Germany)
22-R-Hydroxycholesterol	Sigma-Aldrich (Taufkirchen, Germany)
Dimethylsulfoxide (DMSO)	Merck (Darmstadt, Germany)
Phorbol 12-myristate 13-acetate (PMA)	Sigma-Aldrich (Taufkirchen, Germany)
Oxidized low density lipoprotein (oxLDL)	Autogen Bioclear UK Ltd (Calne, Wiltshire, United Kingdom).
Oil Red O	Alfa Aesar (Karlsruhe, Germany)
Amplex Red Cholesterol Assay Kit	Invitrogen (Karlsruhe, Germany)
Ficoll Paque	GE healthcare (München, Germany)
MACS Monocyte Isolation Kit II	Miltenyi Biotec (Bergisch Gladbach, Germany)
MACS LS columns	Miltenyi Biotec (Bergisch Gladbach, Germany)
Penicillin/Streptamycin	GIBCO (Invitrogen, Karlsruhe, Germany)

CellTiter-Glo	Promega (Mannheim, Germany)
NE-PER Nuclear and Cytoplasmic Extraction Kit	Pierce (Fisher Scientific, Schwerte, Germany)
TrypLE Express	GIBCO (Invitrogen, Karlsruhe, Germany)
Phosphate buffered saline solution (PBS), pH 7.4	GIBCO (Invitrogen, Karlsruhe, Germany)
Trypan Blue Stain	Invitrogen (Karlsruhe, Germany)
TransIT TKO	Mirus (Madison, Wisconsin, USA, distributed by MoBiTec, Göttingen, Germany)
LXRα Silencer Select Validated siRNA ID5458	Ambion (Applied Biosystems, Darmstadt, Germany)
LXRβ Silencer Select Validated siRNA ID s14684	Ambion (Applied Biosystems, Darmstadt, Germany)
Silencer Select Negative Control #1 siRNA	Ambion (Applied Biosystems, Darmstadt, Germany)
Ethanol	Merck (Darmstadt, Germany)
Isopropanol	Merck (Darmstadt, Germany)
RNase-free water	Ambion (Applied Biosystems, Darmstadt, Germany)
RNeasy Plus Mini Kit	QIAGEN (Hilden, Germany)
DNase set	QIAGEN (Hilden, Germany)
High Capacity cDNA Reverse Transcription Kit	Applied Biosystems (Darmstadt, Germany)
Illumina TotalPrep RNA Amplification Kit	Ambion (Applied Biosystems, Darmstadt, Germany)
SYBR GREEN PCR Master Mix	Applied Biosystems (Darmstadt, Germany)
Real-time PCR Primer	Sigma-Aldrich (Taufkirchen, Germany)

Picogreen Quant-iT	Invitrogen (Karlsruhe, Germany)
Sodium dodecyl sulfate (SDS)	Sigma-Aldrich (Taufkirchen, Germany)
Tween-20	Sigma-Aldrich (Taufkirchen, Germany)
1x Phosphatase Inhibitor Cocktail	Sigma-Aldrich (Taufkirchen, Germany)
1x Protease Inhibitor Cocktail	Roche (Mannheim, Germany)
Tris(hydroxymethyl)aminomethane (Tris)	Sigma-Aldrich (Taufkirchen, Germany)
Ethylenediaminetetraacetic acid (EDTA)	Sigma-Aldrich (Taufkirchen, Germany)
Coomassie Brillant Blue R250	Bio-Rad Laboratories (München, Germany)
Precision Plus Protein all blue standards	Bio-Rad Laboratories (München, Germany)
Milk powder	Sigma-Aldrich (Taufkirchen, Germany)
Bovine serum albumin (BSA)	Sigma-Aldrich (Taufkirchen, Germany)
Pierce 660 nm Protein Assay Reagent	Thermo Scientific (Waltham, Massachusetts, USA)
Ponceau S solution	Applichem (Gatersleben, Germany)
anti-LXRα antibody ab 41902	Abcam (Cambridge, UK)
goat anti-mouse IgG-HRP andtibody sc-2005	Santa Cruz Biotechnology (Heidelberg, Germany)
anti-LXRβ antibody ab56237	Abcam (Cambridge, UK)
anti-RXRα antibodies sc-774 X	Santa Cruz Biotechnology (Heidelberg, Germany)
goat anti-rabbit IgG-HRP andtibody sc2004	Santa Cruz Biotechnology (Heidelberg, Germany)
anti-APOE antibody ab1906	Abcam (Cambridge, UK)
anti-ABCA1 antibody ab18180	Abcam (Cambridge, UK)
anti-β-Actin sc-47778, C4	Santa Cruz Biotechnology (Heidelberg, Germany)
anti-H3K4me3 pAB-003-050	Diagenode (Denville, NJ)

anti-H4K20me1 ab9051	Abcam (Cambridge, UK)
anti-IgG kch-819-015	Diagenode (Denville, NJ)
Restore Plus Western Blot Stripping Buffer	Pierce (Fisher Scientific, Schwerte, Germany)
Western Lightning ECL solution	Perkin Elmer (Rodgau, Germany)
Transcription Factor ChIP kit kch-redTBP-012	Diagenode (Denville, NJ)
Proteinase K	Invitrogen (Karlsruhe, Germany)
pGL4.31 Vector	Promega (BioSciences, San Luis Obispo, USA)
pBIND Vector	Promega (BioSciences, San Luis Obispo, USA)
Cholesterol Assay Kit	Invitrogen (Karlsruhe, Germany)
Triglyceride Assay Kit	Invitrogen (Karlsruhe, Germany)
Formaldehyde	Sigma-Aldrich (Taufkirchen, Germany)
Glycine	Sigma-Aldrich (Taufkirchen, Germany)
QIAquick PCR purification kit	QIAGEN (Hilden, Germany)
Phenol/Chloroform	Sigma-Aldrich (Taufkirchen, Germany)
ChIP-Seq Sample Prep Kit	Illumina (Eindhoven, The Netherlands)
In-Fusion HD EcoDry cloning system	Clontech Takara Bio Europe
Lipofectamine	Invitrogen (Karlsruhe, Germany)
E. coli Stellar™ Competent Cells	Clontech (Saint-Germain-en-Laye, France)
QIAprep® Spin Miniprep Kit	QIAGEN (Hilden, Germany)
Dual Luciferase Reporter System	Promega (Mannheim, Germany)

2.13.3 Cells and media

Cell models	**Provider**
THP1 cell line	ATCC (LGC Promochem, Wesel, Germany)
HEK 293T cell line	ATCC (LGC Promochem, Wesel, Germany)
RPMI 1640	Sigma-Aldrich (Taufkirchen, Germany)
Dulbecco's modified Eagle's medium (DMEM)	ATCC (LGC Promochem, Wesel, Germany)
Fetal bovine serum (FBS)	Biochrom (Berlin, Germany)
Human AB serum	First Link UK LTD (Birmingham, United Kingdom)
Optimem	Invitrogen (Karlsruhe, Germany)

2.13.4 Equipments and consumables

Product	**Manufacturer**
384 Well Flat Bottom Polystyrene High Bind Microplate, clear (3700)	Corning Life Sciences (Fisher Scientific, Schwerte, Germany)
384 Well low volume black Polystyrene nontreated microplate (3677)	Corning Life Sciences (Fisher Scientific, Schwerte, Germany)
384 Well Polystyrene cell culture microplate, black (781091)	Greiner Bio-One (Frickenhausen, Germany)
384 Well Polystyrene cell culture microplate, white (781098)	Greiner Bio-One (Frickenhausen, Germany)
384 Well Small Volume HiBase Polystyrene Microplates, black (784076)	Greiner Bio-One (Frickenhausen, Germany)
384 Well Small Volume HiBase Polystyrene	Greiner Bio-One (Frickenhausen, Germany)

Microplates, clear (784101)	
Thermowell 96-well PCR plate	Corning Life Sciences (Fisher Scientific, Schwerte, Germany)
Nunclon cell culture plate 24 well	Nunc (Wiesbaden, Germany)
75 cm² flask	TPP (Biochrom, Berlin, Germany)
150 cm² flask	TPP (Biochrom, Berlin, Germany)
POLARstar Omega	BMG LABTECH (Offenburg, Germany)
TissueLyser	QIAGEN (Hilden, Germany)
ABI Prism 7900HT System	Applied Biosystems (Darmstadt, Germany)
Nanodrop ND-1000	Fisher Scientific (Schwerte, Germany)
Bioanalyzer RNA 6000 Pico Kit	Agilent Technolgies (Böblingen, Germany)
Bioanalyzer 2100	Agilent Technolgies (Böblingen, Germany)
HumanHT-12 v3 Expression BeadChips	Illumina (Eindhoven, The Netherlands)
HumanHT-12 v4 Expression BeadChips	Illumina (Eindhoven, The Netherlands)
BeadStation 500	Illumina (Eindhoven, The Netherlands)
Microvette lithium-heparin coated capillary tubes (CB300)	Sarstedt (Nürnbrecht, Germany)
NuPage Bis-Tris Electrophoresis System	(Invitrogen (Karlsruhe, Germany))
NuPAGE 4-12% Bis-Tris Gel	Invitrogen (Karlsruhe, Germany)
Hybond ECL nitrocellulose membrane	GE Healthcare (München, Germany)
LAS-1000 camera system	Fujifilm (Düsseldorf, Germany)
Illumina Genome Analyzer IIx	Illumina (Eindhoven, The Netherlands)

2.13.5 Software/Internet tools

Software	**Provider**
Microsoft Office	Microsoft Corporation (Redmond, WA, USA)
ScienceSlides	VisiScience Inc. (Chapel Hill, NC, USA)
GraphPad Prism 5	GraphPad Software (La Jolla, CA, USA)
Image Reader LAS-1000 Pro V2.61	Fujifilm (Düsseldorf, Germany)
ImageQuant TL	GE Healthcare (München, Germany)
SDS 2.2	Applied Biosystems (Darmstadt, Germany)
BeadStudio 3.1	Illumina (Eindhoven, The Netherlands)
Solexa Analysis Pipeline	Illumina (Eindhoven, The Netherlands)
DAVID	http://david.abcc.ncifcrf.gov
Mayday 2.8	http://www.zbit.uni-tuebingen.de/pas/software.htm
MeV 4.3	http://www.tm4.org/mev
Gene Set Enrichment Analysis (GSEA)	www.broadinstitute.org/gsea
Connectivity Map, build 02	www.broadinstitute.org/cmap
Primer-BLAST	www.ncbi.nlm.nih.gov/tools/primer-blast
Reactome pathway database	www.reactome.org
Ingenuity pathway analysis (IPA)	www.ingenuity.com/
UCSC genome browser	http://genome.ucsc.edu
Galaxy/Cistrome Analysis Pipelines	http://cistrome.org/ap
HOMER suite	http://biowhat.ucsd.edu/homer/

MEME Suite	http://meme.nbcr.net/meme/
STAMP tool	www.benoslab.pitt.edu/stamp/
FANTOM4Edge express database	http://fantom.gsc.riken.jp/4/edgeexpress
STRING databse	http://string-db.org/
BIOGRID database	http://thebiogrid.org/
NEXTBIO databse	www.nextbio.com/b/corp/content.nb
Nuclear receptor resource database	http://nrresource.org/

3. Results

3.1 Atherosclerosis model and ligand treatment

The THP1 cell line used in this study, is a well-validated human macrophage and foam-cell model (250). THP1-derived macrophages and thereof differentiated foam cells were treated with the highly potent synthetic LXR agonist T0901317 (**Figure 8**).

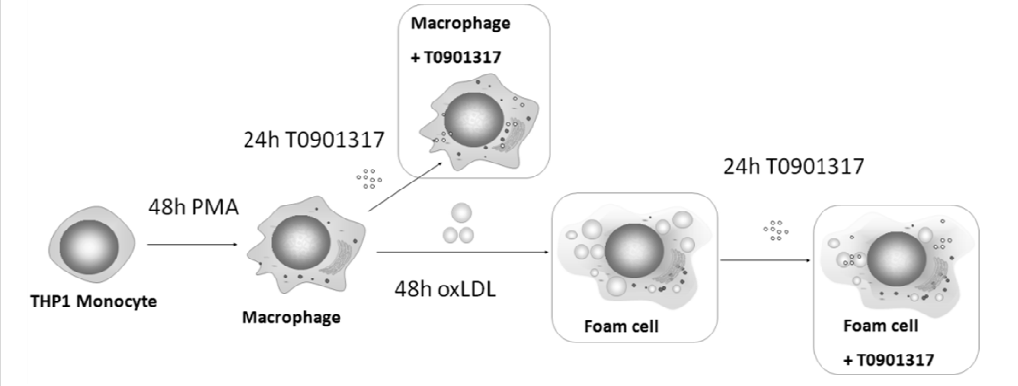

Figure 8: THP1 derived cell models used in this study. THP1 monocytes were stimulated with phorbol 12-myristate 13-acetate (PMA) for 48h to generate macrophages. Macrophages were either treated with the synthetic LXR ligand T0901317 for 24h or with oxidized LDL (oxLDL) for 48h. Foam cells were treated for 24h with T0901317.

3.1.1 Foam cells accumulate lipids

To validate the success of foam cell generation Oil red O staining and a detailed cholesterol composition analyses were applied. Foam cells were visualized as cells with accumulated red lipid droplets after Oil red O staining. After T0901317 treatment, there was a reduction of lipid content observed (**Figure 9A**). The cholesterol composition analysis confirmed the Oil red O observations and revealed an increase of total and free cholesterol in foam cells compared to macrophages. After application of the highly potent synthetic LXR agonist T0901317, total and free cholesterol were significantly reduced (**Figure 9B**). The content of esterified cholesterol, the storage form of cholesterol in cells, stayed surprisingly unchanged between macrophages and foam cells. However, there was

a trend to reduced content of esterified cholesterol after T0901317 treatment (**Figure 9B,** white bar).

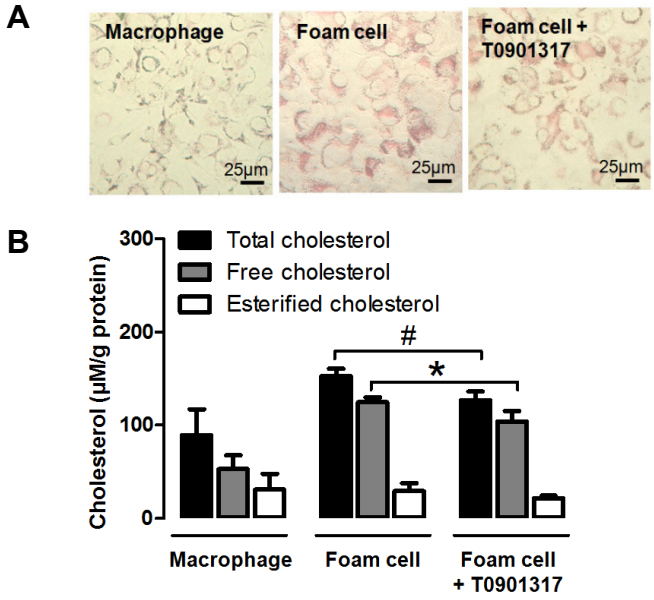

Figure 9: Foam cell formation and T0901317 treatment. (**A**) Cell culture pictures of Oil red O stained macrophages, foam cells and T0901317 treated foam cells (from left to right). (**B**) Cholesterol composition analysis of cell extracts. Data are expressed as mean with ± SD (n=6). Measured cholesterol content was normalized to total protein amount in cell extracts. Significance was calculated with Student's T-test only between foam cells and T0901317 treated foam cells. * = p-value < 0.05, #= p-value < 0.01.

3.1.2 Ligand-dependent autoregulatory upregulation of LXRα

Prior to whole genome binding analyses the amounts of LXRα, LXRβ protein and its heterodimerization partner RXR were examined in our cell models. Therefore western blot method on nuclear extracts, derived from macrophages and foam cells stimulated with T0901317, was applied. Activation of LXRα with its synthetic ligand T0901317 lead to increased protein amounts as well as stimulation with the natural ligand oxysterol (oxLDL), the essential trigger of foam cell formation. Co-administration of T0901317 and oxLDL as observed in T0901317 treated foam cell lead to an additive effect with strong increase of LXRα protein (**Figure 10A**). Whereas LXRα was highly inducible there were overall only low protein amounts of the LXRβ subtype detectable and RXR showed no significant change. Densitometry data revealed that the LXRα subtype

is 38-times more abundant in T0901317 treated foam cells than LXRβ (**Table S1**). This tremendous increase in LXRα protein content in presence of ligands is in accordance with previously published data (145) and can be explained by the feed-forward loop of LXRα (**Figure 10B**). Its autoregulatory function drives upon ligand-based activation its own expression, thereby constantly increasing the protein amount of LXRα. This specific autoregulatory feature of LXRα has not been observed in mouse macrophages (145). In absence of a specific ligand, there was only sparse LXRα protein in human macrophages detectable.

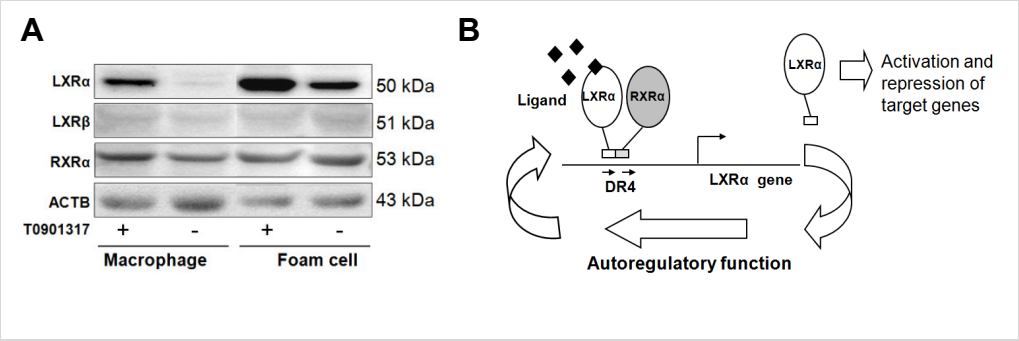

Figure 10: Protein content of LXR and retinoid X receptor (RXR) in analyzed cell models. (**A**) Western blot analysis of LXRα, LXRβ and RXR in macrophages and foam cell in presence and absence of T0901317. (**B**) Sketch of the autoregulatory loop function of LXRα activation. Upon ligand dependent activation, LXRα-RXRα dimer binds to a direct repeat of 4 (DR4) response element in front of *LXRα* gene locus and activates *LXRα* gene expression via a feed-forward loop mechanism.

3.2 Genome-wide binding study

3.2.1 LXRα ChIP-seq

To determine genome-wide LXRα specific binding in THP1 derived macrophages and foam cells, treated and untreated with T0901317, chromatin immunoprecipitation (ChIP) using a well-validated and previously applied antibody (208, 251) followed by massively parallel deep sequencing was applied. This method enables quantification of the DNA-interacting LXRα association with every position in the genome. Therefore, LXRα was crosslinked with interacting DNA sections, chromatin was fragmented and protein-DNA complexes were immunoprecipitated with anti-LXRα antibody. Purified, short DNA fragments represented the position of LXRα binding and were subjected to sequencing followed by alignment to the human genome (252). Density profiles,

generated from aligned sequencing reads, were examined for tag enrichment (LXRα peak or binding site) automatically by MACS (212) and by visual observation. Macrophages and T0901317 treated macrophages were immunoprecipitated and sequenced in biological duplicates. Both biological replicates showed a high degree of correlation (**Figure 11A and 11B**). For improved peak enrichment the sequence tags of biological replicates were

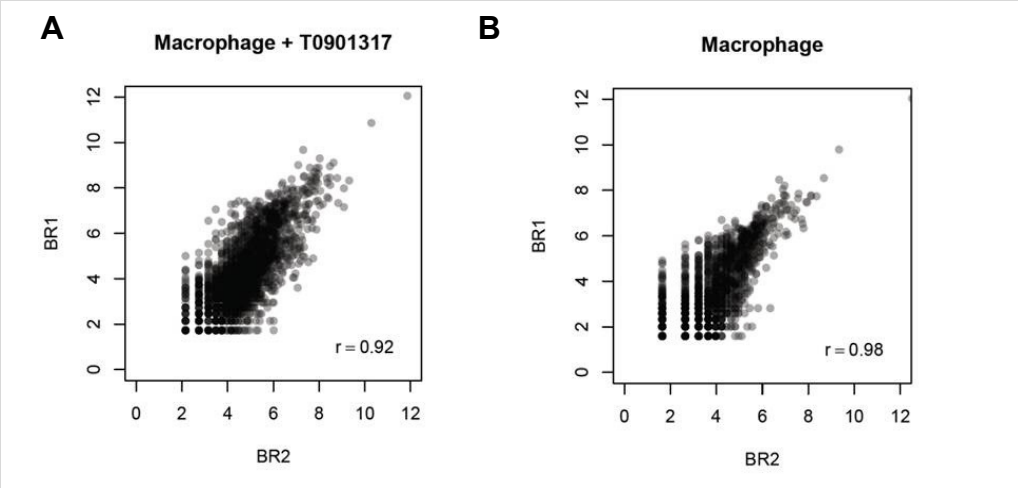

Figure 11: Biological replicates (BR) of ChIP-seq. (**A**) Macrophages treated with T0901317. (**B**) Ligand-free macrophages. Tag counts under the peak intervals were plotted for each biological replicate and correlated with Pearson correlation. Visualized is the log10 scale of tag counts.

combined and peak calling, filtering and all further analyses were performed on pooled sets (this procedure can be found in more detail in the Material and Methods section). Initial peak calling with MACS resulted in thousands of LXRα peaks for each of the cell models (**Table S2**). Unfortunately, it was not possible to find a MACS build-in method for further filtering due to imbalance between ChIP and control sample (215). Further, in cases of very low LXRα enrichments (e.g. ligand-free macrophage) MACS algorithm tended to call false positive peaks. To overcome this problem and to determine a very stringent set of true LXRα binding sites in the cell models, further filtering steps were applied.

3.2.2 LXRα binding is ligand dependent

As observed in western blot analysis, the very low protein amount of LXRα in ligand-free macrophages led to low enrichments at potential binding sites.

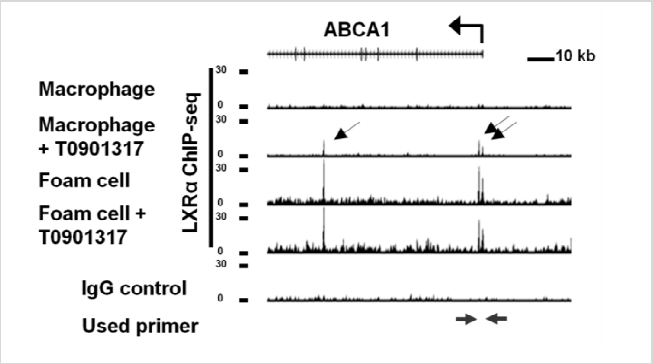

Figure 12: LXRα binding to ABCA1 gene locus. Tag alignment tracks of LXRα ChIP-seq and IgG control at ABCA1 locus selection. Arrows indicate transcription start sites and orientation of transcription. Black arrows over tracks show sites of LXRα enriched binding. Black arrows under tracks show primer position for ChIP-qPCR validation (see Figure 13).

The observation of median raw tag numbers between different treatments revealed significant enrichments of LXRα over IgG control only in ligand treated macrophages and foam cells (**Figure S1**). This observation was corroborated by the low genome-wide sequencing coverage in both biological replicates of ligand-free macrophages (**Figure S2**). Thus, after filtering not any ligand-free macrophage specific binding site could be

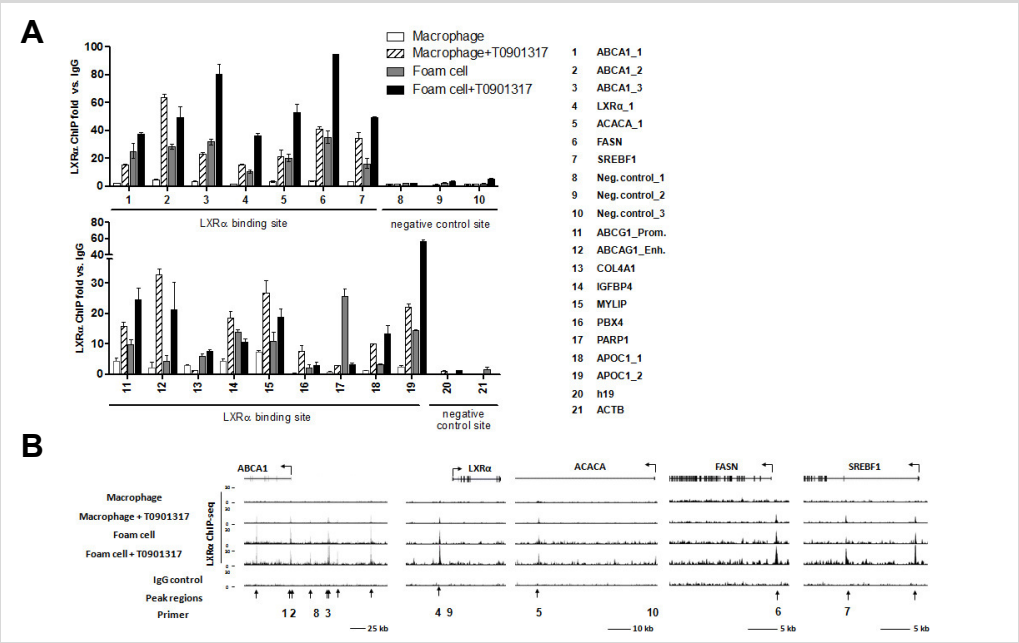

Figure 13: Validation of ChIP-seq with ChIP-qPCR. (A) ChIP-qPCR fold enrichment of LXRα ChIP over input DNA relative to IgG negative control. Selected primer names and positions are depicted on the right. (B) Tag alignment tracks of LXRα and IgG control for selected loci. Arrows under tag alignment track represent LXRα binding sites. Numbers under the arrows represent PCR products related to primers in the ChIP-qPCR.

determined, suggesting that LXRα binding was strictly ligand-induced in the investigated cell models. This observation was contrary to the classic model of constitutive LXR binding and ligand-dependent exchange of co-repressor to co-activator assembly (130, 253). For T0901317 treated macrophages, foam cells and T0901317 treated foam cells 1198,742 and 628 binding sites, respectively were discovered (total: 2652 peaks, **Table S3**). Each binding site was annotated to the next located genes. For example, the ABCA1 gene locus, one of the major LXRα target genes in reverse cholesterol transport, is illustrated in **Figure 12**. In contrast to ligand-free macrophages, T0901317 treatment enriched LXRα significantly at the transcription start site and in intron 5. Similar observations were made for foam cells and T0901317 treated foam cells. The illustrated binding sites represent only a selection of multiple binding sites at this locus. In total, eight binding sites were found in ligand-treated macrophages and foam cells located up to +136kb and -59kb of the transcription start site (**Figure S3**). In order to confirm the robustness of the derived ChIP-seq data the LXRα ChIP experiments were repeated and the enriched material was assessed by qPCR for a selection of 21 LXRα binding sites and negative control sites (**Figure 13**). Visual comparison with ChIP-seq data revealed high concordance. Thus, ChIP-seq-derived peaks were successfully confirmed and again the extremely low enrichment of LXRα in ligand-free macrophages was observed.

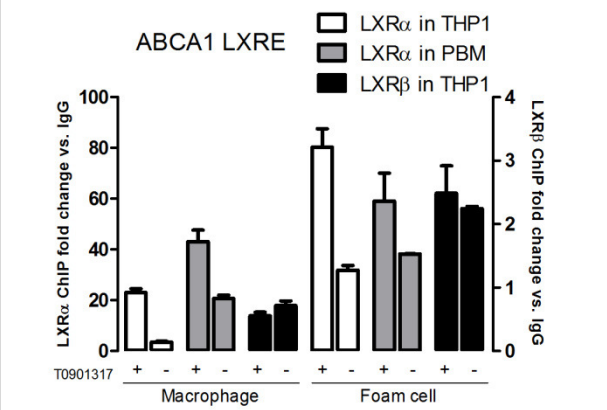

Figure 14: ChIP-qPCR validation of ABCA1 LXRE. LXRα ChIP-qPCR in THP1 derived and human PBM derived cells and LXRβ ChIP-qPCR in THP1 cells. Data are expressed as mean with ± S.D. from biological triplicates relative to IgG.

For example, the LXRα binding site at the transcription start site of ABCA1 gene locus was tested with ChIP-qPCR for LXRα and LXRβ enrichment in THP1-derived macrophages and foam cells in presence and absence of T0901317 (**Figure 14**). As expected, LXRα binding was highly ligand-dependent, whereas LXRβ showed a constitutive and ligand-independent binding profile. Consistently,

an up to 80-fold enrichment of LXRα was observed compared to the only 2.5-fold enrichment of the β-subtype over the IgG control. Further, the THP1 cell models were validated with human peripheral blood monocyte (PBM) derived cell models in absence and presence of T0901317. PBM maturation and T0901317 treatment were controlled by gene expression analyses (**Figure S4**). The LXRα binding profiles of THP1- and PBM-derived macrophages and foam cells were very similar (**Figure 14**).

Interestingly, PBM-derived, ligand-free macrophages showed high binding background. This indicates that the observed lipids in the used donor blood were experimentally interfering. Besides, THP1 cells showed similar binding profiles as PBM-derived cells and provided easy accessible, sufficient and standardized material for all performed analyses. Thus, THP1 cells were the experimental resource of choice.

3.2.3 Shared and differential binding of LXRα to genomic loci in macrophages and foam cells

Cell model and treatment specific effects of LXRα genome binding were assessed by comparative ChIP-seq analysis (218). After sorting the peaks according to their degree of variability, three different peak sets could be categorized. They were visualized as a heat map of tag densities around LXRα binding sites (**Figure 15A**). For completeness, the ligand-free macrophage densities were also included and showed only marginal tag accumulations (grey heat map, **Figure 15A**). The first differential genomic peak set comprised 29% or 769 peaks and showed an increased LXRα binding upon T0901317 treatment. This occupation was observed in T0901317 treated macrophages as well as in T0901317 treated foam cells. This so-called T0901317 specific peak set showed a very poor enrichment of LXRα in foam cells or ligand-free macrophages as illustrated in the left panel of **figure 15A** with a mean tag density of less than 10. The largest peak set discovered (45%, 1193 peaks) was shared among all cell models. The exception was the overall low enrichment of ligand-free macrophages. The third peak set consisted of 690 peaks (26%) and was distinguished by an overall low enrichment of LXRα. However, there was clearly a foam cell-specific enrichment over T0901317-treated cells. This less pronounced enrichment profile could be due to indirect binding of LXRα to the genome, which is more difficult to catch with the

applied crosslink method. Further, chromatin accessibility is associated with active transcriptional regulators and has been recently described as predetermining for TF binding (127, 254).

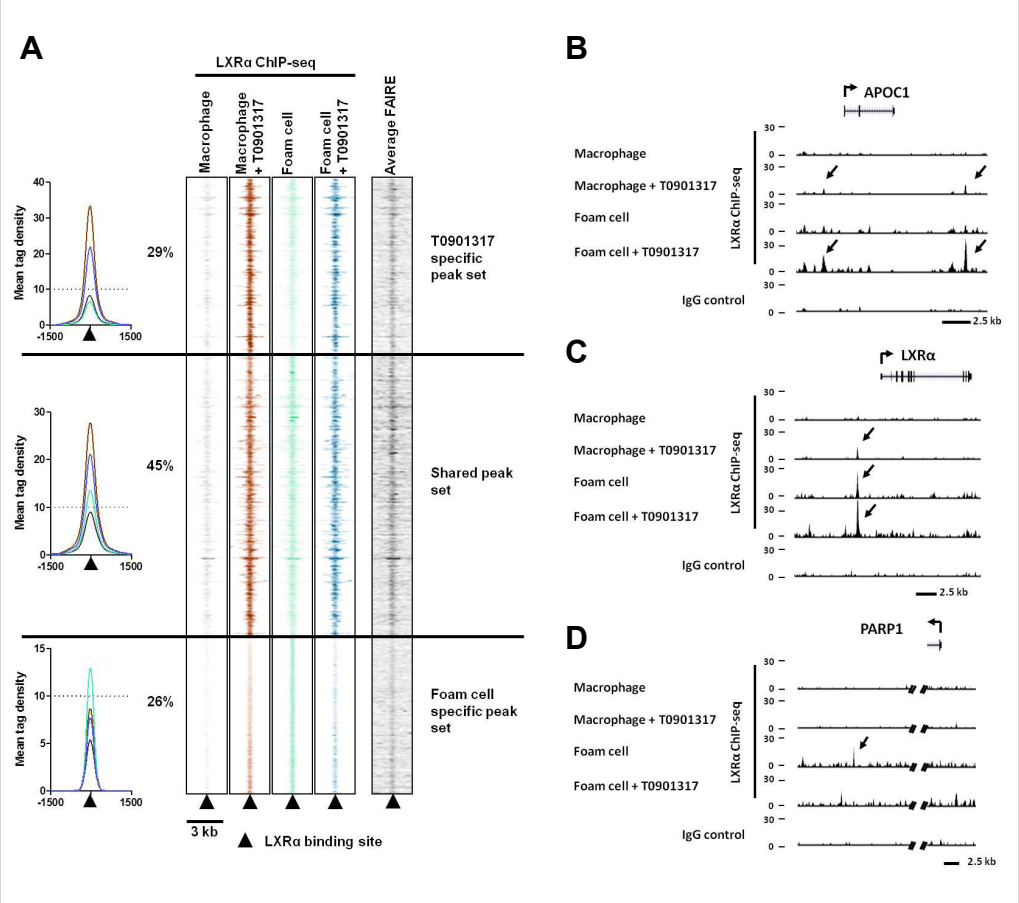

Figure 15: Differential LXRα binding sites in human macrophage and foam cell models. (**A**) Comparative LXRα ChIP-seq enrichment heatmap and mean tag density ±1.5kb from peak center (LXRα binding site). Variability was calculated as log2 fold change between models. The T0901317 specific set comprised 29% of all binding sites. A proportion of 45% binding sites shows similar LXRα enrichments in all cell models and is therefore termed as shared peak set. Foam cell specific peak set is composed of 26% of all binding sites. The left panel shows mean tag densities for each peak set. The right panel shows a plot of the average chromatin openness of the three peak sets derived from FAIRE-seq analyses. Macrophages are depicted in grey, T0901317 treated macrophages in brown, foam cells in green, T0901317 treated foam cells in blue and average FAIRE in black, respectively. (**B**) T0901317 specific peak set tag alignment track example; the *APOC1* locus. (**C**) Shared peak set tag alignment track example; the *LXRα* locus. (**D**) Foam cell specific peak set tag alignment track example; the *PARP1* locus. Arrows indicate transcription start sites and orientation of transcription. Black arrows over tracks show peaks.

Chromatin accessibility can be analyzed by formaldehyde assisted isolation of regulatory elements (FAIRE) followed by massively parallel deep sequencing. Applying this method similar degree of openness could be determined, independent from cell model or treatment (**Figure S5**). Interestingly, within the defined peak sets, chromatin accessibility was changed (Average FAIRE, **Figure 15A**). Whereas genomic loci of the shared peak set were highly accessible, moderate openness in T0901317 specific and only low openness in foam cell specific peak set respectively were observed. Transcriptional regulation is a complex process that mostly involves interplay of several TFs (126, 223). For a first examination, transcription factor binding site (TFBS) data was extracted from Encode. This dataset revealed a pronounced enrichment of co-localized TFBS in shared and T0901317 specific peak sets compared to oxLDL induced foam cell specific binding sites (**Figure 16**). These observations support the assumption that T0901317 and shared peak set harbor gene loci that are occupied by LXRα and co-activator assembly at highly accessible transcriptional hotspots, whereas foam cell specific genomic loci are occupied less tightly by LXRα and few other co-localized TFs in a less open chromatin environment. As characteristic example loci, well-known as well as unexpected and new LXRα target genes were chosen for each LXRα binding set. An example for T0901317 specific binding is the *APOE/C1/C4/C2*-gene cluster (**Figure 15B**). The well-known LXRα target gene, *APOE* is an important promoter of cholesterol efflux and also other members of the cluster can function as cholesterol acceptors. In this study two binding sites were observed, one at promoter region and another 11kb downstream. These two binding regions are located within the multi-enhancer regions ME.1 and ME.2 and

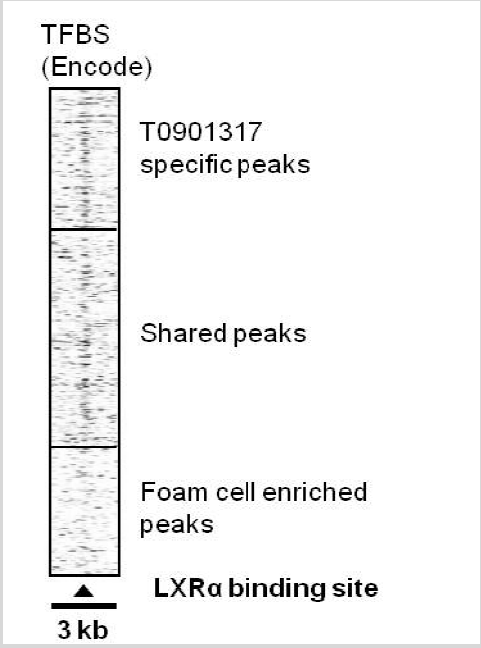

Figure 16: Transcription factor binding site (TFBS) enrichment heatmap extracted from Encode data ± 1.5 kb from LXRα peak center. Regions were sorted according to LXRα peak degree of variability.

direct the expression of APOE and presumably all members of this cluster (255, 256). Another example of T0901317 specific binding is the *PBX4* gene (**Figure S6**). The homeobox protein PBX4, encodes a homeodomain protein that resembles to a TF involved in translocations in pre-B-cell leukemias. In 2008 six new loci, including PBX4 locus were associated with LDL cholesterol (257). In this study, two LXRα binding sites were observed in the first intron. The first binding site was enriched upon T0901317 treatment and slightly in ligand-free macrophages. Notably, the second binding site 2.5kb upstream, was occupied only in foam cells. T0901317 treated foam cells showed a mixed profile with both binding sites occupied. An example for LXRα binding shared among all models is the previously described *ABCA1* gene locus or *LXRα* itself. At the *LXRα* locus, a cell-model independent binding profile was detected with a single binding site 2.8 kb upstream of the transcription start site (**Figure 15C**). An example for foam cell specific binding is the LXRα binding site located 40kb proximal from *PARP1* gene locus (**Figure 15D**). This gene encodes the poly (ADP-ribose) transferase, a chromatin associated enzyme that modulates numerous nuclear proteins and is involved in regulation of differentiation and proliferation, DNA repair and apoptosis. As expected from foam cell specific set an LXRα binding only in foam cells was discovered.

3.2.4 T0901317 sharpens LXRα peak enrichment at promoter sites

The classic model of LXR binding describes its positioning to LXR response elements (LXRE) that contain a consensus sequence of two direct repeats with the core sequence 5'- AGGTCA -3' separated by 4 nucleotides (DR4, (133, 258, 259)). For further characterization of the three sets of LXRα binding sites *de novo* motif search was performed. Surprisingly, significant enrichments of a DR4 motif were found only in T0901317 specific- and shared peak set (**Figure 17A**). The discovered motifs highly resembled the Transfac LXR:RXR motif m00647. For the foam cell specific peak set no *de novo* motif could be significantly enriched. Targeted scanning of the *de novo* derived motif from shared peak set in all peaks resulted in 15% (398 peaks) of binding sites that occupied this motif (**Figure 17B**). In accordance with the *de novo* motif analysis, only 2% thereof were from the foam cell specific set. The low percentage of binding sites that harbor a DR4 motif may be due to the stringent p-value cutoff of 10^{-4}. A more relaxed p-value

cutoff of 10^{-3} revealed 63% of binding sites with a DR4 motif. However, recent studies showed similar low DR4 occupancies and discussed the potential function of the DR4 motif for LXR binding (125, 126). These studies claim that LXR binds

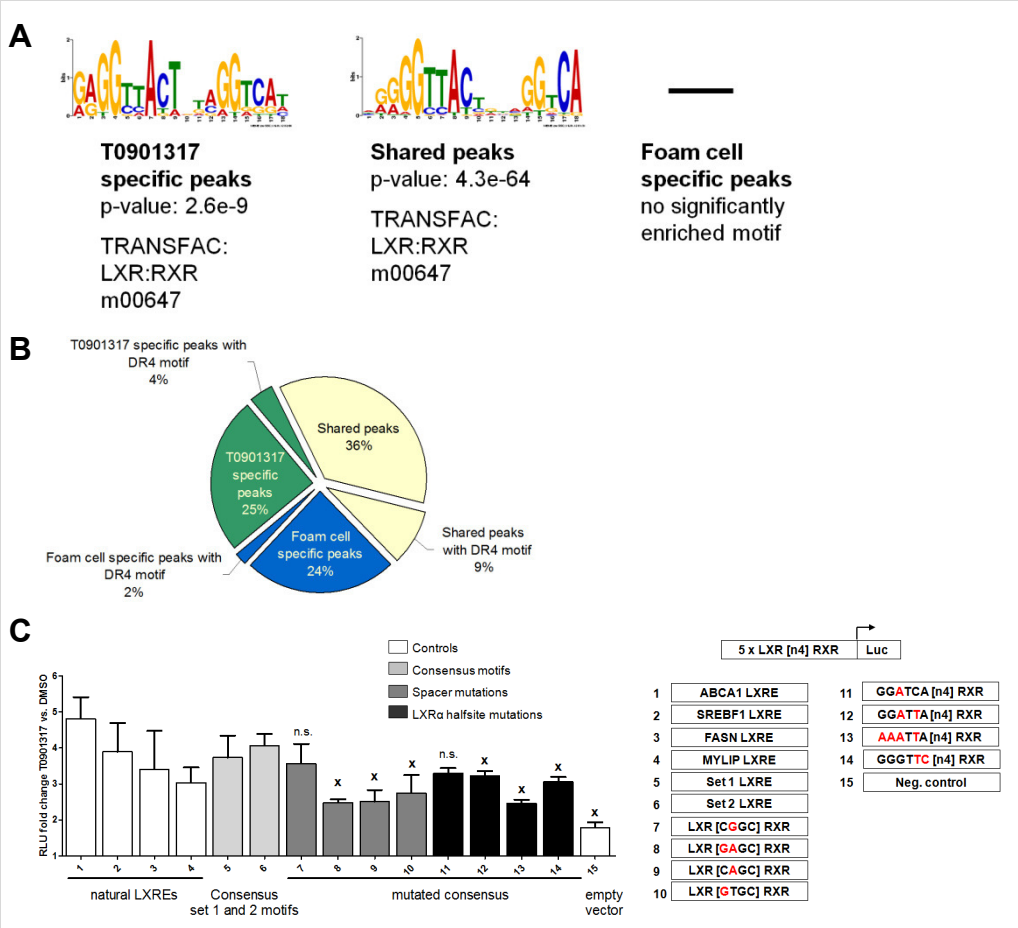

Figure 17: Motif analysis of LXRα peak sets. (**A**) Web logos of direct repeat separated by 4 nucleotides (DR4) sequence motifs identified by *de novo* motif search with top 100 ChIP-seq sequences for each peak set. Motifs with p-value < 10^{-7} were scanned for known motifs with Transfac database. (**B**) Distribution of shared peak set DR4 motif occurrences in all three LXRα peak sets. (**C**) Reporter-gene analysis of natural and synthetic LXREs were analyzed. The relative light unit (RLU) fold-change T0901317 vs. DMSO (n=3, mean± STDEV) is visualized. Significance was calculated by multiple comparison of consensus sharp peak set motif (6) and mutated consensus motifs. x indicates statistically significant, p < 0.05, n.s. indicates statistically not significant.

to fairly degenerated DR elements. To address this question and to biochemically characterize the derived *de novo* motifs transient reporter-gene analyses were performed (**Figure 17C**). In agreement with statements discussed above, single-base changes did not affect LXR binding and subsequent reporter gene activity (**Figure 17C**, sequence 1-4 and 11). Only major mutations with modifications in

the LXRα half-site of the LXR:RXR element led to significantly decreased reporter gene activity (**Figure 17C**, sequence 12-14). Further, analysis of spacer region conservation at position 8 and 9 revealed, that mutations in this region had a strong impact on reporter gene expression. Already minor mutations of one nucleotide (**Figure 17C**, sequence 9, 10) changed significantly the reporter gene expression. So far, only one report on spacer region conservation described the *de novo* derived motif (125), which confirms above described observations.

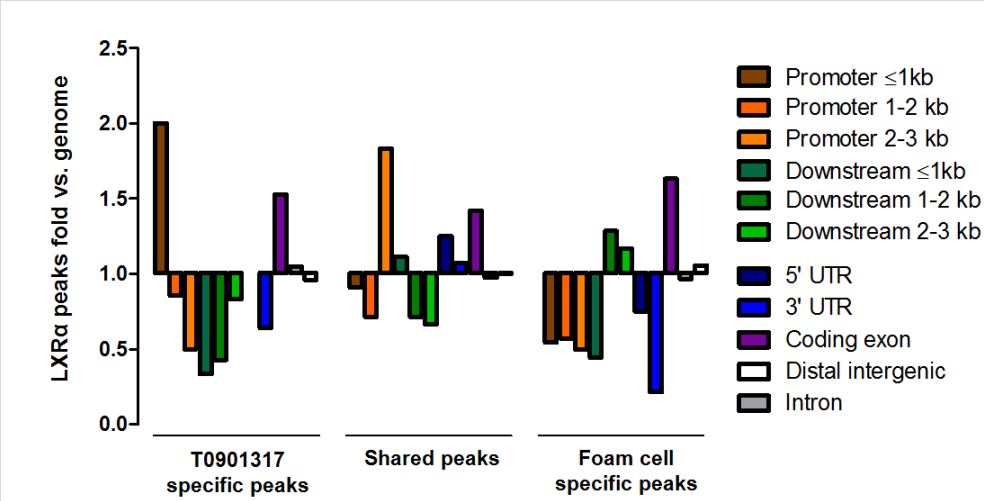

Figure 18: Genomic positions of LXRα peaks. Fold-change of LXRα peak distribution compared to genome composition is visualized for each differential peak set. From left to right: promoter ≤ 1kb, promoter 1-2 kb, promoter 2-3 kb, downstream ≤ 1kb, downstream 1-2 kb, downstream 2-3 kb, 5' UTR (untranslated region), 3' UTR, coding exon, distal intergenic and intron.

Another interesting characteristic feature of binding sites is its position within the genome. This analysis was performed for each individual peak set and revealed increased enrichments around promoters in T0901317-specific LXRα binding sites (**Figure 18**). All peaks enriched LXRα at coding exons. The shared peak set enriched LXRα binding sites in 2-3kb distance from promoters and surprisingly foam cell specific peaks were located more downstream of genes.

Taken together these observations indicate a more pronounced shaping of transcriptional initiation by the synthetic ligand T0901317. Foam cell specific binding seems to be more indirect on distant sites with few other TFs and in less accessible chromatin environment.

3.3 Functional characterization of LXRα binding

3.3.1 Gene expression profiles are mostly similar among cell models

For biological interpretation of LXRα binding data it is imperative to integrate other data types into the analysis (194). Thus, whole genome gene expression and LXR knockdown analyses were performed in all investigated cellular models.

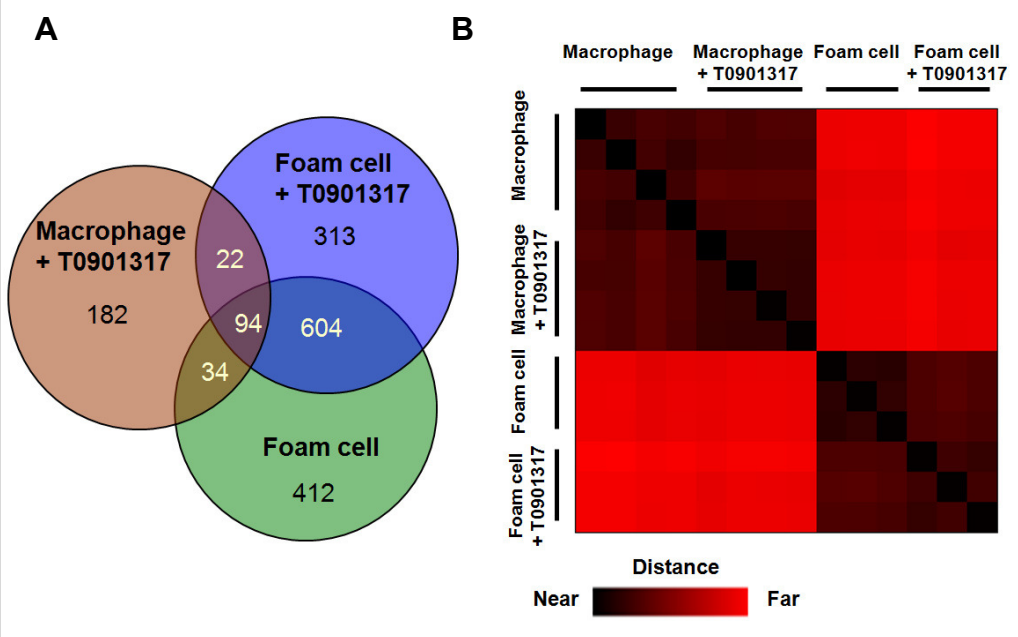

Figure 19: Whole-genome gene expression analysis. (**A**) Visualized is the number of differentially expressed genes with a p-value < 0.05 in each model compared to ligand-free macrophages and their overlap. Total number of genes is the sum of all overlaps and model specific genes. (**B**) Shown is a distance matrix of all expressed genes for each cell model. Squares show the similarity in Euclidean space, ranging from the same properties (black) to completely different (red).

In macrophages upon T0901317 treatment 332 differentially expressed genes were detected compared to ligand-free macrophages. In foam cells and T0901317 treated foam cells 1144 and 1033 differentially expressed genes were detected, respectively (**Figure 19A**). Robustness of microarray data was controlled with qPCR (**Figure S7**). The biggest target gene overlap was between T0901317 treated and untreated foam cells (68%). Similar observations were made with gene distance matrix (GDM) analysis of the complete gene expression data set of all cellular models investigated (**Figure 19B**). Independent from T0901317 treatment similar properties were observed between both macrophage models and

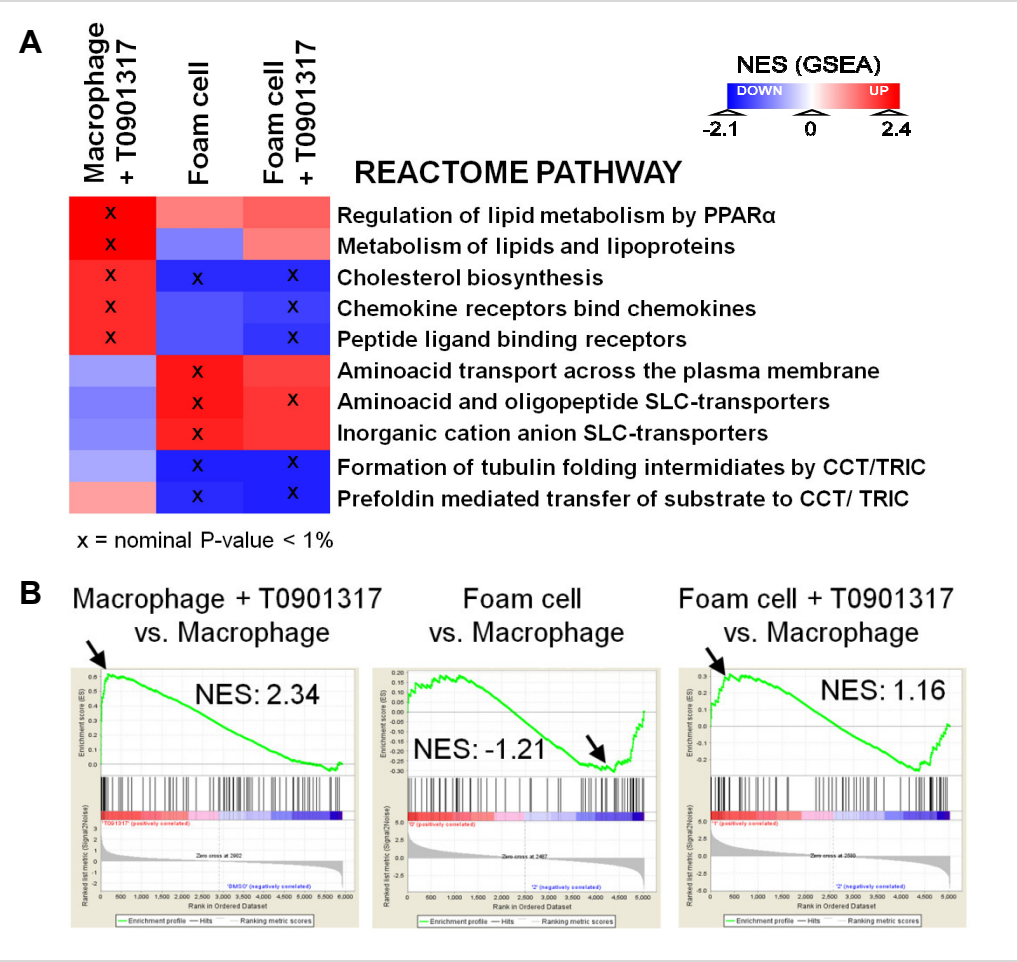

Figure 20: Enriched Reactome pathways in treated cell models compared to ligand-free macrophages extracted from GSEA. (A) The normalized enrichment scores (NES) of each pathway either upregulated (red) or down-regulated (blue) is visualized. The nominal p-value was at least under one condition < 1%. (B) Shown are enrichment scores, ranked list metrics (signal2noise) and NES of genes in gene set metabolism of lipids and lipoproteins for each cell model. The arrow indicates enrichment of positive or negative correlation.

both foam cell models, respectively. In contrast to LXRα binding data, where a strong T0901317 dependent binding profile was observed, whole genome gene expression seemed to be much more dominated by the transformation from macrophage to foam cell. In order to analyze the relevant pathways shared and differential among macrophages and foam cells Gene Set Enrichment Analysis (GSEA) was applied. This method circumvents the limitation of low sensitivity in single gene analysis and is very useful to relate the treatment and model effects to a broader physiological context. T0901317 treated macrophages, foam cells and T0901317treated foam cells expression data was compared to ligand-free

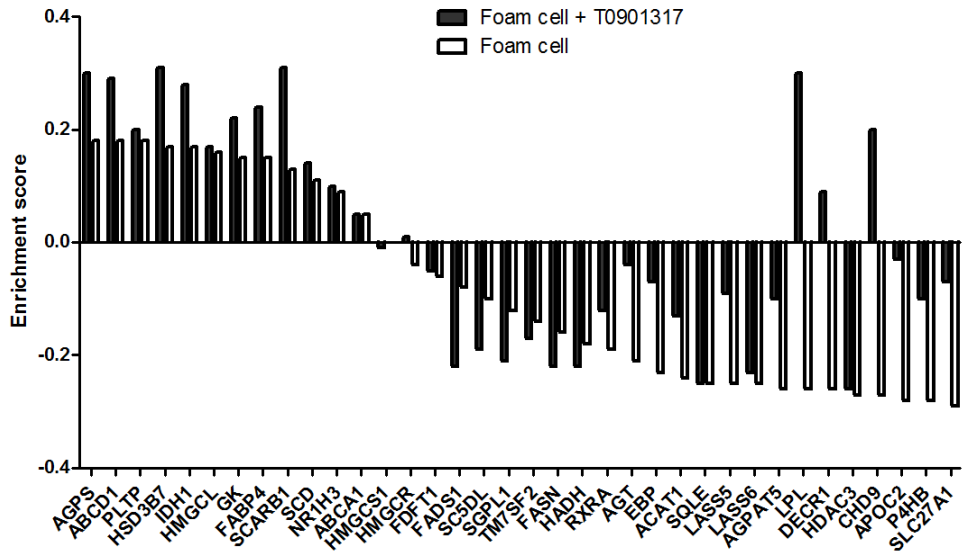

Figure 21: Effects on gene expression related to lipid and lipoprotein metabolism**.** Visualized are normalized enrichment scores for each gene in the analyzed gene set (calculated with compound-specific expression profiles by GSEA). Black bars are T0901317 treated foam cells, white bars are foam cells.

macrophages expression data for the gene sets in reactome pathway database. Gene sets from pathways with significant changes are presented in **Figure 20A**. As expected, all models showed the up- regulation of lipid metabolism pathway by the well-known nuclear receptor PPARα. Interestingly, this pathway and the formation of tubulin folding intermediates represented the only sets regulated similarly by all cell models. Whereas cholesterol biosynthesis and chemokine receptor processes were highly upregulated in T0901317 treated macrophages, both foam cell models showed significant downregulation. The opposite was true for amino acid transport relevant pathways. Notably, there was also the metabolism of lipids and lipoproteins pathway observed to be differentially regulated between foam cells and T0901317 treated foam cells. Whereas in foam cells this process was clearly downregulated, there was a T0901317 dependent upregulation of this gene set (**Figure 20B**).

Further examination of genes comprised in this set revealed interesting differences in target gene regulation between foam cells and T0901317 treated foam cells. For example, the *LPL* gene, which encodes a triglyceride hydrolase and prevents from

many disorders linked to lipoprotein metabolism (260–262), was downregulated in foam cells and upregulated upon T0901317 treatment (**Figure 21**). Another interesting example is the chromodomain helicase DNA binding protein 9

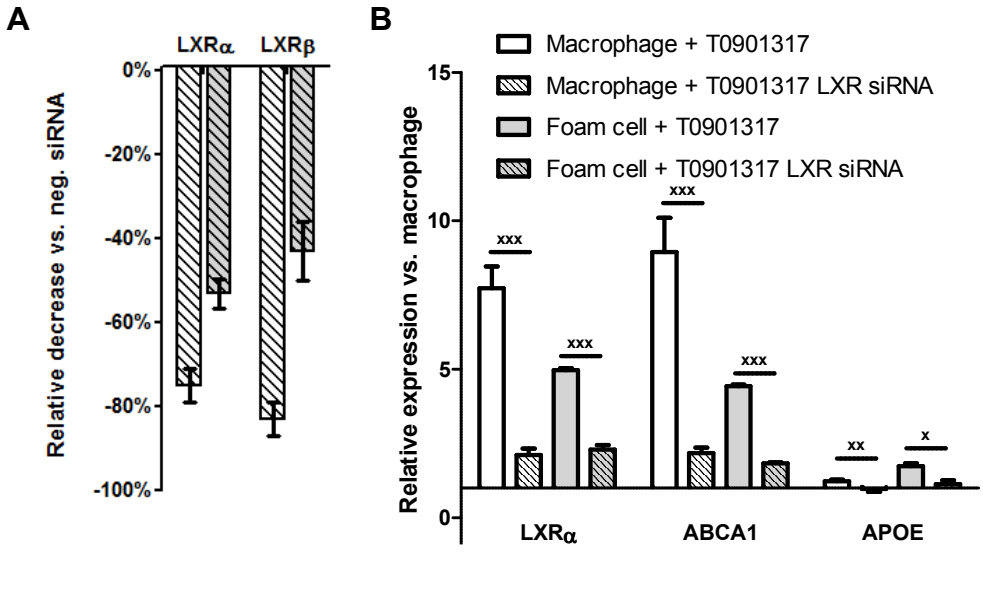

Figure 22: LXR knockdown. (**A**) Knockdown efficiency of LXRα and LXRβ-subtype in macrophages and foam cells. The relative decrease in percent compared to negative siRNA (n=4, mean±SD). (**B**) Ligand dependent gene expression in macrophages and foam cells after siRNA-mediated LXR knockdown for central target genes *LXRα, ABCA1,* and *APOE*. Data is presented as relative expression vs. macrophage. (n=4, mean +SD. x P<0.05, xx P<0.01, xxx P<0.001 vs. neg. siRNA.

(*CHD9*). This, so far undiscovered LXRα target gene encodes a PPARα interacting complex protein, which acts as transcriptional co-activator and may also interact with LXRα. Similar as *LPL*, *CDHC9* gene expression is upregulated upon T0901317 treatment in foam cells. To confirm LXR dependent regulation of differentially expressed target genes LXR knockdown analyses were performed. SiRNA-mediated knockdown achieved an efficiency of 75% for LXRα and 83% for LXRβ in macrophages. Foam cell knockdown was less efficient with 53% and 43% for LXRα and LXRβ, respectively (**Figure 22A**). However, target genes of LXR, that showed a significant increase in protein expression upon T0901317 treatment (**Figure S8**), were extensively downregulated in siRNA-mediated LXR knockdown macrophages and foam cells (**Figure 22B and Figure S9**). Genome-wide expression analysis of LXR knockdown cell models revealed a big proportion of genes that were significantly dependent on LXR for their activation.

Further, many genes, especially in foam cells, were repressed by LXR (**Figure S10**). An example is the malic enzyme (*ME1*), which generates NADPH for fatty acid biosynthesis (263). *ME1* gene was after siRNA-mediated LXR silencing around 50% more expressed compared to control cells with intact LXR expression. Totally, in T0901317 treated macrophages 85 (26% of differentially expressed genes) LXR sensitive genes were detected. In foam cells and T0901317 treated foam cells there were 253 (22% of differentially expressed genes) and 305 (30% of differentially expressed genes) LXR sensitive genes, respectively.

3.3.2 High correlation of gene expression and LXRα binding

In order to generate a robust and highly informative data set, LXRα binding data was correlated with gene expression data. The biggest proportion with 81% of LXRα peaks was located near genes (in ±200kb distance) and only 19% were in gene deserts with distances > 200kb to the next gene. The overlap of LXRα peaks with differentially expressed genes was 19%, thereof 8% with 186 highly significant LXR knockdown sensitive genes (stringent set, **Figure 23A and Figure S11).** To additionally expand the view to potential LXRα target genes not presented in the microarray data, promoter specific changes of important transcriptional initiation and elongation marks H3K4me3 and H4K20me1 (264) were determined at LXRα enriched sites. In combination with FAIRE-seq data for chromatin accessibility, correlation was observed with gene expression profiles (**Figure 23B** and **Figure 23C**, (239)). For prediction analyses, the mean signal fold-change of expression quintile 4 was used. With the addition of 492 predicted LXRα target genes the total correlation of LXRα binding sites with target genes was increased to 30% (**Figure 23A**). Upon correlation of the differential gene expression with LXRα peak enrichment a bimodal regulation pattern was observed in all cell models (**Figure 23D**). Expression levels, separated in quintiles, showed increased LXRα peak enrichment in quintiles -2 to 4 and 2 to 3. Notably, the expression quintile 4 was correlated with decreased peak enrichments in all cell models indicating a regulatory change at very high expression levels. In foam cells, the decrease of LXRα binding was already observed at expression quintile 3. Despite similar expression profiles among foam cells and T0901317 treated foam cells LXRα positioning seemed to be

differentially regulated as already observed at promoter site positioning and DR4 occupancy.

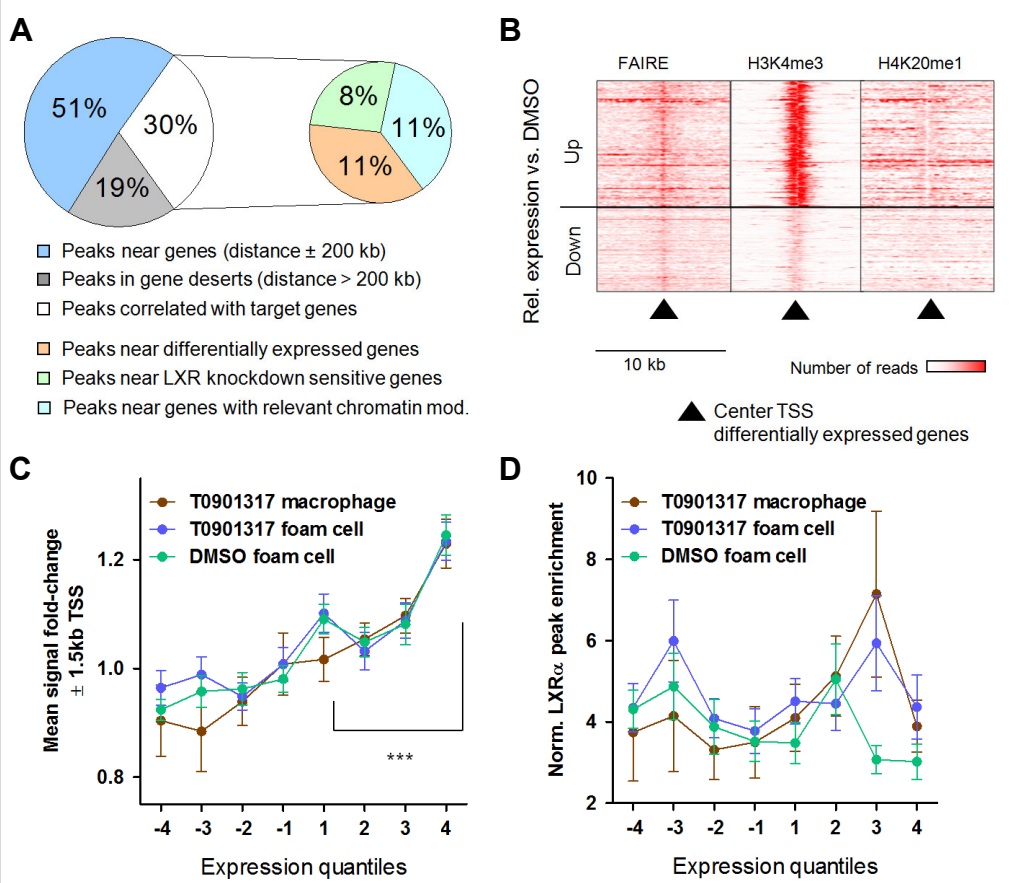

Figure 23: Functional annotation of LXRα binding peaks. (**A**) The left chart shows all peaks and the right chart shows the 30% of peaks, which were correlated with LXRα target genes. (**B**) Comparative H3K4me3, H4K20me1 ChIP-seq and FAIRE-seq enrichment heatmap for T0901317 treated macrophages ±5kb from transcription start site (TSS) center of differentially expressed genes. Relative gene expression vs. ligand free macrophages (DMSO) is separated in up- and down-regulated genes. (**C**) Visualized is the combined mean signal fold-change of FAIRE-seq, H3K4me3 and H4K20me-seq of treated cell models vs. ligand free macrophages. The mean signal ± 1.5kb of the target gene TSS is plotted against differentially expressed genes that were separated in ±4 quintiles for each cell model. *** P<0.001 for quintile 1 vs. quintile 4. (**D**) Correlation of gene expression fold-change (quintiles) with normalized LXRα peak enrichment for all cell models.

Taken together, 30% of peaks showed a correlation with target gene expression. In accordance with LXRα properties as gene-activator or repressor (265), increased LXRα binding was correlated with up- and downregulated genes in all cell models. This bimodal pattern was also observed in foam cells with less

pronounced binding properties, which could be largely induced by T0901317 treatment.

3.3.3 Main functions of LXRα in cholesterol metabolism and interaction with PPARα signaling pathway

To decipher specific pathways enriched in the cell models the stringent set of 186 LXR knockdown sensitive target genes with an associated LXRα binding site was analyzed with DAVID functional annotation clustering analysis (**Table 1**). Individual observation of investigated cell models revealed for T0901317 treated macrophages the fatty acid biosynthesis as most enriched bioprocess. Further, enrichment of BIOCARTA pathway nuclear receptors in lipid metabolism and toxicity was observed. This pathway was also enriched in T0901317 treated foam cells. In foam cells, the mainly enriched bioprocesses were organic acid biosynthesis and regulation of cholesterol storage. Interestingly, regulation of apoptosis was also observed as significantly enriched process. Fourteen genes associated with this process could be identified. This observation pointed towards cell death progression in the context of atherosclerotic plaque formation. On the contrary, T0901317 treatment of the foam cell did not significantly enrich disease-

Table 1: Functional analysis of LXRα target genes.

Cell model	Category	Term	Count	%	P-value	FE	FDR
Macrophage + T0901317	Bioprocess	Fatty acid biosynthetic process	4	8.51	1.74E-03	16.31	2.48
	Kegg Pathway	PPAR signaling pathway	4	8.51	3.95E-03	11.79	3.83
	BIOCARTA	Nuclear Receptors in Lipid Metabolism and Toxicity	3	6.38	1.97E-02	11.98	14.40
Foam cell +T0901317	Bioprocess	Negative regulation of cholesterol storage	3	2.17	9.11E-04	62.63	1.47
	Kegg Pathway	PPAR signaling pathway	5	3.62	5.51E-03	6.82	5.67
	BIOCARTA	Mechanism of Gene Regulation by PPARα	5	3.62	2.63E-03	7.78	2.32
		Nuclear Receptors in Lipid Metabolism and Toxicity	4	2.90	1.41E-02	7.26	11.89
Foam cell	Bioprocess	Organic acid biosynthetic process	8	6.20	1.31E-04	7.05	0.21
		Regulation of cholesterol storage	3	2.33	2.74E-03	37.27	4.33
		Regulation of apoptosis	14	10.85	5.20E-03	2.38	8.07
	Kegg Pathway	Glycine, serine and threonine metabolism	3	3.57	1.59E-02	14.91	14.26
	BIOCARTA	Mechanism of Gene Regulation by PPARα	4	3.10	9.98E-03	8.05	8.12

DAVID functional annotation clustering analysis of gene ontology term bioprocess, Kyoto Encyclopedia of Genes and Genomes (KEGG) and Biocarta pathways for each cellular model. All genes were LXR knockdown sensitive with an associated LXRα binding site. Columns indicate the Category (Bioprocess, Kegg pathway and BIOCARTA), the terms, its count and percentage in the target gene list, as well as the P-value, fold enrichment (FE) and false discovery rate (FDR).

associated processes and showed instead enrichment in athero-protective negative regulation of cholesterol storage.

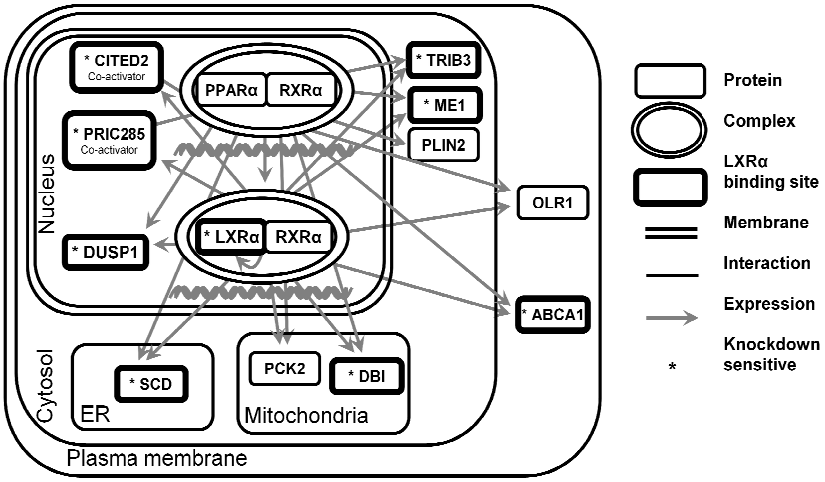

Figure 24: LXRα interactions with PPARα signaling in T0901317 treated foam cells. Shown are important genes in regulation of lipid metabolism by peroxisome proliferators activated receptor alpha (PPARα). The following features are represented: boxes are proteins, circles are protein complexes, bold circled boxes show genes with enriched LXRα binding sites, black lines show interaction, black arrows indicate expression and * indicates LXR knockdown sensitive gene expression.

Notably, all cell models accumulated the PPARα signaling pathway, indicating tight interactions of LXRα and PPARα-regulated pathways (126). Detailed analysis revealed a major proportion of target genes shared among LXRα and PPARα (**Figure 24**). Remarkably, the LXRα complex regulated also two major co-activators of PPARα, Cbp/p300 interacting transactivator with Glu/Asp-rich carboxy-terminal domain 2 (*CITED2*) and peroxisomal proliferator activated receptor A interacting complex 285 (*PRIC 285*).

Analysis of peak set specific functional annotation revealed similar results as for the stringent set of LXRα target genes (**Table S4**). The T0901317 specific peak set enriched processes such as regulation of cholesterol esterification or phospholipid transport. Interestingly, in the shared peak set defense response and in the foam cell specific set the Ras protein signal transduction were enriched.

3.3.4 LXRα binding sites are linked with disease associated SNPs

In order to understand LXRα impact on metabolic disorders and other diseases, a search for significant disease relevant SNPs in proximity to LXRα binding sites was performed. Many GWAS associated successfully a number of SNPs and genomic loci to common diseases (266). However, these studies often lack a functional explanation of causal mechanisms.

Table 2: Correlation of LXRα binding data with GWAS

Function	Disease/ Term	SNP	P-value	Genes	Distance to SNP [kb]
Metabolism	LDL cholesterol	rs10401969	2.0E-08	PBX4	311.5
		rs4420638	1.0E-60	APOC1	5.7
		rs2142672	2.0E-08	MYLIP	52.1
	Triglycerides	rs17216525	4.0E-11	PBX4	57.0
		rs4420638	3.0E-13	APOC1	5.7
		rs7679	7.0E-11	PLTP	33.3
	HDL cholesterol	rs7679	4.0E-09		33.3
	Lipoprotein-associated phospholipase A2 activity and mass	rs1805017	6.0E-14	PLA2G7	40.4
Inflammation	Mean platelet volume	rs12485738	6.0E-31	ARHGEF3	16.0
	Rheumatoid arthritis	rs2062583	2.0E-06		84.4
	C-reactive protein	rs4420638	9.0E-139	APOC1	5.7
Heart	Myocardial infarction (early onset)	rs9982601	6.0E-11	MRPS6	17.2
		rs9982601	4.0E-10		17.2
	Coronary heart disease	rs7801190	3.0E-08	SLC12A9	53.6
		rs10512597	8.0E-11	CD300LF	135.3
	D-dimer levels	rs2774920	1.0E-06	ABCA4	164.3
	Resting heart rate	rs314370	6.0E-10	SLC12A9	58.5
	Diastolic blood pressure	rs1530440	1.0E-09	ARID5B	153.4
Brain	Alzheimer's disease	rs4420638	2.0E-44	APOC1	5.7
	Information processing speed	rs6051520	2.0E-07	TRIB3	6.2
	Multiple sclerosis	rs17174870	1.0E-08	MERTK	93.7
	Amyloid A Levels	rs2896526	4.0E-22	LDHA	92.5
Skin	Melanoma	rs3219090	9.0E-08	PARP1	72.9
		rs2230926	1.0E-17	TNFAIP3	36.6
	Psoriasis	rs610604	9.0E-12		33.2

Columns indicate the general category, associated diseases or terms, and the SNP ID. The P-value indicates the degree of certainty of disease association of the SNP. Next column depicts the reported and potentially disease relevant genes in proximity to the associated SNP. The last column shows the distance between LXRα binding sites and SNPs within the LD block, presented in kilobases (kb).

In this analysis, particular importance was attached on LXRα binding sites being located within LD of the SNPs. Further, reported genes from the GWAS had to match differentially expressed and LXR knockdown sensitive genes in the cell models. By this analysis, it was found that LXRα target genes had central impact

on processes including metabolism and inflammation. Further, heart~, brain~, and skin-disease relevant genes were discovered to be under LXRα control (**Table 2**).

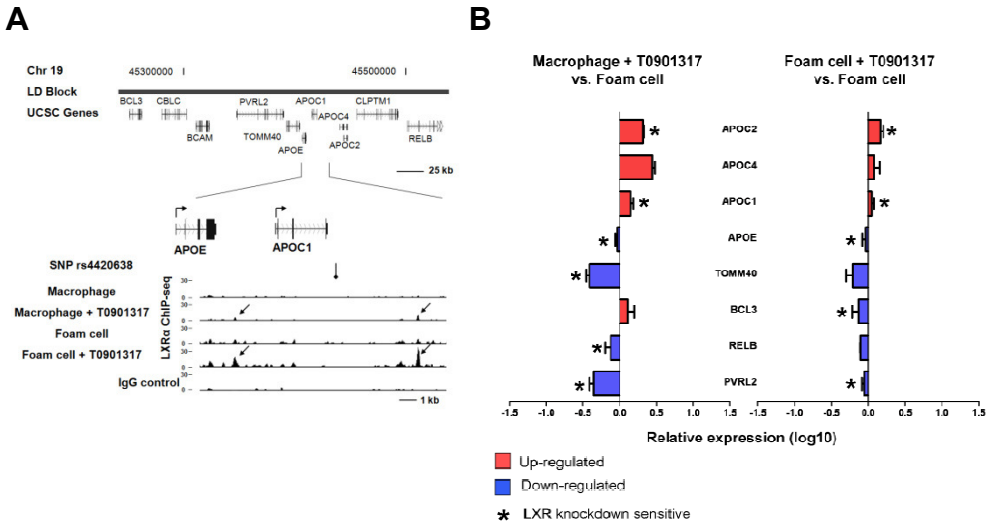

Figure 25: Functional connection between LXRα binding to APOE/C1/C4/C2 locus and disease-relevant SNPs. (**A**) UCSC genome browser picture of the rs4420638 SNP in linkage surrounded area (chr19: 45247846-45544890). SNP position is indicated with a black arrow on top of normalized tag alignment tracks of LXRα ChIP-seq. LXRα binding sites (black arrows over track) around *APOC1*. (**B**) Differential expression of APOE/C1/C4/C2 cluster and enclosed genes compared to foam cell gene expression. (Left) Differential expression of T0901317 treated macrophage vs. foam cell. (Right) Differential expression of T0901317 treated foam cell vs. foam cell (both as log10). Red are upregulated genes, blue are downregulated genes. * LXR knockdown sensitive genes.

Within the metabolism disease group, terms such as LDL/HDL cholesterol and triglycerides were found. Surprisingly, some un-described LXRα target genes (**Table S5**), such as homeobox protein *PBX4* (**Figure S6**), showed significant connection to LDL cholesterol metabolism and the LDL associated phospholipase A2 (*PLA2G7*) was linked with lipoprotein-associated lipase activity and mass. Among others, myocardial infarctions and coronary heart disease relevant genes were also discovered. Notably, there was differential regulation between macrophages and foam cells observed. Further, disorders concerning brain and skin could be associated and confirmed LXRα implications in pathologies such as Alzheimer's disease or Psoriasis (267, 268). Especially skin disorders were downregulated in the foam cell models and peaks were derived solely from foam cell specific peak set. Inflammation was described mainly by C-reactive protein

and rheumatoid arthritis, *APOC1* and *ARHGEF3*, respectively. Whereas the T0901317 macrophage slightly induced these genes, the foam cell decreased their expression.

The most significant association between disease related loci, SNP and LXRα binding site was found with SNP rs4420638 and linked in meta-analyses to C-reactive protein with a p-value of 9^{-139} and LDL cholesterol with a p-value of 1^{-60}, respectively. This SNP is located close to the transcription termination site of *APOC1* and is encircled by two LXRα binding sites that are in 5.7 kb and 6.5 kb distance (**Figure 25A**). LXRα binding at this locus is T0901317 specific (**Figure 15B** and **Figure 25A**). In the foam cell, LXRα was not as efficiently recruited to this locus compared to the recruitment upon T0901317 ligand stimulus. *APOC1* is located within a cluster of genes that are important in plasma lipid metabolism (*APOE*, *APOC*4 and *APOC2* (19)). Further, this locus is also surrounded by genes (*BCL3*, *RELB*, *PVRL2*) that are involved in biological process such as inflammation, immunity, differentiation, cell growth, tumor genesis and apoptosis (first two via NF-kappa-B signaling, (269–271)). Consistently, an improved gene expression profile was also observed for the extended *APOE/C1/C4/C2* cluster (**Figure 25B**). T0901317 treated macrophages and foam cells showed an upregulation of *APOC1*, *APOC2* (both LXR knockdown sensitive) and *APOC4* compared to foam cells. Inflammation and immunity relevant genes were mostly downregulated upon T0901317 treatment.

3.4 Network analyses

3.4.1 LXRα controls a network of responses to activating ligands

Transcriptional network analysis was performed to further investigate the global impact of the LXRα locus on *APOE/C1/C4/C2* gene cluster and thereby on lipid metabolism and immunity. For a broader metabolic context well-known LXRα target genes were included and with the STRING database a network with differential expression data of the foam cell generated (**Figure 26**). This network illustrated the tight relationship between transcriptional regulators and target genes influenced directly (LXRα binding site) or indirectly by LXRα activation.

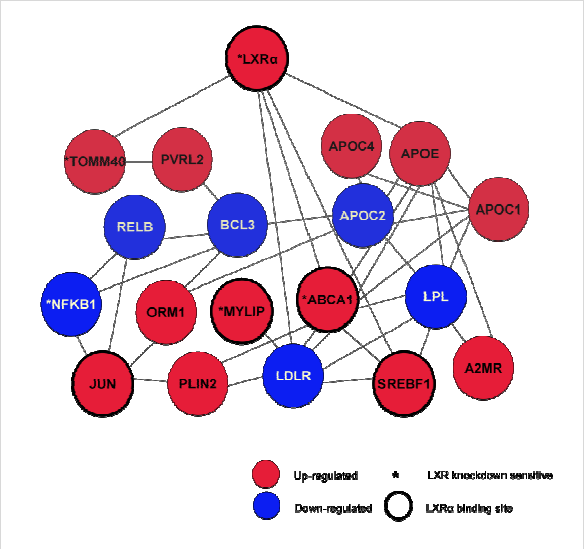

Figure 26: STRING interaction network of genes within the extended *APOE/C1/C4/C2*-gene cluster. Shown is differential expression of foam cells vs. macrophages for the *APOE/C1/C4/C2*-gene cluster genes and well-known LXRα target genes. Red circles represent upregulated and blue circles downregulated genes. Bold circles represent genes with an enriched LXRα binding site. *=LXR knockdown sensitive genes.

Some were also sensitive to LXR knockdown (*LXRα, TOMM40, ABCA1, MYLIP* and *NFkB1*). The induced up- or downregulation of networked genes is of central relevance for metabolic processes such as lipid metabolism, inflammation and apoptosis and supports LXRα influence in these processes (147, 272, 273). Further, the extensive linkage between all genes in the network illustrated the cross-relationship between different metabolic and immunological processes. Thus, it is likely that LXRα induces networks of interacting genes, rather than linear pathways that affect pathologies such as atherosclerosis. Consequently, LXRα-dependent activation of the *APOE/C1/C4/C2* gene cluster supported lowering cholesterol levels (274) by triggering a distinct network of associated genes.

3.4.2 LXRα modulation in foam cells activates carbohydrate metabolism, molecular transport and lipid metabolism

In order to understand the atheroprotective-potential of LXRα ligands the underlying gene networks in foam cells and T0901317 treated foam cells were analyzed. Initially, the focus was on direct effects of LXRα binding in the context of foam cell development. Therefore, a network, composed of all differentially expressed and LXR knockdown sensitive target genes in the foam cell was generated. The interaction data for this network was derived from the FANTOM and STRING database (**Figure 27A**). Foam cell formation induced upregulation of 160 and repression of 93 genes, respectively. Among, several TFs such as

CCAAT-enhancer-binding proteins CEBPB and CEBPG or NFκB1 were detected. This global view on transcriptional interaction underlined once more the broad impact of LXRα activation and its effects, which were either initiated

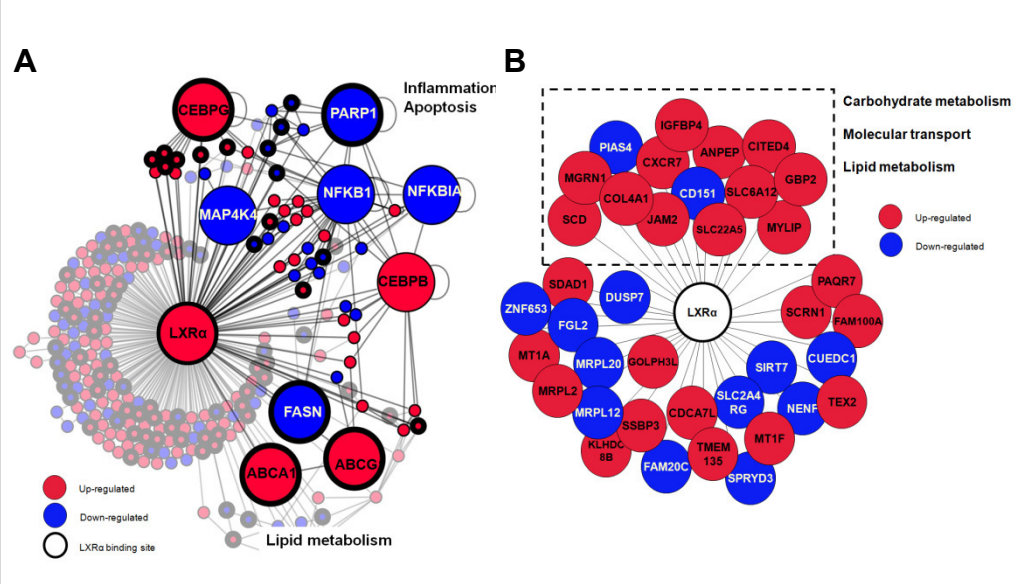

Figure 27: Effects of LXRα modulation with synthetic ligand T0901317 in foam cells. (A) LXRα target gene network in foam cells. Differential expression of LXR knockdown sensitive genes in foam cells vs. macrophages. Target genes in lipid metabolism, inflammation and apoptosis are emphasized. Network data are from FANTOM and STRING network. Bold circles represent genes with an enriched LXRα binding site close by. (B) T0901317 specific LXRα target genes in foam cells associated with LXRα binding. Differential expression of LXR knockdown sensitive genes in T0901317 foam cells vs. foam cells. Connecting lines represent LXR knockdown validated interaction with LXRα. The top associated network functions assigned by IPA show carbohydrate metabolism, molecular transport and lipid metabolism. Red circles display upregulated genes; blue circles display downregulated genes.

directly, through networked genes, or via other TFs on various metabolic processes. In accordance with previous observations molecular functions, such as lipid metabolism, inflammation and cell death (147, 272, 273) were annotated with ingenuity pathway analysis (IPA). Especially the apoptotic function of these cells, which was already shown in **Table 1**, is of central importance in atherogenesis. Apoptosis and necrosis of macrophages leads to necrotic core development and subsequently progresses malign thrombus formation (40). The atheroprotective potential was investigated in foam cells upon T0901317 treatment. Therefore, differentially expressed genes were selected in T0901317

treated foam cells and compared to untreated, diseased foam cells. For increased stringency, only genes that were LXR knockdown sensitive with an LXRα binding site in this model were considered. In total 38 genes were obtained, 25 genes up- and 13 downregulated that met all criteria set in this analysis (**Figure 19B**). Thirty-two genes were not previously described as LXRα target genes and were subsumed as novel LXRα target genes (**Table S6**). For functional classification all 38 genes were subjected to IPA and displayed as top enriched

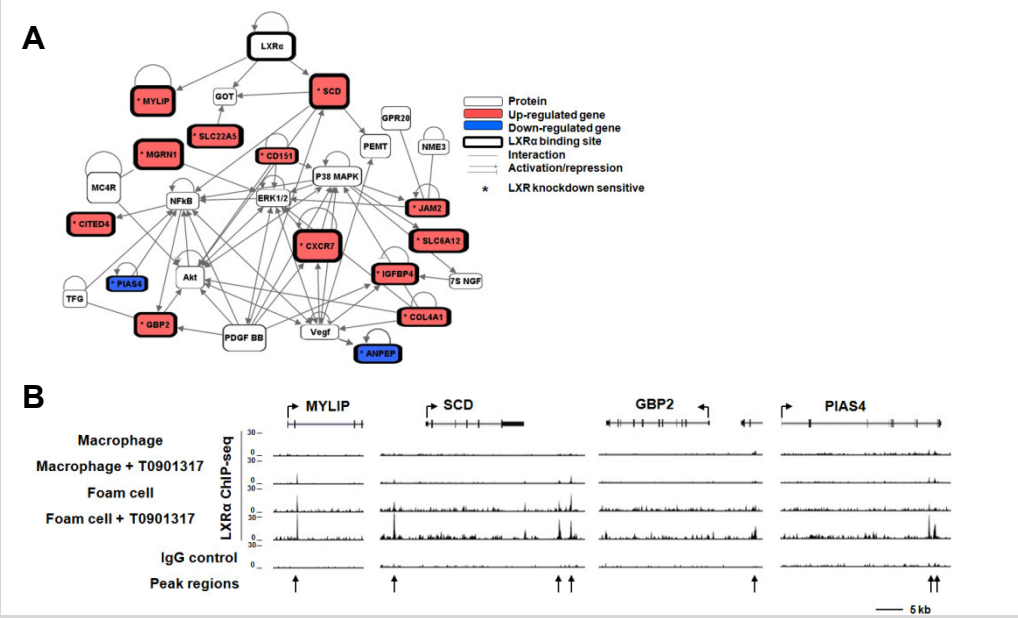

Figure 28: IPA top network for T0901317 treatment specific genes in foam cells. (**A**) Network is associated with functions in carbohydrate metabolism, molecular transport and lipid metabolism. Differential gene expression of knockdown sensitive LXRα target genes upon T0901317 treatment in foam cells vs. foam cells. Red: significantly upregulated genes; blue: significantly downregulated genes. Not significantly regulated gene expression of central proteins is visualized in white. Bold circles represent an enriched LXRα binding site near the gene. (**B**) Tag alignment tracks of LXRα ChIP-seq and IgG control of *MYLIP, SCD, GBP2* and *PIAS4* loci of all cell models. Peak regions are indicated as black arrows under tracks.

molecular functions carbohydrate metabolism, molecular transport and lipid metabolism. Notably, it was not possible to reduce the derived gene set of 38 genes to only one metabolic function. As we already observed in **Figure 26**, there is a tight cross-relationship between different metabolic and immunological processes. One gene could be associated to multiple functions. In addition, this analysis revealed 32 out of 38 genes that have not been associated to LXRα so far.

Therefore, functional classification of the derived gene set was a challenging task. However, in the most enriched network from IPA 14 genes from the gene set were functionally classified and associated with above mentioned network functions, such as carbohydrate metabolism, molecular transport and lipid metabolism (**Figure 28A)**. LXRα activated directly its own expression and mostly upregulated several other target genes in this network. Examples of upregulated and directly connected LXRα target genes are the well known *SCD* (275)), which encodes a key enzyme in fatty acid metabolism and *MYLIP* (155). The striking enrichment of LXRα binding upon T0901317 treatment supports its significant upregulation upon T0901317 treatment in the foam cell (**Figure 28B**).

3.4.3 Novel LXRα target genes with atheroprotective potential in LXR/RXR activation pathway

The LXR/RXR activation pathway was discovered as the top enriched canonical pathway with a p-value of 1.65^{-3} in IPA analysis. To gain more insight in the involvement of the novel LXRα target genes with atheroprotective potential in classical LXR/RXR activation pathway an overlap analysis was performed (**Figure 29**). As described above, two genes with known direct interaction with LXRα, namely *SCD* and *MYLIP* were found. Further, 10 genes that were implicated in LXR/RXR activation via other, networked genes were discovered. The major part of interactions was observed with NFκB complex and TNFA signaling. Underlying overlap data was derived from the Ingenuity Knowledge Base, which relies on experimentally observed and published data. However, in this study all 38 genes were detected as direct LXRα targets with 32 novel, so far not LXRα-associated genes. Thus, it can be concluded that there is a strong bond between LXRα, NFκB and TNFA signaling. Further, for several overlapping genes disease associations were found, which were also previously described for LXRα. For example, arresten (*COL4A1*, collagen chain of basement membranes, (276)) and chemokine orphan receptor 1 (*CXCR7*, member of the G-protein coupled receptor family, (277)) were associated with cardiovascular disease (IPA top disorder, p-value 1.07^{-3}). Both genes were significantly upregulated after T0901317 treatment in foam cells. The highest upregulated gene in this analysis (~6 fold) was interferon-induced guanylate-binding protein 2 (*GBP2*, **Figure 28B**). This GTPase has not been previously linked to LXRα but was associated

with diseases such as psoriasis, rheumatoid arthritis and experimentally induced diabetes (278–280). One of the highest downregulated (~2 fold) genes in this analysis was protein inhibitor of activated STAT 4 (*PIAS4*, **Figure 28B**). This transcriptional co-regulator interacts with the NFκB complex and plays a crucial role in various cellular pathways, including gene silencing (281).

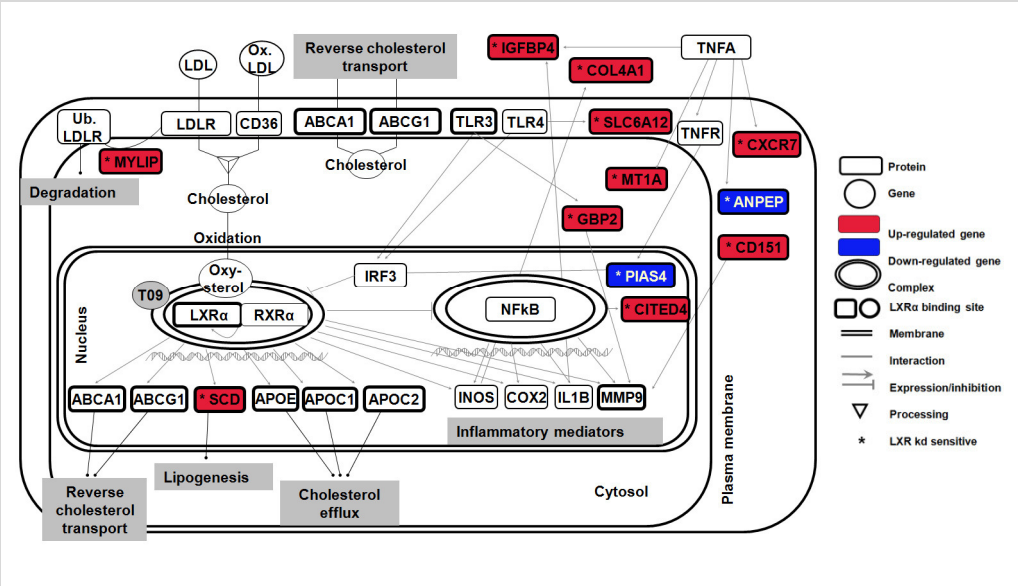

Figure 29: LXR/RXR activation pathway with direct involvement of T0901317 specific LXRα target genes from associated IPA network in foam cells. The differential gene expression of knockdown sensitive LXRα target genes upon T0901317 treatment in foam cells vs. foam cells. Red are significantly upregulated genes; blue are significantly downregulated genes. Unregulated gene expression of central proteins is displayed in white. Bold circles represent an enriched LXRα binding site near the gene.

Taken together, numerous so far unknown LXRα target genes were detected. They contribute to an athero-protective network, associated with functions such as carbohydrate metabolism, molecular transport and lipid metabolism. These new genes are of important value in transcriptional regulation of cellular atherosclerosis processes and ligand-specific activation of LXRα.

3.5 STLX4 - A new LXRα ligand

3.5.1 Chemically optimized stilbenoid activates LXRα

In order to find promising new and selective LXRα agonists, a natural compound library (207) was screened for high affinity binders. The discovered structure with the stilbenoid backbone (ST, **Figure 30A**) showed a promising LXRα binding and activation profile (**Table 3**). This structure was further optimized by chemical modification and addition of an epoxide (STLX4, **Figure 30B**). The new ligand STLX4 displayed in reporter gene assays low nanomolar effective concentration (EC_{50}: 35 nM) with an activation efficiency of 6% (vs. T0901317), which is comparable with the activation potency of the natural LXR ligand 22-R-Hydroxycholesterol (4% vs. T0901317, **Table 3**). Additionally, STLX4 showed in reporter gene assays characteristic specificity for the LXRα subtype that was not observed for the synthetic LXR ligand T0901317 (**Figure S12**). LXRα and LXRβ knockdown

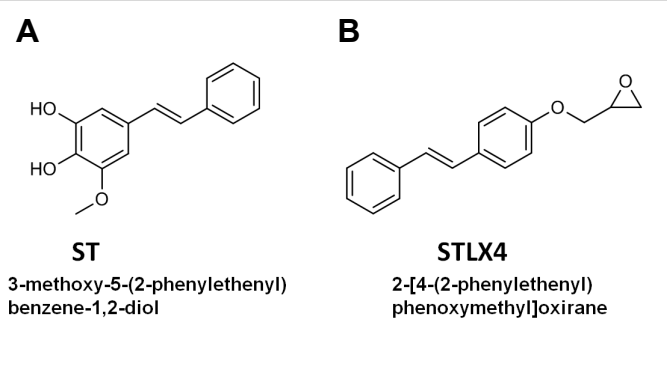

Figure 30: New LXRα ligands with stilbenoid backbone. (**A**) Structure of ST and IUPAC name. (**B**) Structure of the chemically modified stilbenoid, STLX4 and its IUPAC name.

Table 3: LXRα reporter gene assays

Compound	EC_{50}	Efficacy
T0901317	239 nM	100%
22-R-Hydroxycholesterol	13.3 µM	4%
ST	1.8 µM	6%
STLX4	35 nM	6%

Transcriptional activation of LXRα by T0901317 (T09), 22-R-Hydroxycholesterol, ST or STLX4. Visualized is the EC_{50} and the efficacy compared to T09. Data are expressed as mean±SD (n=3).

analyses confirmed the observed LXRα specificity of STLX4 (**Figure 31**). Whereas the absence of both, LXRα and LXRβ influenced T0901317 dependent target gene expression (ABCA1 and LXRα), for STLX4 a clear tendency towards higher LXRα specificity was observed.

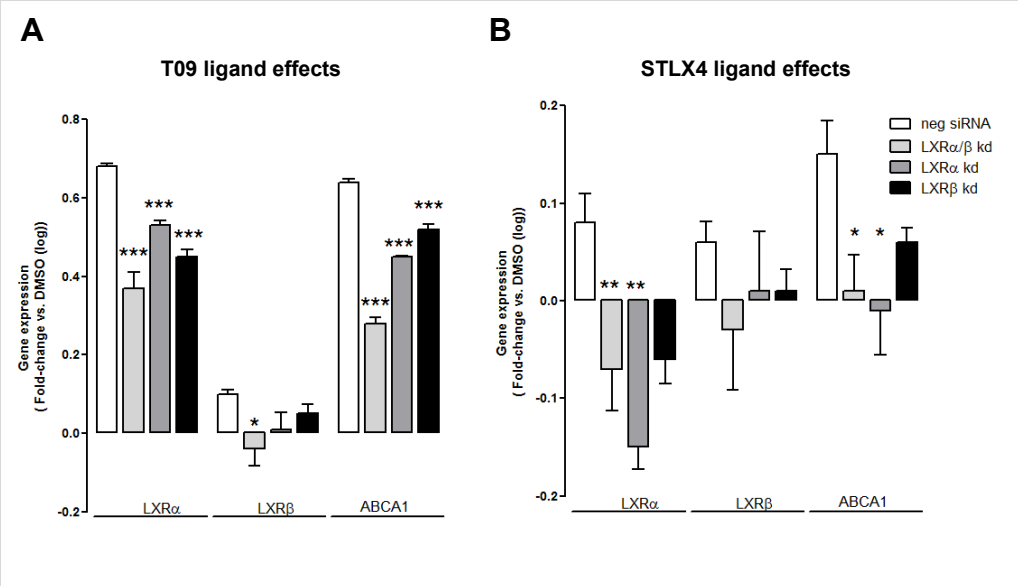

Figure 31: LXRα-subtype specifity of STLX4. Single and combined LXRα/β knockdown influence on gene expression of LXRα, LXRβ and ABCA1. (**A**) T0901317 (T09) ligand effects in foam cells. (**B**) STLX4 ligand effects in foam cells. (mean±SEM, n=4, fold-change vs. DMSO, logarithmised). * P<0.05, ** P<0.01, *** P<0.001 vs. negative siRNA.

3.5.2 STLX4 targets specifically foam cells

As STLX4 was not cytotoxic up to 50 µM (**Figure S13**) it was further investigated for its potential as LXRα ligand in THP1-derived macrophages and foam cells. Therefore, central target genes of LXRα (namely *LXRα, SREBF1, ABCA1,* and *APOE*, **Figure 32A**) were tested by qPCR upon activation with either STLX4 or T0901317. Surprisingly, in foam cells but not in macrophages, STLX4 treatment induced central target gene expression with comparable potency as the synthetic LXR ligand T0901317. Genome-wide gene expression analysis was consistent with qPCR data (**Figure S14**) and showed clearly for STLX4 a foam cell specific activation of genes involved in lipid metabolism **(Figure 32 B)**. Mechanistic analysis of STLX4 binding with a competitive reporter-gene assay (fixed concentration of T0901317 and increasing levels of STLX4) revealed an additive effect on reporter-gene activation (**Figure S15A**). This observation was

also confirmed in an additive target gene expression of *ABCA1* in macrophages (**Figure S15B**). These observations indicate a conditional activation potency of STLX4 only in combination with other LXR ligands or in presence of sufficient oxLDL as observed in diseased foam cells.

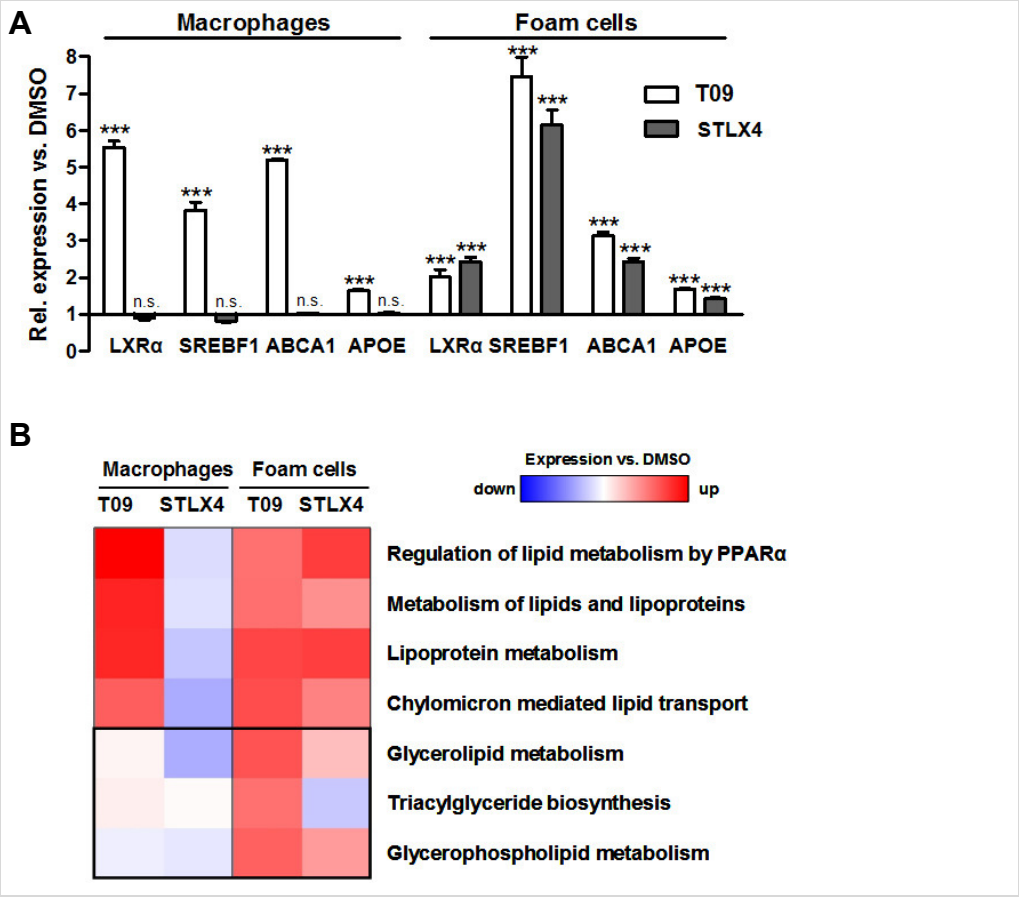

Figure 32: STLX4 targets specifically oxysterol-loaded foam cells. (**A**) Selected target gene expression of *LXRα*, *SREBF1*, *ABCA1* and *APOE* in THP1 macrophages and foam cells after treatment with T0901317 (T09, 10µM) or STLX4 (10µM). Data are expressed as mean ±SEM (n=4). *** P<0.001 vs. DMSO; n.s., not significant. (**B**) Genome-wide gene expression and subsequent gene set enrichment analysis (GSEA) of macrophages and foam cells after treatment with T09 (10µM) or STLX4 (10µM). Regulation of lipid-derived Reactome and KEGG pathways is shown.

3.5.3 STLX4 decreases cholesterol without undesired triglyceride increase

Consistent with the comparable potency of STLX4 and T0901317 to activate genes involved in lipid metabolism, physiological tests displayed also a significant reduction of total and esterified cholesterol content only in foam cells (**Figure 33A, Figure S16**). Interestingly, physiological analysis of triglyceride

levels revealed a striking difference between T0901317 and STLX4 treatments (**Figure 33B**). While T0901317 treatment highly induced the undesired triglyceride content in foam cells, it stayed unchanged upon STLX4 treatment. It was also noted in the genome-wide gene expression analysis that the triacylglyceride biosynthesis process was transcriptionally induced by T0901317 treatment and stayed not regulated or slightly down regulated by STLX4 treatment in foam cells (**Figure 32B**). Notably, this different regulation of triglyceride levels is not based on *SREBF1*, the common marker gene for lipogenesis. Thus, the observed differences in expression (**Figure 32A**) indicate another triglyceride regulation mechanism. Further studies are needed to investigate the underlying effects on this functional pathway.

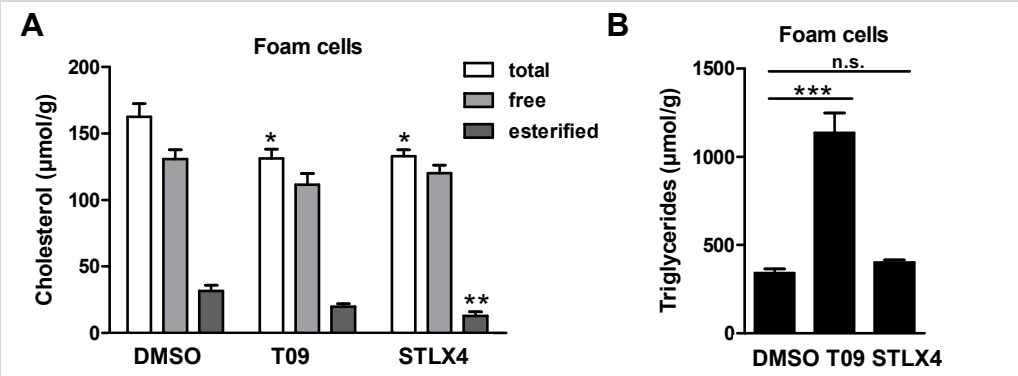

Figure 33: Physiological analyses of STLX4 treatment confirm unique STLX4 properties in foam cells. (**A)** Cholesterol content in foam cells after treatment for 48h with DMSO (0.1%), T0901317 (10µM) or STLX4 (10µM). Data are expressed as mean ±SEM (n=5-6). **(B)** Triglyceride content in foam cells after treatment for 48h with DMSO (0.1%), T0901317 (T09, 10µM) or STLX4 (10µM). * P<0.05, ** P<0.01, *** P<0.001 vs. DMSO; n.s., not significant

In summary, the LXRα agonist STLX4 is a molecule with high potential to decrease excess cholesterol in foam cells without adverse increase in triglycerides.

4. Discussion

The NR LXRα plays a pivotal role in macrophage cholesterol homeostasis and inflammatory response. Ligand-dependent LXRα activation has been shown to efficiently induce anti-atherosclerotic gene expression profiles (146, 251, 282). Despite intensive studies, comprehensive understanding of LXRα mechanisms and the associated molecular pathways of cell metabolism involved in atherogenesis remains elusive. With the recent advent and progress of genome-wide studies it is now possible to perform such comprehensive analyses to understand the complex molecular networks that underlie cell physiology and common diseases (283).

The present study reports for the first time of the genome-wide investigation of LXRα ligand-dependent networks of transcriptional regulation and pharmacological intervention in macrophages and foam cells. Moreover, this study introduces a novel, LXRα subtype specific ligand that particularly targets diseased foam cells.

4.1 Significance of data

The focus of this study was on LXRα-dependent gene networks modulated by either natural ligands or pharmacological intervention including new molecules rather than on individual target genes, as often analyzed in conventional molecular biological studies. Therefore, multiple datasets were integrated. To obtain significant biological information on interconnected molecular pathways in cell metabolism it was essential to validate each data set thoroughly and in-depth. This procedure included validating control experiments, replicates and stringent cutoffs. The applied ChIP-seq technique is a still evolving method and the strength of the derived signals is a continuum with more weak- than strong binding sites. Consequently, for the composition of the final peak list it is of upmost importance to set specific parameter settings and stringent thresholds in order to exclude a high proportion of false positives (199).

ChIP-seq data was carefully filtered and comprised only LXRα loci that showed significant effects on gene expression and were at the same time sensitive to LXR

knockdown (**Figure S11**). Moreover, the data set was strengthened through comparative ChIP-seq analysis and combination with histone occupancy and publicly available data of TFBS.

The analyzed THP1 cell line is a widely used model for human foam cell development (250) and showed similar effects on LXRα binding patterns and gene expression as primary macrophages (PBM). The performed comprehensive analysis was only possible with the standardized THP1 cell line as lipids from donor blood interfered with the analysis in PBM-derived cells (**Figure 14**). Additionally, human macrophages were advantageous over mouse macrophages for LXRα research in atherosclerosis. One of the central features of human LXRα is its autoregulatory loop activation which is absent in mouse macrophages (145). This feedback loop provides a mechanism to amplify the ligand stimulus and thereby promotes cholesterol efflux attenuating foam cell formation (144). Differences between mice and humans indicate that LXRα activation in human cells is regulated differently from other species.

4.2 LXRα cistrome

4.2.1 Ligand requirement for LXRα binding

In contrast to the classic model of LXRα transactivation, this study revealed a strong ligand requirement for all binding sites in macrophages and foam cells. Recent genome-wide studies already challenged the classic model and introduced new concepts of alternative activation modes (124–126, 131). Boergesen and colleagues observed an unexpected ligand requirement for the majority of detected binding sites (126). In absence of a ligand chromatin has a more closed structure and is less accessible for LXRα binding. Upon ligand activation LXRα in conjunction with co-regulators such as GPS2, and chromatin modifiers (e.g. histone demethylase) binds DNA (132), preferably in so-called hotspots of TF binding (125). Consequently, LXR recruitment leads to a more accessible chromatin environment and to the activation of target genes (126).

In contrast to recent genome-wide LXR studies (125, 126), the present study could not confirm significant basal binding of LXRα. Absence of basal binding was also attested by ChIP-qPCR analyses (**Figure 13**) and is in accordance with

the overall low LXRα protein level in ligand-free macrophages (**Figure 10A**). For example the widely tested LXRα target genes *ABCA1* and *ABCG1* were investigated for LXRα occupancy by ChIP-seq and ChIP-qPCR (**Figure 13**). The two cholesterol transporter ABCA1 and ABCG1 are highly induced LXRα target genes and play a central role in the anti-atherogenic effects of LXR ligands (284). Notably, these genes were associated with multiple and, in part, novel LXRα binding sites, which support their importance in metabolism and indicate a balancing mechanism for gene expression levels **(Figure S3**). As expected, these loci were also clearly increasingly occupied by LXRα upon T0901317 treatment. In absence of a ligand there was only sparse LXRα binding, which was mostly in the range of negative control binding sites.

Deviating outcomes of this study when compared to previous studies on LXR binding could be explained by setting of more stringent cutoffs and filtering criteria. Endpoint ChIP-PCR analyses, as applied by Jakobsson et al. 2010 (132) may lead to different results in terms of accurate relative quantification compared to ChIP-qPCR using real-time detection. Furthermore, the subtype specificity of the LXR antibody is a crucial factor for reliable data interpretation. It is important to mention that - although ChIP-seq is a powerful genome-wide screening technology - comparative analyses between different experiments remain very challenging (200). As exemplified by Bardet et al. 2012 (218), differences in sequencing depth and lane-to-lane variation can lead to very different peak sets and thus different biological interpretation of data.

The NR LXRα is a highly flexible and sensitive sensor for diverse metabolites and reacts quickly to pharmacological intervention in the human body. Thus, for an instant response to changing environment it is crucial for DNA binding and positioning to remain elastic. For many NRs the occupancy time at the DNA is in the range of microseconds (119). From observed results it can be assumed that LXRα, in the ligand-free state, constantly samples DNA without being engaged in stable interactions. Its low abundance in absence of ligands aggravates significant enrichment at potential target sites. Upon ligand activation, conformational changes may direct LXRα to engage at high affinity and high accessibility sites in a more stable interaction where it can interact with other TFs. Higher affinity of NR-DNA binding mostly correlates with stronger transcriptional activity.

Consequently, the protein level of LXRα is increased through the autoregulatory function and significant enrichment at specific LXRα-target sites can be observed.

4.2.2 Different peak patterns between T0901317 and foam cell-specific loci

Comparative ChIP-seq analysis revealed increased flexibility of LXRα binding upon activation via a synthetic or natural ligand. Shared and differential binding of LXRα to genomic loci was observed in macrophages and foam cells as response to different stimuli (**Figure 15**). Dependent on the individual requirements of the macrophage or the foam cell, LXRα seemed to bind with varying affinity to individual target gene sites. Stimulus by synthetic ligand T0901317 appeared to enrich LXRα at target sites stronger than the naturally occurring oxysterol ligands from oxLDL treatment of foam cells. Surprisingly, 45% of binding sites were common among different treatments indicating that - despite biological transformation from macrophage to foam cell - LXRα function remains established for many genes.

The T0901317 specific peak set and the shared peak set were comprised of genes known to be involved in cholesterol and fatty acid metabolism as well as defense response (**Table S4**). Notably, the foam cell-specific peak set was enriched with genes encoding bioprocesses including ras protein signal transduction. Ras is a membrane associated protein that is normally activated by extracellular signals and affects many cellular functions including cell proliferation, differentiation as well as apoptosis (285). It has been proposed that Ras can also be directly activated by reactive free radicals and cellular redox stress (286, 287), which is in accordance with the diseased, oxLDL loaded foam cell model.

The different peak patterns between the shared, T0901317-specific and foam cell-specific peak sets are of particular interest to uncover the differential transcriptional regulation of involved genes by LXRα. Remarkably, the foam cell specific binding sites were less pronounced enriched, showed decreased chromatin accessibility (**Figure 15**) and were less enriched with co-occurring TFBS (**Figure 16**), which indicates that LXRα bound less tight or indirect via other TFs to these genomic sites. Especially, the trans-repressive function of LXRα can involve long-range cis-interactions or tethering of LXRα to other

factors (288). Moreover, weak enrichment may also indicate a pioneering function of LXRα at these sites as only few other TFBS were co-localized.

An interesting and novel LXRα target gene *PARP1,* identified from the foam cell-specific peak set (**Figure 15D**), represents an enzyme that is known to be involved in DNA damage repair. This function is in contrast to the mostly lipid and inflammation relevant target genes of shared and T0901317-specific peak sets. Notably, a recent study postulated that PARP1 inhibitors can act against pathologies such as diabetes, stroke and cardiovascular diseases (289). Inhibition of PARP1 leads in particular in brown adipose tissue and skeletal muscle to enhanced mitochondrial metabolism via activation of the histone deacetylase SIRT1, which culminated in protection against metabolic diseases (61). As observed in diseased foam cells, increased levels of oxysterols triggered LXRα binding at this locus, whereas T0901317 therapy prevented LXRα from binding to *PARP1* locus. This finding could point towards a so far unexplored role of LXRα in counteracting metabolically undesired effects of foam cells.

4.2.3 Motif requirement and positioning of LXRα

As an evolutionary rather new nuclear receptor, LXRα showed comparably poor defined sequence-specificity in this study. LXRα motif analyses showed that single base changes of the derived motif did not alter reporter gene activity. Notably, mutations of the spacer region decreased LXRα binding affinity indicating a potential stereo-chemical role of the spacer region for LXRα binding, which has not been considered relevant so far. However, binding specificity in the chromatin context is far different from *in vitro* assays. In this study, only 15% of ChIP-seq derived binding sites occupied the DR4 motif. Especially in the case of foam cell-specific binding sites almost only DR4 motif independent and relatively promoter distant binding patterns were detected (**Figure 17**, **Figure 18**). Genome-wide ChIP-seq studies pointed towards much more promiscuous NR-binding to DNA sequences than expected from consensus motif studies (126). In recently published LXR ChIP-seq studies, only 6.3% -8% of peaks contained a DR4-type RE (124–126). A large number of NR-binding sites in these studies had no resemblance to a specific NR-RE (124–126). There are several mechanisms that could explain specific recruitment in absence of a motif, including stabilizing interactions with other TFs (126), via looping, ‘piggyback’ binding or assisted

binding through specifically modified histones with an open chromatin environment (114). It could be shown e.g. for the glucocorticoid receptor (GR), that chromatin accessibility predetermines its binding to DNA (127). Consistently, increased chromatin accessibility and an enrichment of co-localized TFs could be observed for the shared and T0901317 specific peak sets (**Figure 15A**, **Figure 16**). The less pronounced openness of the foam cell-specific peak set could be due to indirect binding of LXRα to the genome, pointing towards a regulatory function as distant enhancer or repressor of gene expression.

One further aspect supporting this hypothesis is the relative genomic position of foam cell-specific LXRα peaks. In contrast to the observed promoter site enrichment of T0901317-specific and shared peak set, the foam cell-specific set was enriched downstream of genes. Thus, it can be assumed that in foam cells, LXRα acts as long-range enhancer or repressor rather than a classic promoter-associated TF.

In general, the synthetic ligand T0901317 seems to have the potential for pronounced sharpening of LXRα genome-binding patterns. Foam cell-specific binding is less pronounced and might hint to trans-repressive mechanisms of LXRα in foam cells or a pioneering function of LXRα at distant enhancer regions. However, for comprehensive understanding of all observed effects, further studies are needed.

4.3 LXRα transcriptome

4.3.1 Cell type dominates gene expression

The gene expression profiles between foam cells and T0901317 treated foam cells as well as macrophages and T0901317 treated macrophages were mostly comparable (**Figure 19B**). In contrast to LXRα binding, where the T0901317 stimulus was pre-determining, in gene expression the transformation process from macrophage to foam cell dominated the profiles. The applied GSEA method to decipher functional pathways, proved advantageous to relate the treatment effects to a broader physiological context (236). In contrast, single gene analyses are more limited and often show only small expression level changes that accumulate merely for a specific pathway. The chosen GSEA method revealed an interesting

upregulation of lipid and lipoprotein metabolism upon T090137 treatment in foam cells (**Figure 20**), which could explain some of the described anti-atherogenic properties of T0901317 (186).

4.3.2 Tight interaction of LXRα and PPARα regulated pathways

Transcriptional regulation is a complex process that mostly involves the tight interplay of several TFs (126, 223). The functional annotation of the derived data set revealed an interesting involvement of LXRα in the PPARα signaling pathway. Induction of LXR by PPAR members is well described (288). However, apart from the expected up regulation of the lipid metabolism pathway via PPARα (**Figure 20A**) the present study revealed an LXRα-dependent regulation of two major co-regulators of PPARα, *CITED2* and *PRIC 285* (**Figure 24**). Boergesen et al. 2012 recently reported a tight crosstalk between PPARα and LXR in mouse liver (126). PPARα and LXR seem to share a substantial proportion of common binding sites. In the macrophage 16.5% of discovered LXR peaks shared a binding site with PPARγ (125). In line with these studies, it can be concluded that LXRα also influences PPARα target genes and that there is a tight crosstalk between these two NRs.

4.4 Data integration

To fully address complex biological mechanisms it is important to apply system-based strategies that integrate numerous genomic, molecular and physiological data (38). To get a very stringent data set for subsequent network studies, integrative data analysis was applied. A highly confident set of LXRα target genes was generated by the integration of ChIP-seq and gene expression profiles. An additional layer of information was derived by correlation with histone ChIP-seq data, FAIRE-seq data and publicly available data of TFBS. Greatly enriched FAIRE regions can be identified near known regulatory active transcription start sites (291). FAIRE-seq derived chromatin landscapes at LXRα binding sites confirmed chromatin accessibility as highly correlated with transcriptional regulation of target genes. Combination of promoter specific changes of H3K4me3, H4K20me1 and chromatin accessibility at potential target genes, determined by FAIRE-seq, were supportive and predictive for gene expression regulation (239) (**Figure 23**). In total, 30% of LXRα binding sites could be

directly correlated with target gene expression. This rate is in range with similar reports comparing ChIP-seq and microarray data (125, 292).

4.4.1 Disease-associated genetic variation data

Several groups have previously reported on potential correlations between LXR and diseases including diabetes and obesity. However, to date, the data are conflicting and mechanistic links between SNPs and human (patho-) physiology remain to be established (293). To gain deeper understanding on potential links between LXRα target genes and different diseases, GWAS information were combined with the derived LXRα binding and expression data sets.

The applied analysis confirmed already known as well as identified novel LXRα target genes with central impact on pathological processes concerning metabolism and inflammation (**Table 2**). The most significant association was identified between a SNP located close to *APOC1* gene and disease terms LDL cholesterol and C-reactive protein. The *APOC1* gene was flanked by two T0901317-specific LXRα binding sites that were almost completely absent in foam cells (**Figure 25A**). In accordance with the presented data, LXR has been shown to induce activation of multi-enhancer regions ME.1 and ME.2 which presumably drive the expression of the whole *APOE/C1/C2/C4* gene cluster (20, 255, 256). Apart from gene induction relevant for lipid metabolism, adjacent, inflammation and apoptosis relevant genes were also shown to be regulated by LXRα upon T0901317 treatment (**Figure 25**). This interplay is supported by a recent large-scale association study that reported on a significant crosstalk between lipid metabolism and inflammation pathways (294).

The identified strong association suggests that ligand-induced specific LXRα binding at this locus is significant for establishing a key network of genes that contribute to the reversal of cholesterol efflux and attenuation of inflammation processes in foam cells, which ultimately helps to prevent atherogenesis.

4.5 Network analyses

It has been stated that biological function emerges from complex interaction networks of genes rather than from single gene analyses (295). The network concept was successfully applied in multiple studies (205, 206, 294) and was

therefore chosen for the present research work. Herein, it was essential to analyze the generated large-scale genomic data and to establish molecular networks based on DNA, RNA and protein interactions to elucidate gene regulatory networks, molecular pathways and their interplay in healthy and diseased states.

4.5.1 Gene networks in foam cells vs. T0901317 treated foam cells

The athero-protective potential of LXRα ligands was analyzed by direct comparison of the foam cell-specific gene network with the T0901317-modulated network in foam cells. The transformation of macrophage to foam cell triggered the expression of multiple genes that were directly or indirectly connected with LXRα (**Figure 27A**). Among the identified genes, there were multiple TFs, including CEBPs and NFkB, known to be important in the regulation of several pathways such as inflammatory responses (296, 297) and apoptosis (298). This network illustrated nicely the complexity of LXRα triggered gene regulatory process. Activated TFs were shown to be connected to a vast number of differentially expressed genes. The derived network represented several levels of transcriptional control including intracellular signaling pathways of LXRα, recruited co-factors and other TFs that are potentially required for the maximal expression or repression of downstream genes. Therefore, each node of the network could be in principle a critical component of LXRα transcriptional program. Through intense crosstalk of various factors different cascades of genes could be regulated and thereby finally define the cellular response to foam cell transformation or pharmacological intervention with T0901317.

IPA analysis of the foam cell network annotated molecular functions to analyzed genes including lipid metabolism, inflammation and cell death. These functions were also previously described to be influenced by LXRα (147, 272, 273). Notably, the apoptotic function of these cells is in accordance with the diseased foam cell model. Excessive apoptosis is thought to promote atherosclerosis. OxLDL can trigger ER-stress and subsequently activate proteins correlated to apoptosis and plaque vulnerability (103). Furthermore, defective anti-inflammatory signaling can lead to ineffective efferocytosis and cause plaque necrosis (78). Remarkably, in the early stages of atherosclerosis, increased

apoptosis protects from atherosclerosis development presumably due to the removal of macrophages in the early plaque development (299).

Differential analysis of LXRα ligand-dependent modulation of the diseased foam cell network revealed 38 genes vulnerable to T0901317 therapy (**Figure 27B**). Surprisingly, 32 of these genes were novel LXRα target genes, discovered in the present study (**Table S6**). Their novelty made functional classification and association with LXRα challenging. Despite lacking database-information on LXRα connection with most genes in this set, it was still possible with IPA to annotate and functionally classify 14 genes in network functions such as carbohydrate metabolism, molecular transport and lipid metabolism (**Figure 28A**). All these processes have been previously described as associated with LXRα function (300), which confirms the significance of the new target genes and discloses new pharmacologically treatable gene networks with athero-protective potential. The derived 32 novel LXRα target genes should be further tested for their athero-beneficial potential and their impact on other metabolic diseases such as diabetes.

Due to limitations in the IPA database, only a subset of 10 novel LXRα target genes could be further analyzed for their involvement in the LXR/RXR activation pathway (**Figure 29**). These 10 genes were indirectly connected to LXRα through networked genes, mainly via the NFκB complex and TNFA. NFκB is a protein complex that has a key role in regulating immune responses to infections. Additionally, NFκB is involved in cellular responses to various stimuli including stress, free radicals and oxLDL (297, 301). Inhibition of the NFκB pathway leads to decreased production of inflammatory cytokines such as IL6 and TNFA (79). It has been reported that LXR's anti-inflammatory properties also comprise the inhibition of NFκB-mediated signaling in macrophages (83, 139). In cardiomyocytes LXRs have been shown to suppress NFκB-signaling and thereby reduce cardiac growth and inflammation (302). In the present study, no direct LXRα binding at the *NFκB* locus could be observed. However, there is a clear relation between LXRα, NFκB and TNFA signaling (**Figure 29**). Several novel LXRα target genes interact directly with the NFκB-complex or indirectly via TLR and TNFA. An interesting example of highly suppressed LXRα target genes is *PIAS4*, an E3 SUMO-protein ligase, also known as protein inhibitor of activated

STAT protein 4. This transcriptional co-regulator interacts with the NFκB complex and plays a crucial role in various cellular pathways with involvement in gene silencing (281). Further, PIAS4 has been shown to activate NFκB in response to stress (303). Together, these observations could suggest suppression of PIAS4 as one of the upstream activator mechanisms of inflammatory response and represent an explanation for the anti-inflammatory effects of T0901317 in inflammatory foam cells.

Notably, several novel LXRα target genes in network were also found to be associated with diseases that were previously linked to LXRα, including CVD and psoriasis. Thus, the novel LXRα target genes could be used to explain at least in part the implications of disease-associated genetic variation data.

Taken together, integration of multiple datasets and identification of involved networks that comprehensively responded to pharmacological intervention provided a powerful approach in this study to investigate the complex biological foam cell system and its pharmacological modulation with the LXRα ligand T0901317.

4.6 STLX4 - A novel disease specific LXRα ligand

Development of selective LXR modulators without deleterious side effects is key to effectively combat atherosclerosis and CVD (183). One of the present study findings is the introduction of the novel LXR agonist STLX4. Screening a diverse natural compound library and subsequent optimization of the derived stilbenoid structure resulted in the identification of a foam cell-specific, anti-atherogenic LXRα ligand.

4.6.1 STLX4 mode of action

The performed analyses displayed that the unique conditional activation potential of STLX4 in diseased foam cells is highly dependent on a partner ligand (**Figure S15**). One of the explanations for this property could be allosteric binding of STLX4 to the LBD. Alternatively, STLX4 could recruit a changed set of transcriptional LXR co-factors in foam cells and thereby drive its specific actions. Notably, the amount of LXRα protein is due to its autoregulatory activation potential highly increased in foam cells compared to macrophages (145). This

could explain the lack of activation potential of STLX4 in macrophages. Further, STLX4 showed LXRα-subtype specificity. This could be connected with the predominant levels of LXRα-subtype compared to LXRβ in foam cells (**Figure 10, Table S1**). Alpha-subtype specificity was further confirmed in reporter gene analysis and by trend in knockdown experiments (**Figure 31**, **Figure S12**).

4.6.2 Physiological effects of STLX4

In contrast to most LXR ligands, including T0901317 and GW3965 (190, 191), STLX4 decreased cellular content of total and esterified cholesterol without the undesirable increase in triglyceride levels (**Figure 33**). Interestingly, this effect was observed despite the detected up regulation of *SREBF1* (**Figure 32A**), the central activator of lipogenesis. Hence, there must be a different regulatory mechanism for triglyceride metabolism upon STLX4 modulation.

This new foam cell-specific LXRα ligand can be used as a tool compound for further investigation of mechanistic aspects of anti-atherogenic processes. Moreover, STLX4 is an interesting ligand for the analysis of ligand-dependent fine-tuning of LXRα-regulated gene expression via differential co-factor recruitment. Comprehensive analysis of STLX4-triggered networks of transcriptional regulation that shape gene expression patterns will further elucidate the complex interconnected molecular pathways in cell metabolism during atherogenesis.

The specific anti-atherogenic spectrum of the STLX4 in foam cells makes it a promising LXRα ligand for further pharmaceutical development. Further chemical optimization and modification of the presented STLX4 lead structure may improve the presented effects and make the new ligand readily applicable for *ex-* and *in vivo* models to study gene regulation processes and resulting metabolic effects. Prior to *in vivo* models, testing of chemical stability and potential side effects including for example binding tests with NRs will be necessary. Additionally, the pharmaceutical properties of STLX4 should be assessed in standard test panels including absorption, distribution, metabolism and excretion (ADME) prior to application *in vivo*.

Taken together, STLX4 is a potent compound that specifically activates only selected metabolic features of LXRα in diseased but not in normal macrophage cells. This compound provides new avenues for further mechanistic studies and future innovative treatment strategies of atherosclerosis and CVD.

4.7 Conclusions and future perspectives

The presented data describes an LXRα ligand-dependent network of transcriptional regulation, which can be modulated by small molecules that efficiently activate LXRα and shape gene expression patterns. The applied integrative analysis revealed a highly complex interplay between multiple regulatory levels. DNA binding of a NR can trigger multiple processes including activation or repression of several other factors or their recruitment to a specific site. It is obvious that LXRα cooperates with other factors and regulates broad networks via interaction with other TFs, including PPARα or NFκB. Future studies should involve system-biological approaches and incorporate analysis of several associated TFs.

Moreover, ligand-dependent differential interaction with transcriptional co-factors can easily lead to varying responses on the gene network level and thereby modulate the gene expression patterns (207). Hence, the generated integrative data set of the present study may provide a resource for developing further mechanistic LXR-studies to analyze ligand-dependent fine-tuning of gene expression via differential co-factor recruitment. Such studies could be performed with a panel of alternative small molecule activators of LXR such as GW3965 (304) or the new foam cell-specific LXRα ligand STLX4.

Quantitative LXRα binding studies could as well be applied on clinical samples of diseased patients. Such studies will have the potential to explain the functional impact of genetic variation in a certain locus for cardiovascular or other diseases.

Future studies will certainly benefit from an additional layer of complementary information by integration of gene, protein or metabolic networks (305, 306). Such analyses will potentially provide an even more comprehensive understanding of interconnected molecular pathways in atherosclerosis and reveal optimized treatment strategies for CVD.

5. Summary

Atherosclerosis is the leading cause of cardiovascular diseases (CVD) and an enormous health burden. The ligand dependent nuclear receptor liver X receptor alpha (LXRα) is an important target for anti-atherosclerotic compounds due to its essential role in the adaptation of macrophages to lipid overload. Unfortunately, treatment with currently investigated LXRα modulating ligands is associated with deleterious side effects such as hypertriglyceridemia. Thus, it is of fundamental interest to investigate LXRα contribution to gene regulatory networks in macrophages, atherosclerotic foam cells and changes upon modulation with known anti-atherosclerotic LXRα ligands as well as the discovery of novel, selective LXRα modulators. Applying a highly integrative approach, global LXRα cistrome, epigenome and transcriptome data in macrophages, foam cells and with LXRα ligand T0901317 treated cell models were generated. Subsequent network analyses revealed that LXRα regulates broad networks via interaction with other factors, including PPARα and NFκB. The diseased foam cell network could be successfully modulated by pharmacological intervention with T0901317 resulting in the discovery of 32 novel LXRα target genes with potential athero-beneficial effects, which in part explained the implications of disease-associated genetic variation data. The identified networks provide a powerful platform to investigate the complex biological foam cell system and will in future help to find new avenues for treating systematically atherosclerosis and related diseases. Additionally, the presented work debuts a novel LXRα ligand, STLX4. The optimized stilbenoid-based molecule binds preferably the LXRα-subtype and selectively induces its anti-atherogenic potential in diseased foam cells but not in macrophages. STLX4 has similar potency to reduce excess cholesterol in foam cells as T0901317 without the adverse increase in triglycerides. Thus, STLX4 is a novel LXRα ligand with outstanding potential for future pharmaceutical development.

6. Zusammenfassung

Atherosklerose ist die Hauptursache für die Entstehung von kardiovaskulären Erkrankungen und stellt ein großes Gesundheitsproblem unserer Gesellschaft dar. Der ligandenabhängige nukleare Rezeptor Leber X Rezeptor alpha (LXRα) ist ein wichtiger Zielrezeptor für anti-atherosklerotische Substanzen, da er von zentraler Bedeutung für die Bewältigung der Lipidüberladung von Makrophagen ist. Leider weisen aktuell erforschte LXRα-modulierende Substanzen Nebenwirkungen, wie zum Beispiel Hypertriglyzeridämie, auf. Daher ist es von besonderem Interesse, den Beitrag von LXRα zu genregulatorischen Netzwerken, sowie dessen anti-atherosklerotische Modulation in Makrophagen und Schaumzellen zu untersuchen. Darüber hinaus steht auch die Entwicklung neuer und selektiver LXRα-Modulatoren im Vordergrund. Durch die Anwendung eines überaus integrativen Ansatzes wurden genomweite Cistrom-, Epigenom- und Transkriptomdaten für LXRα in Makrophagen, Schaumzellen und mit dem LXRα liganden T0901317 behandelten Zellmodellen generiert. Die anschließende Netzwerkanalyse zeigte, dass LXRα weitreichende Netzwerke durch Interaktion mit anderen Faktoren, wie PPARα und NFκB, reguliert. Das pathologische Schaumzellnetzwerk konnte durch die pharmakologische Intervention mit T0901317 moduliert werden und ermöglichte die Identifikation von 32 neuen LXRα-Zielgenen, die ein hohes athero-protektives Potential bergen und zum Teil die Auswirkungen von krankheitsassoziierten genetischen Variationsdaten erklären können. Die identifizierten Netzwerke sind eine hervorragende Basis für die Analyse der komplexen Biologie des Schaumzellsystems und werden in Zukunft dazu beitragen, neue Wege für die systematische Behandlung von Atherosklerose und ähnlichen Erkrankungen zu finden. Im Rahmen der vorliegenden Arbeit gelang es zudem, mit STLX4 einen neuen LXRα Liganden zu identifizieren. Das optimierte, auf einem Stilbenoid basierende Molekül, bindet bevorzugt den LXRα-Subtyp und induziert sein anti-atherogenes Potential nur in Schaumzellen und nicht in Makrophagen. Das Potential von STLX4, überschüssiges Cholesterin zu reduzieren, ist vergleichbar mit dem von T0901317, allerdings ruft STLX4 keinen unerwünschten Anstieg an Triglyzeriden hervor. STLX4 ist ein neuer LXRα-Ligand mit einem herausragenden Potential für weitere zukünftige pharmakologische Entwicklungen.

7. References

1. World Health Organization (2011) Global atlas on cardiovascular disease prevention and control. *World Health Organ Tech Rep Ser*, **1**, 164.

2. Anand,S.S., Islam,S., Rosengren,A., Franzosi,M.G., Steyn,K., Yusufali,A.H., Keltai,M., Diaz,R., Rangarajan,S. and Yusuf,S. (2008) Risk factors for myocardial infarction in women and men: insights from the INTERHEART study. *European heart journal*, **29**, 932–40.

3. Stein,A.D., Thompson,A.M. and Waters,A. (2005) Childhood growth and chronic disease: evidence from countries undergoing the nutrition transition. *Maternal & child nutrition*, **1**, 177–84.

4. Hu,F.B. (2008) Globalization of food patterns and cardiovascular disease risk. *Circulation*, **118**, 1913–4.

5. Critchley,J., Liu,J., Zhao,D., Wei,W. and Capewell,S. (2004) Explaining the increase in coronary heart disease mortality in Beijing between 1984 and 1999. *Circulation*, **110**, 1236–44.

6. Leal,J., Luengo-Fernández,R., Gray,A., Petersen,S. and Rayner,M. (2006) Economic burden of cardiovascular diseases in the enlarged European Union. *European heart journal*, **27**, 1610–9.

7. Institute of Medicine (IOM) (2010) Promoting Cardiovascular Health in the Developing World: A Critical Challenge to Achieve Global Health Valentin Fuster; Bridget B. Kelly (ed) The National Academies Press (US), Washington, DC.

8. Christensen,K., Doblhammer,G., Rau,R. and Vaupel,J.W. (2009) Ageing populations: the challenges ahead. *Lancet*, **374**, 1196–208.

9. Rich,M.W. and Mensah,G.A. (2009) Fifth Pivotal Research in Cardiology in the Elderly (PRICE-V) symposium: preventive cardiology in the elderly-executive summary. Part I: morning session. *Preventive cardiology*, **12**, 198–204.

10. McKay,J.A. and Mathers,J.C. (2011) Diet induced epigenetic changes and their implications for health. *Acta physiologica (Oxford, England)*, **202**, 103–18.

11. McCay CM, Crowell MF,M. LA (1935) The effect of retarded growth upon the length of life span and upon the ultimate body size. *The Journal of nutrition*, **10**, 63–79.

12. Ribarič,S. (2012) Diet and aging. *Oxidative medicine and cellular longevity*, **2012**, 741468.

13. Fontana,L., Villareal,D.T., Weiss,E.P., Racette,S.B., Steger-May,K., Klein,S. and Holloszy,J.O. (2007) Calorie restriction or exercise: effects on coronary heart

disease risk factors. A randomized, controlled trial. *American journal of physiology. Endocrinology and metabolism*, **293**, E197–202.

14. Hanukoglu,I. (1992) Steroidogenic enzymes: structure, function, and role in regulation of steroid hormone biosynthesis. *The Journal of steroid biochemistry and molecular biology*, **43**, 779–804.

15. Ikonen,E. (2006) Mechanisms for cellular cholesterol transport: defects and human disease. *Physiological reviews*, **86**, 1237–61.

16. Walker HK, Hall WD, Hurst JW, Editors.Walker HK, Hall WD, Hurst JW,E. (1990) Clinical Methods: The History, Physical, and Laboratory Examinations. 3rd ed. Butterworths, Boston.

17. Murray RK, Granner DK, Mayes PA,R.V. (1993) Harper's Biochemistry 23rd ed. Appleton and Lange, Norwalk.

18. Devlin,T.M. (1992) Textbook of Biochemistry with Clinical Correlations Wiley-Liss, New York.

19. Ken-Dror,G., Talmud,P.J., Humphries,S.E. and Drenos,F. APOE/C1/C4/C2 gene cluster genotypes, haplotypes and lipid levels in prospective coronary heart disease risk among UK healthy men. *Molecular medicine (Cambridge, Mass.)*, **16**, 389–99.

20. Plump,A.S., Smith,J.D., Hayek,T., Aalto-Setälä,K., Walsh,A., Verstuyft,J.G., Rubin,E.M. and Breslow,J.L. (1992) Severe hypercholesterolemia and atherosclerosis in apolipoprotein E-deficient mice created by homologous recombination in ES cells. *Cell*, **71**, 343–353.

21. Lin,C.Y., Duan,H. and Mazzone,T. (1999) Apolipoprotein E-dependent cholesterol efflux from macrophages: kinetic study and divergent mechanisms for endogenous versus exogenous apolipoprotein E. *Journal of lipid research*, **40**, 1618–27.

22. Wilson,M.D. and Rudel,L.L. (1994) Review of cholesterol absorption with emphasis on dietary and biliary cholesterol. *Journal of lipid research*, **35**, 943–55.

23. Goldstein,J.L. and Brown,M.S. (1977) Atherosclerosis: The low-density lipoprotein receptor hypothesis. *Metabolism*, **26**, 1257–1275.

24. Brown,M.S. and Goldstein,J.L. (1986) A receptor-mediated pathway for cholesterol homeostasis. *Science (New York, N.Y.)*, **232**, 34–47.

25. Steinberg,D. and Gotto,A.M. (1999) Preventing coronary artery disease by lowering cholesterol levels: fifty years from bench to bedside. *JAMA : the journal of the American Medical Association*, **282**, 2043–50.

26. Ginsberg,H.N. (1998) Lipoprotein physiology. *Endocrinology and metabolism clinics of North America*, **27**, 503–19.

27. Yoshikawa,T., Shimano,H., Amemiya-Kudo,M., Yahagi,N., Hasty,A.H., Matsuzaka,T., Okazaki,H., Tamura,Y., Iizuka,Y., Ohashi,K., et al. (2001) Identification of liver X receptor-retinoid X receptor as an activator of the sterol regulatory element-binding protein 1c gene promoter. *Molecular and cellular biology*, **21**, 2991–3000.

28. Yusuf,S., Hawken,S., Ounpuu,S., Dans,T., Avezum,A., Lanas,F., McQueen,M., Budaj,A., Pais,P., Varigos,J., et al. Effect of potentially modifiable risk factors associated with myocardial infarction in 52 countries (the INTERHEART study): case-control study. *Lancet*, **364**, 937–52.

29. Kannel,W.B., Castelli,W.P., Gordon,T. and McNamara,P.M. (1971) Serum cholesterol, lipoproteins, and the risk of coronary heart disease. The Framingham study. *Annals of internal medicine*, **74**, 1–12.

30. Manninen,V., Tenkanen,L., Koskinen,P., Huttunen,J.K., Mänttäri,M., Heinonen,O.P. and Frick,M.H. (1992) Joint effects of serum triglyceride and LDL cholesterol and HDL cholesterol concentrations on coronary heart disease risk in the Helsinki Heart Study. Implications for treatment. *Circulation*, **85**, 37–45.

31. Gotto,A.M. (2005) Evolving concepts of dyslipidemia, atherosclerosis, and cardiovascular disease: the Louis F. Bishop Lecture. *Journal of the American College of Cardiology*, **46**, 1219–24.

32. Collins,R., Armitage,J., Parish,S., Sleight,P. and Peto,R. (2004) Effects of cholesterol-lowering with simvastatin on stroke and other major vascular events in 20536 people with cerebrovascular disease or other high-risk conditions. *Lancet*, **363**, 757–67.

33. Bhardwaj,S., Misra,A., Khurana,L., Gulati,S., Shah,P. and Vikram,N.K. (2008) Childhood obesity in Asian Indians: a burgeoning cause of insulin resistance, diabetes and sub-clinical inflammation. *Asia Pacific journal of clinical nutrition*, **17 Suppl 1**, 172–5.

34. Després,J.P., Lemieux,I. and Prud'homme,D. (2001) Treatment of obesity: need to focus on high risk abdominally obese patients. *BMJ (Clinical research ed.)*, **322**, 716–20.

35. Poirier,P., Giles,T.D., Bray,G.A., Hong,Y., Stern,J.S., Pi-Sunyer,F.X. and Eckel,R.H. (2006) Obesity and cardiovascular disease: pathophysiology, evaluation, and effect of weight loss: an update of the 1997 American Heart Association Scientific Statement on Obesity and Heart Disease from the Obesity Committee of the Council on Nutrition, Physical. *Circulation*, **113**, 898–918.

36. Innerarity,T.L., Mahley,R.W., Weisgraber,K.H., Bersot,T.P., Krauss,R.M., Vega,G.L., Grundy,S.M., Friedl,W., Davignon,J. and McCarthy,B.J. (1990) Familial defective apolipoprotein B-100: a mutation of apolipoprotein B that causes hypercholesterolemia. *Journal of lipid research*, **31**, 1337–49.

37. Arking,D.E. and Chakravarti,A. (2009) Understanding cardiovascular disease through the lens of genome-wide association studies. *Trends in genetics : TIG*, **25**, 387–94.

38. Lusis,A.J., Attie,A.D. and Reue,K. (2008) Metabolic syndrome: from epidemiology to systems biology. *Nat Rev Genet*, **9**, 819–830.

39. Arnett,D.K., Baird,A.E., Barkley,R.A., Basson,C.T., Boerwinkle,E., Ganesh,S.K., Herrington,D.M., Hong,Y., Jaquish,C., McDermott,D.A., et al. (2007) Relevance of genetics and genomics for prevention and treatment of cardiovascular disease: a scientific statement from the American Heart Association Council on Epidemiology and Prevention, the Stroke Council, and the Functional Genomics and Translational. *Circulation*, **115**, 2878–901.

40. Lee,R.T. and Libby,P. (1997) The unstable atheroma. *Arteriosclerosis, thrombosis, and vascular biology*, **17**, 1859–67.

41. World Health Organization (2007) Prevention of cardiovascular disease: Guideline for assessment and management of cardiovascular risk. *World Health Organ Tech Rep Ser*.

42. Libby,P. (2000) Changing concepts of atherogenesis. *Journal of internal medicine*, **247**, 349–58.

43. Bobryshev,Y. V (2006) Monocyte recruitment and foam cell formation in atherosclerosis. *Micron (Oxford, England : 1993)*, **37**, 208–22.

44. Libby,P. Inflammation in atherosclerosis. *Nature*, **420**, 868–74.

45. Ross,R. (1999) Atherosclerosis--an inflammatory disease. *The New England journal of medicine*, **340**, 115–26.

46. Mestas,J. and Ley,K. (2008) Monocyte-endothelial cell interactions in the development of atherosclerosis. *Trends in cardiovascular medicine*, **18**, 228–32.

47. Hoff,H.F., O'Neil,J., Pepin,J.M. and Cole,T.B. (1990) Macrophage uptake of cholesterol-containing particles derived from LDL and isolated from atherosclerotic lesions. *Eur. Heart J.*, **11**, 105–115.

48. Maton,A. (1993) Human biology and health lst ed. Prentice Hall, Englewood Cliffs N.J.

49. Virchow,R. (1856) Phlogose und Thrombose im Gefasssystem. *Gesammelte Abhandlungen zur Wissenschaftlichen Medicin, Fankfurt*.

50. Ross,R., Glomset,J. and Harker,L. (1977) Response to injury and atherogenesis. *The American journal of pathology*, **86**, 675–84.

51. Deanfield,J., Donald,A., Ferri,C., Giannattasio,C., Halcox,J., Halligan,S., Lerman,A., Mancia,G., Oliver,J.J., Pessina,A.C., et al. (2005) Endothelial function and dysfunction. Part I: Methodological issues for assessment in the

different vascular beds: a statement by the Working Group on Endothelin and Endothelial Factors of the European Society of Hypertension. *Journal of hypertension*, **23**, 7–17.

52. Fabricant,C.G. and Fabricant,J. (1999) Atherosclerosis induced by infection with Marek's disease herpesvirus in chickens. *American heart journal*, **138**, S465–8.

53. Hsu,H.Y., Nicholson,A.C., Pomerantz,K.B., Kaner,R.J. and Hajjar,D.P. (1995) Altered cholesterol trafficking in herpesvirus-infected arterial cells. Evidence for viral protein kinase-mediated cholesterol accumulation. *The Journal of biological chemistry*, **270**, 19630–7.

54. Cheng,J., Ke,Q., Jin,Z., Wang,H., Kocher,O., Morgan,J.P., Zhang,J. and Crumpacker,C.S. (2009) Cytomegalovirus infection causes an increase of arterial blood pressure. *PLoS pathogens*, **5**, e1000427.

55. Koren,O., Spor,A., Felin,J., Fåk,F., Stombaugh,J., Tremaroli,V., Behre,C.J., Knight,R., Fagerberg,B., Ley,R.E., et al. (2011) Human oral, gut, and plaque microbiota in patients with atherosclerosis. *Proceedings of the National Academy of Sciences of the United States of America*, **108 Suppl** , 4592–8.

56. Brown,M.S. and Goldstein,J.L. (1976) Analysis of a mutant strain of human fibroblasts with a defect in the internalization of receptor-bound low density lipoprotein. *Cell*, **9**, 663–74.

57. Goldstein,J.L., Ho,Y.K., Basu,S.K. and Brown,M.S. (1979) Binding site on macrophages that mediates uptake and degradation of acetylated low density lipoprotein, producing massive cholesterol deposition. *Proceedings of the National Academy of Sciences of the United States of America*, **76**, 333–7.

58. Williams,K.J. and Tabas,I. (1998) The response-to-retention hypothesis of atherogenesis reinforced. *Current opinion in lipidology*, **9**, 471–4.

59. Libby,P., Ridker,P.M. and Hansson,G.K. (2011) Progress and challenges in translating the biology of atherosclerosis. *Nature*, **473**, 317–325.

60. Petricoin,E.F., Ardekani,A.M., Hitt,B.A., Levine,P.J., Fusaro,V.A., Steinberg,S.M., Mills,G.B., Simone,C., Fishman,D.A., Kohn,E.C., et al. (2002) Use of proteomic patterns in serum to identify ovarian cancer. *Lancet.*, **359**, 572–7.

61. Steinberg,D., Parthasarathy,S., Carew,T.E., Khoo,J.C. and Witztum,J.L. (1989) Beyond cholesterol. Modifications of low-density lipoprotein that increase its atherogenicity. *The New England journal of medicine*, **320**, 915–24.

62. Steinbrecher,U.P., Parthasarathy,S., Leake,D.S., Witztum,J.L. and Steinberg,D. (1984) Modification of low density lipoprotein by endothelial cells involves lipid peroxidation and degradation of low density lipoprotein phospholipids. *Proceedings of the National Academy of Sciences of the United States of America*, **81**, 3883–7.

63. Sparrow,C.P. and Olszewski,J. (1993) Cellular oxidation of low density lipoprotein is caused by thiol production in media containing transition metal ions. *Journal of lipid research*, **34**, 1219–28.

64. Cathcart,M.K., Morel,D.W. and Chisolm,G.M. (1985) Monocytes and neutrophils oxidize low density lipoprotein making it cytotoxic. *Journal of leukocyte biology*, **38**, 341–50.

65. Glass,C.K. and Witztum,J.L. (2001) Atherosclerosis. the road ahead. *Cell*, **104**, 503–16.

66. Flood,C., Gustafsson,M., Richardson,P.E., Harvey,S.C., Segrest,J.P. and Borén,J. (2002) Identification of the proteoglycan binding site in apolipoprotein B48. *The Journal of biological chemistry*, **277**, 32228–33.

67. Hulley,S., Grady,D., Bush,T., Furberg,C., Herrington,D., Riggs,B. and Vittinghoff,E. (1998) Randomized trial of estrogen plus progestin for secondary prevention of coronary heart disease in postmenopausal women. Heart and Estrogen/progestin Replacement Study (HERS) Research Group. *JAMA : the journal of the American Medical Association*, **280**, 605–13.

68. Kastelein,J.J.P., Van Leuven,S.I., Burgess,L., Evans,G.W., Kuivenhoven,J.A., Barter,P.J., Revkin,J.H., Grobbee,D.E., Riley,W.A., Shear,C.L., et al. (2007) Effect of torcetrapib on carotid atherosclerosis in familial hypercholesterolemia. *The New England journal of medicine*, **356**, 1620–30.

69. Kastelein,J.J.P., Akdim,F., Stroes,E.S.G., Zwinderman,A.H., Bots,M.L., Stalenhoef,A.F.H., Visseren,F.L.J., Sijbrands,E.J.G., Trip,M.D., Stein,E.A., et al. (2008) Simvastatin with or without ezetimibe in familial hypercholesterolemia. *The New England journal of medicine*, **358**, 1431–43.

70. Keizer,H.G. (2012) The “Mevalonate hypothesis”: A cholesterol-independent alternative for the etiology of atherosclerosis. *Lipids in health and disease*, **11**, 149.

71. Ravnskov,U. (2003) High cholesterol may protect against infections and atherosclerosis. *QJM*, **96**, 927–934.

72. Allam,A.H., Thompson,R.C., Wann,L.S., Miyamoto,M.I., Nur El-Din,A.E.-H., El-Maksoud,G.A., Al-Tohamy Soliman,M., Badr,I., El-Rahman Amer,H.A., Sutherland,M.L., et al. (2011) Atherosclerosis in ancient Egyptian mummies: the Horus study. *JACC. Cardiovascular imaging*, **4**, 315–27.

73. Krauss,R.M. (2002) Is the size of low-density lipoprotein particles related to the risk of coronary heart disease? *JAMA : the journal of the American Medical Association*, **287**, 712–3.

74. Moore,K.J. and Tabas,I. (2011) Macrophages in the pathogenesis of atherosclerosis. *Cell*, **145**, 341–355.

75. McLaren,J.E., Michael,D.R., Ashlin,T.G. and Ramji,D.P. (2011) Cytokines, macrophage lipid metabolism and foam cells: implications for cardiovascular disease therapy. *Progress in lipid research*, **50**, 331–47.

76. Takahashi,K., Takeya,M. and Sakashita,N. (2002) Multifunctional roles of macrophages in the development and progression of atherosclerosis in humans and experimental animals. *Medical electron microscopy : official journal of the Clinical Electron Microscopy Society of Japan*, **35**, 179–203.

77. Johnson,J.L. and Newby,A.C. (2009) Macrophage heterogeneity in atherosclerotic plaques. *Current opinion in lipidology*, **20**, 370–8.

78. Tabas,I. (2010) Macrophage death and defective inflammation resolution in atherosclerosis. *Nature reviews. Immunology*, **10**, 36–46.

79. Mosser,D.M. and Zhang,X. (2008) Interleukin-10: new perspectives on an old cytokine. *Immunological reviews*, **226**, 205–18.

80. Martinez,F.O., Helming,L. and Gordon,S. (2009) Alternative activation of macrophages: an immunologic functional perspective. *Annual review of immunology*, **27**, 451–83.

81. Huynh,M.-L.N., Fadok,V.A. and Henson,P.M. (2002) Phosphatidylserine-dependent ingestion of apoptotic cells promotes TGF-beta1 secretion and the resolution of inflammation. *The Journal of clinical investigation*, **109**, 41–50.

82. Frutkin,A.D., Otsuka,G., Stempien-Otero,A., Sesti,C., Du,L., Jaffe,M., Dichek,H.L., Pennington,C.J., Edwards,D.R., Nieves-Cintrón,M., et al. (2009) TGF-[beta]1 limits plaque growth, stabilizes plaque structure, and prevents aortic dilation in apolipoprotein E-null mice. *Arteriosclerosis, thrombosis, and vascular biology*, **29**, 1251–7.

83. Hong,C. and Tontonoz,P. (2008) Coordination of inflammation and metabolism by PPAR and LXR nuclear receptors. *Curr Opin Genet Dev*, **18**, 461–467.

84. Feig,J.E., Pineda-Torra,I., Sanson,M., Bradley,M.N., Vengrenyuk,Y., Bogunovic,D., Gautier,E.L., Rubinstein,D., Hong,C., Liu,J., et al. (2010) LXR promotes the maximal egress of monocyte-derived cells from mouse aortic plaques during atherosclerosis regression. *The Journal of clinical investigation*, **120**, 4415–24.

85. Cuchel,M. and Rader,D.J. (2006) Macrophage reverse cholesterol transport: key to the regression of atherosclerosis? *Circulation*, **113**, 2548–55.

86. Tabas,I. (2011) Pulling down the plug on atherosclerosis: finding the culprit in your heart. *Nature Medicine*, **17**, 791–793.

87. Itabe,H., Obama,T. and Kato,R. (2011) The Dynamics of Oxidized LDL during Atherogenesis. *Journal of lipids*, **2011**, 418313.

88. Profumo,E., Buttari,B. and Riganò,R. (2011) Oxidative stress in cardiovascular inflammation: its involvement in autoimmune responses. *International journal of inflammation*, **2011**, 295705.

89. Arvieux,J., Regnault,V., Hachulla,E., Darnige,L., Berthou,F. and Youinou,P. (2001) Oxidation of beta2-glycoprotein I (beta2GPI) by the hydroxyl radical alters phospholipid binding and modulates recognition by anti-beta2GPI autoantibodies. *Thrombosis and haemostasis*, **86**, 1070–6.

90. Skålén,K., Gustafsson,M., Rydberg,E.K., Hultén,L.M., Wiklund,O., Innerarity,T.L. and Borén,J. (2002) Subendothelial retention of atherogenic lipoproteins in early atherosclerosis. *Nature*, **417**, 750–4.

91. Li,A.C. and Glass,C.K. (2002) The macrophage foam cell as a target for therapeutic intervention. *Nature medicine*, **8**, 1235–42.

92. Buttari,B., Profumo,E., Petrone,L., Pietraforte,D., Siracusano,A., Margutti,P., Delunardo,F., Ortona,E., Minetti,M., Salvati,B., et al. (2007) Free hemoglobin: a dangerous signal for the immune system in patients with carotid atherosclerosis? *Annals of the New York Academy of Sciences*, **1107**, 42–50.

93. Traber,M.G. and Kayden,H.J. (1980) Low density lipoprotein receptor activity in human monocyte-derived macrophages and its relation to atheromatous lesions. *Proceedings of the National Academy of Sciences of the United States of America*, **77**, 5466–70.

94. Moore,K.J. and Freeman,M.W. (2006) Scavenger receptors in atherosclerosis: beyond lipid uptake. *Arteriosclerosis, thrombosis, and vascular biology*, **26**, 1702–11.

95. Walton,K.A., Cole,A.L., Yeh,M., Subbanagounder,G., Krutzik,S.R., Modlin,R.L., Lucas,R.M., Nakai,J., Smart,E.J., Vora,D.K., et al. (2003) Specific phospholipid oxidation products inhibit ligand activation of toll-like receptors 4 and 2. *Arteriosclerosis, thrombosis, and vascular biology*, **23**, 1197–203.

96. Hazen,S.L. (2008) Oxidized phospholipids as endogenous pattern recognition ligands in innate immunity. *The Journal of biological chemistry*, **283**, 15527–31.

97. Chinetti-Gbaguidi,G. and Staels,B. (2009) Lipid ligand-activated transcription factors regulating lipid storage and release in human macrophages. *Biochim Biophys Acta*, **1791**, 486–493.

98. Duewell,P., Kono,H., Rayner,K.J., Sirois,C.M., Vladimer,G., Bauernfeind,F.G., Abela,G.S., Franchi,L., Nuñez,G., Schnurr,M., et al. (2010) NLRP3 inflammasomes are required for atherogenesis and activated by cholesterol crystals. *Nature*, **464**, 1357–61.

99. Tall,A.R., Yvan-Charvet,L., Terasaka,N., Pagler,T. and Wang,N. (2008) HDL, ABC transporters, and cholesterol efflux: implications for the treatment of atherosclerosis. *Cell metabolism*, **7**, 365–75.

100. Greenow,K., Pearce,N.J. and Ramji,D.P. (2005) The key role of apolipoprotein E in atherosclerosis. *Journal of molecular medicine (Berlin, Germany)*, **83**, 329–42.

101. Schrijvers,D.M., De Meyer,G.R.Y., Kockx,M.M., Herman,A.G. and Martinet,W. (2005) Phagocytosis of apoptotic cells by macrophages is impaired in atherosclerosis. *Arteriosclerosis, thrombosis, and vascular biology*, **25**, 1256–61.

102. Lusis,A.J. (2000) Atherosclerosis. *Nature*, **407**, 233–41.

103. Seimon,T. and Tabas,I. (2009) Mechanisms and consequences of macrophage apoptosis in atherosclerosis. *Journal of lipid research*, **50 Suppl**, S382–7.

104. Henson,P.M., Bratton,D.L. and Fadok,V.A. (2001) Apoptotic cell removal. *Current biology : CB*, **11**, R795–805.

105. Barish,G.D. and Evans,R.M. PPARs and LXRs: atherosclerosis goes nuclear. *Trends in endocrinology and metabolism: TEM*, **15**, 158–65.

106. Zhang,Z., Burch,P.E., Cooney,A.J., Lanz,R.B., Pereira,F.A., Wu,J., Gibbs,R.A., Weinstock,G. and Wheeler,D.A. (2004) Genomic analysis of the nuclear receptor family: new insights into structure, regulation, and evolution from the rat genome. *Genome research*, **14**, 580–90.

107. Germain,P., Staels,B., Dacquet,C., Spedding,M. and Laudet,V. (2006) Overview of nomenclature of nuclear receptors. *Pharmacological reviews*, **58**, 685–704.

108. Owen,G.I. and Zelent,A. (2000) Origins and evolutionary diversification of the nuclear receptor superfamily. *Cell Mol Life Sci*, **57**, 809–827.

109. Mangelsdorf,D.J. and Evans,R.M. (1995) The RXR heterodimers and orphan receptors. *Cell*, **83**, 841–50.

110. Kumar,R. and Thompson,E.B. (1999) The structure of the nuclear hormone receptors. *Steroids*, **64**, 310–9.

111. Sonoda,J., Pei,L. and Evans,R.M. (2008) Nuclear receptors: decoding metabolic disease. *FEBS letters*, **582**, 2–9.

112. Jin,L. and Li,Y. (2010) Structural and functional insights into nuclear receptor signalling. *Advanced drug delivery reviews*, **62**, 1218–26.

113. Hilser,V.J. and Thompson,E.B. (2011) Structural dynamics, intrinsic disorder, and allostery in nuclear receptors as transcription factors. *The Journal of biological chemistry*, **286**, 39675–82.

114. Farnham,P.J. (2009) Insights from genomic profiling of transcription factors. *Nat Rev Genet*, **10**, 605–616.

115. Khorasanizadeh,S. and Rastinejad,F. (2001) Nuclear-receptor interactions on DNA-response elements. *Trends in Biochemical Sciences*, **26**, 384–390.

116. Wright,W.E. and Funk,W.D. (1993) CASTing for multicomponent DNA-binding complexes. *Trends in biochemical sciences*, **18**, 77–80.

117. Willy,P.J. and Mangelsdorf,D.J. (1997) Unique requirements for retinoid-dependent transcriptional activation by the orphan receptor LXR. *Genes & Development*, **11**, 289–298.

118. Pabo,C.O. and Sauer,R.T. (1984) Protein-DNA recognition. *Annual review of biochemistry*, **53**, 293–321.

119. Van Tilborg,P.J., Mulder,F.A., De Backer,M.M., Nair,M., Van Heerde,E.C., Folkers,G., Van der Saag,P.T., Karimi-Nejad,Y., Boelens,R. and Kaptein,R. (1999) Millisecond to microsecond time scale dynamics of the retinoid X and retinoic acid receptor DNA-binding domains and dimeric complex formation. *Biochemistry*, **38**, 1951–6.

120. Nordeen,S.K. (1997) DNA Intersegment Transfer, How Steroid Receptors Search for A Target Site. *Journal of Biological Chemistry*, **272**, 1061–1068.

121. Voss,T.C., Schiltz,R.L., Sung,M.-H., Yen,P.M., Stamatoyannopoulos,J.A., Biddie,S.C., Johnson,T.A., Miranda,T.B., John,S. and Hager,G.L. (2011) Dynamic exchange at regulatory elements during chromatin remodeling underlies assisted loading mechanism. *Cell*, **146**, 544–54.

122. Geserick,C., Meyer,H.-A. and Haendler,B. (2005) The role of DNA response elements as allosteric modulators of steroid receptor function. *Molecular and cellular endocrinology*, **236**, 1–7.

123. Meijsing,S.H., Pufall,M.A., So,A.Y., Bates,D.L., Chen,L. and Yamamoto,K.R. (2009) DNA binding site sequence directs glucocorticoid receptor structure and activity. *Science (New York, N.Y.)*, **324**, 407–10.

124. Heinz,S., Benner,C., Spann,N., Bertolino,E., Lin,Y.C., Laslo,P., Cheng,J.X., Murre,C., Singh,H. and Glass,C.K. (2010) Simple combinations of lineage-determining transcription factors prime cis-regulatory elements required for macrophage and B cell identities. *Molecular cell*, **38**, 576–89.

125.Pehkonen,P., Welter-Stahl,L., Diwo,J., Ryynanen,J., Wienecke-Baldacchino,A., Heikkinen,S., Treuter,E., Steffensen,K.R. and Carlberg,C. (2012) Genome-wide landscape of liver X receptor chromatin binding and gene regulation in human macrophages. *BMC Genomics*, **13**, 50.

126. Boergesen,M., Pedersen,T.A., Gross,B., Van Heeringen,S.J., Hagenbeek,D., Bindesboll,C., Caron,S., Lalloyer,F., Steffensen,K.R., Nebb,H.I., et al. (2012) Genome-wide profiling of liver X receptor, retinoid X receptor, and peroxisome proliferator-activated receptor alpha in mouse liver reveals extensive sharing of binding sites. *Molecular and Cellular Biology*, **32**, 852–867.

127. John,S., Sabo,P.J., Thurman,R.E., Sung,M.-H., Biddie,S.C., Johnson,T.A., Hager,G.L. and Stamatoyannopoulos,J.A. (2011) Chromatin accessibility pre-determines glucocorticoid receptor binding patterns. *Nature genetics*, **43**, 264–8.

128. Lee,T.I. and Young,R.A. (2000) Transcription of eukaryotic protein-coding genes. *Annual review of genetics*, **34**, 77–137.

129. Chen,T. (2008) Nuclear receptor drug discovery. *Curr Opin Chem Biol*, **12**, 418–426.

130.Wagner,B.L., Valledor,A.F., Shao,G., Daige,C.L., Bischoff,E.D., Petrowski,M., Jepsen,K., Baek,S.H.H., Heyman,R.A., Rosenfeld,M.G., et al. (2003) Promoter-specific roles for liver X receptor/corepressor complexes in the regulation of ABCA1 and SREBP1 gene expression. *Molecular and cellular biology*, **23**, 5780–5789.

131. Venteclef,N., Jakobsson,T., Steffensen,K.R. and Treuter,E. (2011) Metabolic nuclear receptor signalling and the inflammatory acute phase response. *Trends in endocrinology and metabolism: TEM*, **22**, 333–43.

132. Jakobsson,T., Venteclef,N., Toresson,G., Damdimopoulos,A.E., Ehrlund,A., Lou,X., Sanyal,S., Steffensen,K.R., Gustafsson,J.-A.A. and Treuter,E. (2009) GPS2 is required for cholesterol efflux by triggering histone demethylation, LXR recruitment, and coregulator assembly at the ABCG1 locus. *Molecular cell*, **34**, 510–518.

133. Willy,P.J., Umesono,K., Ong,E.S., Evans,R.M., Heyman,R.A. and Mangelsdorf,D.J. (1995) LXR, a nuclear receptor that defines a distinct retinoid response pathway. *Genes & development*, **9**, 1033–45.

134. Song,C., Kokontis,J.M., Hiipakka,R.A. and Liao,S. (1994) Ubiquitous receptor: a receptor that modulates gene activation by retinoic acid and thyroid hormone receptors. *Proceedings of the National Academy of Sciences of the United States of America*, **91**, 10809–13.

135. Schuster,G.U. (2002) Accumulation of foam cells in liver X receptor-deficient mice. *Circulation*, **106**, 1147–1153.

136.Bradley,M.N., Hong,C., Chen,M., Joseph,S.B., Wilpitz,D.C., Wang,X., Lusis,A.J., Collins,A., Hseuh,W.A., Collins,J.L., et al. (2007) Ligand activation of LXR beta reverses atherosclerosis and cellular cholesterol overload in mice lacking LXR alpha and apoE. *J Clin Invest*, **117**, 2337–2346.

137. Tangirala,R.K., Bischoff,E.D., Joseph,S.B., Wagner,B.L., Walczak,R., Laffitte,B.A., Daige,C.L., Thomas,D., Heyman,R.A., Mangelsdorf,D.J., et al. (2002) Identification of macrophage liver X receptors as inhibitors of atherosclerosis. *Proceedings of the National Academy of Sciences of the United States of America*, **99**, 11896–901.

138. Joseph,S.B., McKilligin,E., Pei,L., Watson,M.A., Collins,A.R., Laffitte,B.A., Chen,M., Noh,G., Goodman,J., Hagger,G.N., et al. (2002) Synthetic LXR ligand

inhibits the development of atherosclerosis in mice. *Proc. Natl Acad. Sci. USA*, **99**, 7604–7609.

139. Zelcer,N. and Tontonoz,P. (2006) Liver X receptors as integrators of metabolic and inflammatory signalling. *The Journal of clinical investigation*, **116**, 607–14.

140. Krasowski,M.D., Ni,A., Hagey,L.R. and Ekins,S. (2011) Evolution of promiscuous nuclear hormone receptors: LXR, FXR, VDR, PXR, and CAR. *Molecular and Cellular Endocrinology*, **334**, 39–48.

141. Auboeuf,D., Rieusset,J., Fajas,L., Vallier,P., Frering,V., Riou,J.P., Staels,B., Auwerx,J., Laville,M. and Vidal,H. (1997) Tissue distribution and quantification of the expression of mRNAs of peroxisome proliferator-activated receptors and liver X receptor-alpha in humans: no alteration in adipose tissue of obese and NIDDM patients. *Diabetes*, **46**, 1319–27.

142. Repa,J.J. and Mangelsdorf,D.J. (2000) The role of orphan nuclear receptors in the regulation of cholesterol homeostasis. *Annual review of cell and developmental biology*, **16**, 459–81.

143. Li,Y., Bolten,C., Bhat,B.G., Woodring-Dietz,J., Li,S., Prayaga,S.K., Xia,C. and Lala,D.S. (2002) Induction of human liver X receptor alpha gene expression via an autoregulatory loop mechanism. *Mol Endocrinol*, **16**, 506–514.

144. Whitney,K.D., Watson,M.A., Goodwin,B., Galardi,C.M., Maglich,J.M., Wilson,J.G., Willson,T.M., Collins,J.L. and Kliewer,S.A. (2001) Liver X receptor (LXR) regulation of the LXRalpha gene in human macrophages. *J Biol Chem*, **276**, 43509–43515.

145. Laffitte,B.A., Joseph,S.B., Walczak,R., Pei,L., Wilpitz,D.C., Collins,J.L. and Tontonoz,P. (2001) Autoregulation of the human liver X receptor alpha promoter. *Mol Cell Biol*, **21**, 7558–7568.

146. Bischoff,E.D., Daige,C.L., Petrowski,M., Dedman,H., Pattison,J., Juliano,J., Li,A.C. and Schulman,I.G. (2010) Non-redundant roles for LXRalpha and LXRbeta in atherosclerosis susceptibility in low density lipoprotein receptor knockout mice. *Journal of lipid research*, **51**, 900–6.

147. Peet,D.J., Turley,S.D., Ma,W., Janowski,B.A., Lobaccaro,J.M., Hammer,R.E. and Mangelsdorf,D.J. (1998) Cholesterol and bile acid metabolism are impaired in mice lacking the nuclear oxysterol receptor LXR alpha. *Cell*, **93**, 693–704.

148. Repa,J.J., Liang,G., Ou,J., Bashmakov,Y., Lobaccaro,J.M., Shimomura,I., Shan,B., Brown,M.S., Goldstein,J.L. and Mangelsdorf,D.J. (2000) Regulation of mouse sterol regulatory element-binding protein-1c gene (SREBP-1c) by oxysterol receptors, LXRalpha and LXRbeta. *Genes Dev*, **14**, 2819–2830.

149. Alberti,S., Schuster,G., Parini,P., Feltkamp,D., Diczfalusy,U., Rudling,M., Angelin,B., Björkhem,I., Pettersson,S. and Gustafsson,J.A. (2001) Hepatic

cholesterol metabolism and resistance to dietary cholesterol in LXRbeta-deficient mice. *The Journal of clinical investigation*, **107**, 565–73.

150. Ferré,P. and Foufelle,F. (2007) SREBP-1c transcription factor and lipid homeostasis: clinical perspective. *Hormone research*, **68**, 72–82.

151. Barbier,O., Trottier,J., Kaeding,J., Caron,P. and Verreault,M. (2009) Lipid-activated transcription factors control bile acid glucuronidation. *Molecular and cellular biochemistry*, **326**, 3–8.

152.Volle,D.H., Repa,J.J., Mazur,A., Cummins,C.L., Val,P., Henry-Berger,J., Caira,F., Veyssiere,G., Mangelsdorf,D.J. and Lobaccaro,J.-M.A. (2004) Regulation of the aldo-keto reductase gene akr1b7 by the nuclear oxysterol receptor LXRalpha (liver X receptor-alpha) in the mouse intestine: putative role of LXRs in lipid detoxification processes. *Molecular endocrinology (Baltimore, Md.)*, **18**, 888–98.

153. Lo Sasso,G., Murzilli,S., Salvatore,L., D'Errico,I., Petruzzelli,M., Conca,P., Jiang,Z.-Y., Calabresi,L., Parini,P. and Moschetta,A. (2010) Intestinal specific LXR activation stimulates reverse cholesterol transport and protects from atherosclerosis. *Cell metabolism*, **12**, 187–93.

154. Wang,X., Collins,H.L., Ranalletta,M., Fuki,I. V, Billheimer,J.T., Rothblat,G.H., Tall,A.R. and Rader,D.J. (2007) Macrophage ABCA1 and ABCG1, but not SR-BI, promote macrophage reverse cholesterol transport in vivo. *The Journal of clinical investigation*, **117**, 2216–24.

155. Zelcer,N., Hong,C., Boyadjian,R. and Tontonoz,P. (2009) LXR regulates cholesterol uptake through Idol-dependent ubiquitination of the LDL receptor. *Science*, **325**, 100–104.

156. Wang,Y., Rogers,P.M., Su,C., Varga,G., Stayrook,K.R. and Burris,T.P. (2008) Regulation of cholesterologenesis by the oxysterol receptor, LXRalpha. *The Journal of biological chemistry*, **283**, 26332–26339.

157. Mitro,N., Mak,P.A., Vargas,L., Godio,C., Hampton,E., Molteni,V., Kreusch,A. and Saez,E. (2007) The nuclear receptor LXR is a glucose sensor. *Nature*, **445**, 219–223.

158. Korach-André,M., Archer,A., Barros,R.P., Parini,P. and Gustafsson,J.-Å. (2011) Both liver-X receptor (LXR) isoforms control energy expenditure by regulating brown adipose tissue activity. *Proceedings of the National Academy of Sciences of the United States of America*, **108**, 403–8.

159. Stenson,B.M., Rydén,M., Venteclef,N., Dahlman,I., Pettersson,A.M.L., Mairal,A., Aström,G., Blomqvist,L., Wang,V., Jocken,J.W.E., et al. (2011) Liver X receptor (LXR) regulates human adipocyte lipolysis. *The Journal of biological chemistry*, **286**, 370–9.

160. A-Gonzalez,N., Bensinger,S.J., Hong,C., Beceiro,S., Bradley,M.N., Zelcer,N., Deniz,J., Ramirez,C., Díaz,M., Gallardo,G., et al. (2009) Apoptotic

cells promote their own clearance and immune tolerance through activation of the nuclear receptor LXR. *Immunity*, **31**, 245–58.

161. Blaschke,F., Takata,Y., Caglayan,E., Collins,A., Tontonoz,P., Hsueh,W.A. and Tangirala,R.K. (2006) A nuclear receptor corepressor-dependent pathway mediates suppression of cytokine-induced C-reactive protein gene expression by liver X receptor. *Circulation research*, **99**, e88–99.

162. Koldamova,R. and Lefterov,I. (2007) Role of LXR and ABCA1 in the pathogenesis of Alzheimer's disease - implications for a new therapeutic approach. *Current Alzheimer research*, **4**, 171–8.

163. Leoni,V. and Caccia,C. (2011) Oxysterols as biomarkers in neurodegenerative diseases. *Chemistry and physics of lipids*, **164**, 515–24.

164. Zelcer,N., Khanlou,N., Clare,R., Jiang,Q., Reed-Geaghan,E.G., Landreth,G.E., Vinters,H. V and Tontonoz,P. (2007) Attenuation of neuroinflammation and Alzheimer's disease pathology by liver x receptors. *Proceedings of the National Academy of Sciences of the United States of America*, **104**, 10601–6.

165. Koldamova,R., Fitz,N.F. and Lefterov,I. (2010) The role of ATP-binding cassette transporter A1 in Alzheimer's disease and neurodegeneration. *Biochimica et biophysica acta*, **1801**, 824–30.

166. Francis,G.A. (2010) The complexity of HDL. *Biochimica et biophysica acta*, **1801**, 1286–93.

167. Tontonoz,P. and Mangelsdorf,D.J. (2003) Liver X receptor signalling pathways in cardiovascular disease. *Molecular endocrinology (Baltimore, Md.)*, **17**, 985–93.

168. Rigamonti,E., Helin,L., Lestavel,S., Mutka,A.L., Lepore,M., Fontaine,C., Bouhlel,M.A., Bultel,S., Fruchart,J.C., Ikonen,E., et al. (2005) Liver X receptor activation controls intracellular cholesterol trafficking and esterification in human macrophages. *Circ Res*, **97**, 682–689.

169. Venkateswaran,A., Laffitte,B.A., Joseph,S.B., Mak,P.A., Wilpitz,D.C., Edwards,P.A. and Tontonoz,P. (2000) Control of cellular cholesterol efflux by the nuclear oxysterol receptor LXR alpha. *Proceedings of the National Academy of Sciences of the United States of America*, **97**, 12097–102.

170. Repa,J.J. (2000) Regulation of Absorption and ABC1-Mediated Efflux of Cholesterol by RXR Heterodimers. *Science*, **289**, 1524–1529.

171. Tangirala,R.K., Bischoff,E.D., Joseph,S.B., Wagner,B.L., Walczak,R., Laffitte,B.A., Daige,C.L., Thomas,D., Heyman,R.A., Mangelsdorf,D.J., et al. (2002) Identification of macrophage liver X receptors as inhibitors of atherosclerosis. *Proc Natl Acad Sci U S A*, **99**, 11896–11901.

172. Wójcicka,G., Jamroz-Wiśniewska,A., Horoszewicz,K. and Bełtowski,J. (2007) Liver X receptors (LXRs). Part I: structure, function, regulation of activity, and role in lipid metabolism. *Postępy higieny i medycyny doświadczalnej (Online)*, **61**, 736–59.

173. Laffitte,B.A., Repa,J.J., Joseph,S.B., Wilpitz,D.C., Kast,H.R., Mangelsdorf,D.J. and Tontonoz,P. (2001) LXRs control lipid-inducible expression of the apolipoprotein E gene in macrophages and adipocytes. *Proceedings of the National Academy of Sciences*, **98**, 507–512.

174. Luo,Y. and Tall,A.R. (2000) Sterol upregulation of human CETP expression in vitro and in transgenic mice by an LXR element. *The Journal of clinical investigation*, **105**, 513–20.

175. Zhang,Y., Repa,J.J., Gauthier,K. and Mangelsdorf,D.J. (2001) Regulation of lipoprotein lipase by the oxysterol receptors, LXRalpha and LXRbeta. *The Journal of biological chemistry*, **276**, 43018–24.

176. Gui,T., Shimokado,A., Sun,Y., Akasaka,T. and Muragaki,Y. (2012) Diverse roles of macrophages in atherosclerosis: from inflammatory biology to biomarker discovery. *Mediators of inflammation*, **2012**, 693083.

177. Janowski,B.A., Willy,P.J., Devi,T.R., Falck,J.R. and Mangelsdorf,D.J. (1996) An oxysterol signalling pathway mediated by the nuclear receptor LXRα. *Nature*, **383**, 728–731.

178. Björkhem,I. (2002) Do oxysterols control cholesterol homeostasis? *The Journal of clinical investigation*, **110**, 725–30.

179. Janowski,B., Grogan,M., Jones,S., Wisely,G., Kliewer,S., Corey,E. and Mangelsdorf,D. (1999) Structural requirements of ligands for the oxysterol liver X receptors LXRalpha and LXRbeta. *Proceedings of the National Academy of Sciences of the United States of America*, **96**, 266–271.

180. Bethany A. Janowski, Michael J. Grogan, Stacey A. Jones, G. Bruce Wisely, Steven A. Kliewer, Elias J. Corey,D.J.M. (1999) Structural requirements of ligands for the oxysterol liver X receptors LXRa and LXRb. *Proc. Natl. Acad. Sci. USA*, **96**, 266–271.

181. Lehmann,J.M., Kliewer,S.A., Moore,L.B., Smith-Oliver,T.A., Oliver,B.B., Su,J.L., Sundseth,S.S., Winegar,D.A., Blanchard,D.E., Spencer,T.A., et al. (1997) Activation of the nuclear receptor LXR by oxysterols defines a new hormone response pathway. *The Journal of biological chemistry*, **272**, 3137–40.

182. Färnegårdh,M., Bonn,T., Sun,S., Ljunggren,J., Ahola,H., Wilhelmsson,A., Gustafsson,J.-A. and Carlquist,M. (2003) The three-dimensional structure of the liver X receptor beta reveals a flexible ligand-binding pocket that can accommodate fundamentally different ligands. *The Journal of biological chemistry*, **278**, 38821–8.

183. Viennois,E., Mouzat,K., Dufour,J., Morel,L., Lobaccaro,J.-M. and Baron,S. (2012) Selective liver X receptor modulators (SLiMs): what use in human health? *Molecular and cellular endocrinology*, **351**, 129–41.

184. Gronemeyer,H., Gustafsson,J.A. and Laudet,V. (2004) Principles for modulation of the nuclear receptor superfamily. *Nat Rev Drug Discov*, **3**, 950–964.

185. Jakobsson,T., Treuter,E., Gustafsson,J.-Å. and Steffensen,K.R. (2012) Liver X receptor biology and pharmacology: new pathways, challenges and opportunities. *Trends in Pharmacological Sciences*, **33**, 394–404.

186. Terasaka,N., Hiroshima,A., Koieyama,T., Ubukata,N., Morikawa,Y., Nakai,D. and Inaba,T. (2003) T-0901317, a synthetic liver X receptor ligand, inhibits development of atherosclerosis in LDL receptor-deficient mice. *FEBS Letters*, **536**, 6–11.

187. Levin,N., Bischoff,E.D., Daige,C.L., Thomas,D., Vu,C.T., Heyman,R.A., Tangirala,R.K. and Schulman,I.G. (2005) Macrophage liver X receptor is required for antiatherogenic activity of LXR agonists. *Arteriosclerosis, thrombosis, and vascular biology*, **25**, 135–42.

188. Verschuren,L., De Vries-van der Weij,J., Zadelaar,S., Kleemann,R. and Kooistra,T. (2009) LXR agonist suppresses atherosclerotic lesion growth and promotes lesion regression in apoE*3Leiden mice: time course and mechanisms. *J. Lipid Res.*, **50**, 301–311.

189. Laffitte,B.A., Chao,L.C., Li,J., Walczak,R., Hummasti,S., Joseph,S.B., Castrillo,A., Wilpitz,D.C., Mangelsdorf,D.J., Collins,J.L., et al. (2003) Activation of liver X receptor improves glucose tolerance through coordinate regulation of glucose metabolism in liver and adipose tissue. *Proc Natl Acad Sci U S A*, **100**, 5419–5424.

190. Schultz,J.R. (2000) Role of LXRs in control of lipogenesis. *Genes & Development*, **14**, 2831–2838.

191. Grefhorst,A., Elzinga,B.M., Voshol,P.J., Plösch,T., Kok,T., Bloks,V.W., Van der Sluijs,F.H., Havekes,L.M., Romijn,J.A., Verkade,H.J., et al. (2002) Stimulation of lipogenesis by pharmacological activation of the liver X receptor leads to production of large, triglyceride-rich very low density lipoprotein particles. *The Journal of biological chemistry*, **277**, 34182–90.

192. Heintzman,N.D., Stuart,R.K., Hon,G., Fu,Y., Ching,C.W., Hawkins,R.D., Barrera,L.O., Van Calcar,S., Qu,C., Ching,K.A., et al. (2007) Distinct and predictive chromatin signatures of transcriptional promoters and enhancers in the human genome. *Nat Genet*, **39**, 311–318.

193. Cai,Y.-H. and Huang,H. (2012) Advances in the study of protein-DNA interaction. *Amino acids*, **43**, 1141–6.

194. Park,P.J. (2009) ChIP-seq: advantages and challenges of a maturing technology. *Nat Rev Genet*, **10**, 669–680.

195. Hao,H. (2012) Genome-wide occupancy analysis by ChIP-chip and ChIP-Seq. *Advances in experimental medicine and biology*, **723**, 753–9.

196. Mikkelsen,T.S., Ku,M., Jaffe,D.B., Issac,B., Lieberman,E., Giannoukos,G., Alvarez,P., Brockman,W., Kim,T.-K., Koche,R.P., et al. (2007) Genome-wide maps of chromatin state in pluripotent and lineage-committed cells. *Nature*, **448**, 553–60.

197. Barski,A. and Zhao,K. (2009) Genomic location analysis by ChIP-Seq. *Journal of cellular biochemistry*, **107**, 11–8.

198. Mardis,E.R. (2007) ChIP-seq: welcome to the new frontier. *Nature methods*, **4**, 613–4.

199. Landt,S.G., Marinov,G.K., Kundaje,A., Kheradpour,P., Pauli,F., Batzoglou,S., Bernstein,B.E., Bickel,P., Brown,J.B., Cayting,P., et al. (2012) ChIP-seq guidelines and practices of the ENCODE and modENCODE consortia. *Genome research*, **22**, 1813–31.

200. Li,Q., Brown,J.B., Huang,H. and Bickel,P.J. (2011) Measuring reproducibility of high-throughput experiments. *The Annals of Applied Statistics*, **5**, 1752–1779.

201. Rye,M.B., Sætrom,P. and Drabløs,F. (2011) A manually curated ChIP-seq benchmark demonstrates room for improvement in current peak-finder programs. *Nucleic acids research*, **39**, e25.

202. Ma,W. and Wong,W.H. (2011) The analysis of ChIP-Seq data. *Methods in enzymology*, **497**, 51–73.

203. Ghazalpour,A., Doss,S., Yang,X., Aten,J., Toomey,E.M., Nas,A. Van, Wang,S., Drake,T.A. and Lusis,A.J. (2004) Thematic review series: The Pathogenesis of Atherosclerosis. Toward a biological network for atherosclerosis. *Journal of Lipid Research*, **45**, 1793–1805.

204. Schadt,E.E. and Lum,P.Y. (2006) Thematic review series: systems biology approaches to metabolic and cardiovascular disorders. Reverse engineering gene networks to identify key drivers of complex disease phenotypes. *Journal of lipid research*, **47**, 2601–13.

205. Duarte,N.C., Becker,S.A., Jamshidi,N., Thiele,I., Mo,M.L., Vo,T.D., Srivas,R. and Palsson,B.Ø. (2007) Global reconstruction of the human metabolic network based on genomic and bibliomic data. *Proceedings of the National Academy of Sciences of the United States of America*, **104**, 1777–82.

206. Weiss,J.N., Yang,L. and Qu,Z. (2006) Systems biology approaches to metabolic and cardiovascular disorders: network perspectives of cardiovascular metabolism. *Journal of lipid research*, **47**, 2355–66.

207. Weidner,C., De Groot,J.C., Prasad,A., Freiwald,A., Quedenau,C., Kliem,M., Witzke,A., Kodelja,V., Han,C.-T., Giegold,S., et al. (2012) Amorfrutins are potent antidiabetic dietary natural products. *Proceedings of the National Academy of Sciences*, **109**, 7257–62.

208. Nedumaran,B., Kim,G.S., Hong,S., Yoon,Y.-S., Kim,Y.-H., Lee,C.-H., Lee,Y.C., Koo,S.-H. and Choi,H.-S. (2010) Orphan nuclear receptor DAX-1 acts as a novel corepressor of liver X receptor alpha and inhibits hepatic lipogenesis. *The Journal of biological chemistry*, **285**, 9221–32.

209. Chinetti-Gbaguidi,G., Baron,M., Bouhlel,M.A., Vanhoutte,J., Copin,C., Sebti,Y., Derudas,B., Mayi,T., Bories,G., Tailleux,A., et al. (2011) Human Atherosclerotic Plaque Alternative Macrophages Display Low Cholesterol Handling but High Phagocytosis Because of Distinct Activities of the PPAR and LXR Pathways. *Circulation Research*, **108**, 985–995.

210. Mogilenko,D.A., Shavva,V.S., Dizhe,E.B., Orlov,S. V and Perevozchikov,A.P. (2010) PPARγ activates ABCA1 gene transcription but reduces the level of ABCA1 protein in HepG2 cells. *Biochemical and biophysical research communications*, **402**, 477–482.

211. Langmead,B., Trapnell,C., Pop,M. and Salzberg,S.L. (2009) Ultrafast and memory-efficient alignment of short DNA sequences to the human genome. *Genome biology*, **10**, R25.

212. Zhang,Y., Liu,T., Meyer,C.A., Eeckhoute,J., Johnson,D.S., Bernstein,B.E., Nusbaum,C., Myers,R.M., Brown,M., Li,W., et al. (2008) Model-based analysis of ChIP-Seq (MACS). *Genome biology*, **9**, R137.

213. Kent,W.J., Zweig,A.S., Barber,G., Hinrichs,A.S. and Karolchik,D. (2010) BigWig and BigBed: enabling browsing of large distributed datasets. *Bioinformatics (Oxford, England)*, **26**, 2204–7.

214. Karolchik,D., Hinrichs,A.S. and Kent,W.J. (2011) The UCSC Genome Browser. *Current protocols in human genetics / editorial board, Jonathan L. Haines ... [et al.]*, **Chapter 18**, Unit18.6.

215. Xu,H., Handoko,L., Wei,X., Ye,C., Sheng,J., Wei,C.-L., Lin,F. and Sung,W.-K. (2010) A signal-noise model for significance analysis of ChIP-seq with negative control. *Bioinformatics (Oxford, England)*, **26**, 1199–204.

216. Ye,T., Krebs,A.R., Choukrallah,M.-A., Keime,C., Plewniak,F., Davidson,I. and Tora,L. (2011) seqMINER: an integrated ChIP-seq data interpretation platform. *Nucleic acids research*, **39**, e35.

217. Heintzman,N.D., Hon,G.C., Hawkins,R.D., Kheradpour,P., Stark,A., Harp,L.F., Ye,Z., Lee,L.K., Stuart,R.K., Ching,C.W., et al. (2009) Histone modifications at human enhancers reflect global cell-type-specific gene expression. *Nature*, **459**, 108–12.

218. Bardet,A.F., He,Q., Zeitlinger,J. and Stark,A. (2012) A computational pipeline for comparative ChIP-seq analyses. *Nat. Protocols*, **7**, 45–61.

219. Giresi,P.G. and Lieb,J.D. (2009) Isolation of active regulatory elements from eukaryotic chromatin using FAIRE (Formaldehyde Assisted Isolation of Regulatory Elements). *Methods (San Diego, Calif.)*, **48**, 233–9.

220. Boyle,A.P., Davis,S., Shulha,H.P., Meltzer,P., Margulies,E.H., Weng,Z., Furey,T.S. and Crawford,G.E. (2008) High-resolution mapping and characterization of open chromatin across the genome. *Cell*, **132**, 311–22.

221. Moorman,C., Sun,L. V, Wang,J., De Wit,E., Talhout,W., Ward,L.D., Greil,F., Lu,X.-J., White,K.P., Bussemaker,H.J., et al. (2006) Hotspots of transcription factor colocalization in the genome of Drosophila melanogaster. *Proceedings of the National Academy of Sciences of the United States of America*, **103**, 12027–32.

222. Li,X.-Y., Thomas,S., Sabo,P.J., Eisen,M.B., Stamatoyannopoulos,J.A. and Biggin,M.D. (2011) The role of chromatin accessibility in directing the widespread, overlapping patterns of Drosophila transcription factor binding. *Genome biology*, **12**, R34.

223. Siersbæk,R., Nielsen,R., John,S., Sung,M.-H., Baek,S., Loft,A., Hager,G.L. and Mandrup,S. (2011) Extensive chromatin remodelling and establishment of transcription factor "hotspots" during early adipogenesis. *The EMBO journal*, **30**, 1459–72.

224. Myers,R.M., Stamatoyannopoulos,J., Snyder,M., Dunham,I., Hardison,R.C., Bernstein,B.E., Gingeras,T.R., Kent,W.J., Birney,E., Wold,B., et al. (2011) A user's guide to the encyclopedia of DNA elements (ENCODE). *PLoS biology*, **9**, e1001046.

225. Machanick,P. and Bailey,T.L. (2011) MEME-ChIP: motif analysis of large DNA datasets. *Bioinformatics (Oxford, England)*, **27**, 1696–7.

226. Matys,V., Fricke,E., Geffers,R., Gössling,E., Haubrock,M., Hehl,R., Hornischer,K., Karas,D., Kel,A.E., Kel-Margoulis,O. V, et al. (2003) TRANSFAC: transcriptional regulation, from patterns to profiles. *Nucleic acids research*, **31**, 374–8.

227. Mahony,S. and Benos,P. V (2007) STAMP: a web tool for exploring DNA-binding motif similarities. *Nucleic acids research*, **35**, W253–8.

228. Shin,H., Liu,T., Manrai,A.K. and Liu,X.S. (2009) CEAS: cis-regulatory element annotation system. *Bioinformatics (Oxford, England)*, **25**, 2605–6.

229. Teif,V.B. (2010) Predicting gene-regulation functions: lessons from temperate bacteriophages. *Biophysical journal*, **98**, 1247–56.

230. Fujita,P.A., Rhead,B., Zweig,A.S., Hinrichs,A.S., Karolchik,D., Cline,M.S., Goldman,M., Barber,G.P., Clawson,H., Coelho,A., et al. (2011) The UCSC Genome Browser database: update 2011. *Nucleic acids research*, **39**, D876–82.

231. Livak,K.J. and Schmittgen,T.D. (2001) Analysis of relative gene expression data using real-time quantitative PCR and the 2(-Delta Delta C(T)) Method. *Methods (San Diego, Calif.)*, **25**, 402–8.

232. Rozen,S. and Skaletsky,H. (2000) Primer3 on the WWW for general users and for biologist programmers. *Methods in molecular biology (Clifton, N.J.)*, **132**, 365–86.

233. National Center for Biotechnology Information (NCBI) (2000) No Title. *Primer-BLAST*.

234. Benjamini, Yoav; Hochberg,Y. (1995) Controlling the false discovery rate: a practical and powerful approach to multiple testing. *Journal of the Royal Statistical Society*, **Series B (**, 289–300.

235. Saeed,A.I., Sharov,V., White,J., Li,J., Liang,W., Bhagabati,N., Braisted,J., Klapa,M., Currier,T., Thiagarajan,M., et al. (2003) TM4: a free, open-source system for microarray data management and analysis. *Biotechniques*, **34**, 374–378.

236. Subramanian,A., Tamayo,P., Mootha,V.K., Mukherjee,S., Ebert,B.L., Gillette,M.A., Paulovich,A., Pomeroy,S.L., Golub,T.R., Lander,E.S., et al. (2005) Gene set enrichment analysis: a knowledge-based approach for interpreting genome-wide expression profiles. *Proc Natl Acad Sci U S A*, **102**, 15545–15550.

237. Huang,D.W., Sherman,B.T. and Lempicki,R.A. (2009) Systematic and integrative analysis of large gene lists using DAVID bioinformatics resources. *Nature protocols*, **4**, 44–57.

238. Battke,F., Symons,S. and Nieselt,K. (2010) Mayday--integrative analytics for expression data. *BMC bioinformatics*, **11**, 121.

239. Karlić,R., Chung,H.-R., Lasserre,J., Vlahovicek,K. and Vingron,M. (2010) Histone modification levels are predictive for gene expression. *Proceedings of the National Academy of Sciences of the United States of America*, **107**, 2926–31.

240. Van Dijk,K., Ding,Y., Malkaram,S., Riethoven,J.-J.M., Liu,R., Yang,J., Laczko,P., Chen,H., Xia,Y., Ladunga,I., et al. (2010) Dynamic changes in genome-wide histone H3 lysine 4 methylation patterns in response to dehydration stress in Arabidopsis thaliana. *BMC plant biology*, **10**, 238.

241. Haw,R.A., Croft,D., Yung,C.K., Ndegwa,N., D'Eustachio,P., Hermjakob,H. and Stein,L.D. (2011) The Reactome BioMart. *Database : the journal of biological databases and curation*, **2011**, bar031.

242. Calvano,S.E., Xiao,W., Richards,D.R., Felciano,R.M., Baker,H. V, Cho,R.J., Chen,R.O., Brownstein,B.H., Cobb,J.P., Tschoeke,S.K., et al. (2005) A network-based analysis of systemic inflammation in humans. *Nature*, **437**, 1032–7.

243. Hindorff,L.A., Sethupathy,P., Junkins,H.A., Ramos,E.M., Mehta,J.P., Collins,F.S. and Manolio,T.A. (2009) Potential etiologic and functional implications of genome-wide association loci for human diseases and traits. *Proceedings of the National Academy of Sciences of the United States of America*, **106**, 9362–7.

244. Pallejà,A., Horn,H., Eliasson,S. and Jensen,L.J. (2012) DistiLD Database: diseases and traits in linkage disequilibrium blocks. *Nucleic acids research*, **40**, D1036–40.

245. Kawaji,H., Severin,J., Lizio,M., Forrest,A.R.R., Van Nimwegen,E., Rehli,M., Schroder,K., Irvine,K., Suzuki,H., Carninci,P., et al. (2011) Update of the FANTOM web resource: from mammalian transcriptional landscape to its dynamic regulation. *Nucleic acids research*, **39**, D856–60.

246. Jensen,L.J., Kuhn,M., Stark,M., Chaffron,S., Creevey,C., Muller,J., Doerks,T., Julien,P., Roth,A., Simonovic,M., et al. (2009) STRING 8--a global view on proteins and their functional interactions in 630 organisms. *Nucleic acids research*, **37**, D412–6.

247. Smoot,M.E., Ono,K., Ruscheinski,J., Wang,P.-L. and Ideker,T. (2011) Cytoscape 2.8: new features for data integration and network visualization. *Bioinformatics (Oxford, England)*, **27**, 431–2.

248. Stark,C., Breitkreutz,B.-J., Reguly,T., Boucher,L., Breitkreutz,A. and Tyers,M. (2006) BioGRID: a general repository for interaction datasets. *Nucleic acids research*, **34**, D535–9.

249. Kupershmidt,I., Su,Q.J., Grewal,A., Sundaresh,S., Halperin,I., Flynn,J., Shekar,M., Wang,H., Park,J., Cui,W., et al. (2010) Ontology-based meta-analysis of global collections of high-throughput public data. *PloS one*, **5**.

250. Auwerx,J. (1991) The human leukemia cell line, THP-1: a multifacetted model for the study of monocyte-macrophage differentiation. *Experientia*, **47**, 22–31.

251. Watanabe,Y., Jiang,S., Takabe,W., Ohashi,R., Tanaka,T., Uchiyama,Y., Katsumi,K., Iwanari,H., Noguchi,N., Naito,M., et al. (2005) Expression of the LXRalpha protein in human atherosclerotic lesions. *Arterioscler Thromb Vasc Biol*, **25**, 622–627.

252. Leleu,M., Lefebvre,G. and Rougemont,J. (2010) Processing and analyzing ChIP-seq data: from short reads to regulatory interactions. *Briefings in functional genomics*, **9**, 466–76.

253. Hu,X., Li,S., Wu,J., Xia,C. and Lala,D.S. (2003) Liver X receptors interact with corepressors to regulate gene expression. *Molecular endocrinology (Baltimore, Md.)*, **17**, 1019–26.

254. Cockerill,P.N. (2011) Structure and function of active chromatin and DNase I hypersensitive sites. *The FEBS journal*, **278**, 2182–210.

255. Laffitte,B.A., Repa,J.J., Joseph,S.B., Wilpitz,D.C., Kast,H.R., Mangelsdorf,D.J. and Tontonoz,P. (2001) LXRs control lipid-inducible expression of the apolipoprotein E gene in macrophages and adipocytes. *PNAS*, **98**, 507–512.

256. Mak,P.A., Laffitte,B.A., Desrumaux,C., Joseph,S.B., Curtiss,L.K., Mangelsdorf,D.J., Tontonoz,P. and Edwards,P.A. (2002) Regulated expression of the apolipoprotein E/C-I/C-IV/C-II gene cluster in murine and human macrophages. A critical role for nuclear liver X receptors alpha and beta. *The Journal of biological chemistry*, **277**, 31900–8.

257. Kathiresan,S., Melander,O., Guiducci,C., Surti,A., Burtt,N.P., Rieder,M.J., Cooper,G.M., Roos,C., Voight,B.F., Havulinna,A.S., et al. (2008) Six new loci associated with blood low-density lipoprotein cholesterol, high-density lipoprotein cholesterol or triglycerides in humans. *Nature Genetics*, **40**, 189–197.

258. Apfel,R., Benbrook,D., Lernhardt,E., Ortiz,M.A., Salbert,G. and Pfahl,M. (1994) A novel orphan receptor specific for a subset of thyroid hormone-responsive elements and its interaction with the retinoid/thyroid hormone receptor subfamily. *Molecular and cellular biology*, **14**, 7025–35.

259. Repa,J.J. and Mangelsdorf,D.J. (1999) Nuclear receptor regulation of cholesterol and bile acid metabolism. *Current opinion in biotechnology*, **10**, 557–63.

260. Otarod,J.K. and Goldberg,I.J. (2004) Lipoprotein lipase and its role in regulation of plasma lipoproteins and cardiac risk. *Curr Atheroscler Rep*, **6**, 335–342.

261. Stein,Y. and Stein,O. (2003) Lipoprotein lipase and atherosclerosis. *Atherosclerosis*, **170**, 1–9.

262. Wang,H. and Eckel,R.H. (2009) Lipoprotein lipase: from gene to obesity. *American journal of physiology. Endocrinology and metabolism*, **297**, E271–88.

263. Zhang,Y., Adams,I.P. and Ratledge,C. (2007) Malic enzyme: the controlling activity for lipid production? Overexpression of malic enzyme in Mucor circinelloides leads to a 2.5-fold increase in lipid accumulation. *Microbiology (Reading, England)*, **153**, 2013–25.

264. Schneider,R. and Grosschedl,R. (2007) Dynamics and interplay of nuclear architecture, genome organization, and gene expression. *Genes & development*, **21**, 3027–43.

265. Freeman,M.W. and Moore,K.J. (2003) eLiXiRs for restraining inflammation. *Nat Med*, **9**, 168–169.

266. McCarthy,M.I., Abecasis,G.R., Cardon,L.R., Goldstein,D.B., Little,J., Ioannidis,J.P.A. and Hirschhorn,J.N. (2008) Genome-wide association studies for complex traits: consensus, uncertainty and challenges. *Nature reviews. Genetics*, **9**, 356–69.

267. Patel,N. V and Forman,B.M.M. (2004) Linking lipids, Alzheimer's and LXRs? *Nuclear receptor signalling*, **2**.

268. Gupta,D.S., Kaul,D., Kanwar,A.J. and Parsad,D. (2009) Psoriasis: crucial role of LXR-α RNomics. *Genes and Immunity*, **11**, 37–44.

269. Ge,B., Li,O., Wilder,P., Rizzino,A. and McKeithan,T.W. (2003) NF-{kappa}B Regulates BCL3 Transcription in T Lymphocytes Through an Intronic Enhancer. *J. Immunol.*, **171**, 4210–4218.

270. Xia,Y., Pauza,M.E., Feng,L. and Lo,D. (1997) RelB regulation of chemokine expression modulates local inflammation. *The American journal of pathology*, **151**, 375–87.

271. Porcellini,E., Carbone,I., Ianni,M. and Licastro,F. (2010) Alzheimer's disease gene signature says: beware of brain viral infections. *Immunity & ageing : I & A*, **7**, 16.

272. Shibata,N. and Glass,C.K. (2009) Regulation of macrophage function in inflammation and atherosclerosis. *Journal of lipid research*, **50 Suppl**, S277–81.

273. Valledor,A.F., Hsu,L.-C., Ogawa,S., Sawka-Verhelle,D., Karin,M. and Glass,C.K. (2004) Activation of liver X receptors and retinoid X receptors prevents bacterial-induced macrophage apoptosis. *Proceedings of the National Academy of Sciences of the United States of America*, **101**, 17813–8.

274. Calkin,A.C. and Tontonoz,P. (2010) Liver x receptor signalling pathways and atherosclerosis. *Arteriosclerosis, thrombosis, and vascular biology*, **30**, 1513–1518.

275. Chu,K., Miyazaki,M., Man,W.C. and Ntambi,J.M. (2006) Stearoyl-coenzyme A desaturase 1 deficiency protects against hypertriglyceridemia and increases plasma high-density lipoprotein cholesterol induced by liver X receptor activation. *Molecular and cellular biology*, **26**, 6786–98.

276. Paradis,V., Bièche,I., Dargère,D., Cazals-Hatem,D., Laurendeau,I., Saada,V., Belghiti,J., Bezeaud,A., Vidaud,M., Bedossa,P., et al. (2005) Quantitative gene expression in Budd-Chiari syndrome: a molecular approach to the pathogenesis of the disease. *Gut*, **54**, 1776–81.

277. Sierro,F., Biben,C., Martínez-Muñoz,L., Mellado,M., Ransohoff,R.M., Li,M., Woehl,B., Leung,H., Groom,J., Batten,M., et al. (2007) Disrupted cardiac development but normal hematopoiesis in mice deficient in the second

CXCL12/SDF-1 receptor, CXCR7. *Proceedings of the National Academy of Sciences of the United States of America*, **104**, 14759–64.

278. Bowcock,A.M., Shannon,W., Du,F., Duncan,J., Cao,K., Aftergut,K., Catier,J., Fernandez-Vina,M.A. and Menter,A. (2001) Insights into psoriasis and other inflammatory diseases from large-scale gene expression studies. *Human molecular genetics*, **10**, 1793–805.

279. Lequerré,T., Bansard,C., Vittecoq,O., Derambure,C., Hiron,M., Daveau,M., Tron,F., Ayral,X., Biga,N., Auquit-Auckbur,I., et al. (2009) Early and long-standing rheumatoid arthritis: distinct molecular signatures identified by gene-expression profiling in synovia. *Arthritis research & therapy*, **11**, R99.

280. Gerhardinger,C., Costa,M.B., Coulombe,M.C., Toth,I., Hoehn,T. and Grosu,P. (2005) Expression of acute-phase response proteins in retinal Müller cells in diabetes. *Investigative ophthalmology & visual science*, **46**, 349–57.

281. Zhang,J., Xu,L.-G., Han,K.-J., Wei,X. and Shu,H.-B. (2004) PIASy represses TRIF-induced ISRE and NF-kappaB activation but not apoptosis. *FEBS letters*, **570**, 97–101.

282. Zhao,C. and Dahlman-Wright,K. (2010) Liver X receptor in cholesterol metabolism. *The Journal of endocrinology*, **204**, 233–40.

283. Sauer,S., Lange,B.M.H., Gobom,J., Nyarsik,L., Seitz,H. and Lehrach,H. (2005) Miniaturization in functional genomics and proteomics. *Nature reviews. Genetics*, **6**, 465–76.

284. Wang,N. and Tall,A.R. (2003) Regulation and mechanisms of ATP-binding cassette transporter A1-mediated cellular cholesterol efflux. *Arteriosclerosis, thrombosis, and vascular biology*, **23**, 1178–84.

285. Rommel,C. and Hafen,E. (1998) Ras - a versatile cellular switch. *Current Opinion in Genetics & Development*, **8**, 412–418.

286. Lander,H.M., Ogiste,J.S., Teng,K.K. and Novogrodsky,A. (1995) p21ras as a common signalling target of reactive free radicals and cellular redox stress. *The Journal of biological chemistry*, **270**, 21195–8.

287. Deora,A.A. (1998) A Redox-triggered Ras-Effector Interaction. RECRUITMENT OF PHOSPHATIDYLINOSITOL 3'-KINASE TO Ras BY REDOX STRESS. *Journal of Biological Chemistry*, **273**, 29923–29928.

288. Li,A.C. and Glass,C.K. (2004) PPAR- and LXR-dependent pathways controlling lipid metabolism and the development of atherosclerosis. *Journal of lipid research*, **45**, 2161–73.

289. Pacher,P. and Szabó,C. (2007) Role of poly(ADP-ribose) polymerase 1 (PARP-1) in cardiovascular diseases: the therapeutic potential of PARP inhibitors. *Cardiovascular drug reviews*, **25**, 235–260.

290. Bai,P., Canto,C., Oudart,H., Brunyanszki,A., Cen,Y., Thomas,C., Yamamoto,H., Huber,A., Kiss,B., Houtkooper,R.H., et al. (2011) PARP-1 inhibition increases mitochondrial metabolism through SIRT1 activation. *Cell Metab*, **13**, 461–468.

291. Gaulton,K.J., Nammo,T., Pasquali,L., Simon,J.M., Giresi,P.G., Fogarty,M.P., Panhuis,T.M., Mieczkowski,P., Secchi,A., Bosco,D., et al. (2010) A map of open chromatin in human pancreatic islets. *Nature genetics*, **42**, 255–9.

292. Ramagopalan,S. V, Heger,A., Berlanga,A.J., Maugeri,N.J., Lincoln,M.R., Burrell,A., Handunnetthi,L., Handel,A.E., Disanto,G., Orton,S.M., et al. A ChIP-seq defined genome-wide map of vitamin D receptor binding: associations with disease and evolution. *Genome Res*, **20**, 1352–1360.

293. Calkin,A.C. and Tontonoz,P. (2012) Transcriptional integration of metabolism by the nuclear sterol-activated receptors LXR and FXR. *Nature reviews. Molecular cell biology*, **13**, 213–24.

294. Deloukas,P., Kanoni,S., Willenborg,C., Farrall,M., Assimes,T.L., Thompson,J.R., Ingelsson,E., Saleheen,D., Erdmann,J., Goldstein,B.A., et al. (2012) Large-scale association analysis identifies new risk loci for coronary artery disease. *Nature Genetics*, **45**, 25–33.

295. Lee,D.-S., Park,J., Kay,K.A., Christakis,N.A., Oltvai,Z.N. and Barabási,A.-L. (2008) The implications of human metabolic network topology for disease comorbidity. *Proceedings of the National Academy of Sciences of the United States of America*, **105**, 9880–5.

296. Bradley,M.N., Zhou,L. and Smale,S.T. (2003) C/EBP Regulation in Lipopolysaccharide-Stimulated Macrophages. *Molecular and Cellular Biology*, **23**, 4841–4858.

297. Gilmore,T.D. (2006) Introduction to NF-kappaB: players, pathways, perspectives. *Oncogene*, **25**, 6680–4.

298. Radhakrishnan,S.K. and Kamalakaran,S. (2006) Pro-apoptotic role of NF-kappaB: implications for cancer therapy. *Biochimica et biophysica acta*, **1766**, 53–62.

299. Im,S.-S.S. and Osborne,T.F. (2011) Liver x receptors in atherosclerosis and inflammation. *Circulation research*, **108**, 996–1001.

300. Steffensen,K.R. and Gustafsson,J.-A. (2004) Putative Metabolic Effects of the Liver X Receptor (LXR). *Diabetes*, **53**, 36S–42.

301. Tian,B. and Brasier,A.R. (2003) Identification of a nuclear factor kappa B-dependent gene network. *Recent progress in hormone research*, **58**, 95–130.

302. Wu,S., Yin,R., Ernest,R., Li,Y., Zhelyabovska,O., Luo,J., Yang,Y. and Yang,Q. (2009) Liver X receptors are negative regulators of cardiac hypertrophy via suppressing NF-kappaB signalling. *Cardiovascular research*, **84**, 119–26.

303. Mabb,A.M., Wuerzberger-Davis,S.M. and Miyamoto,S. (2006) PIASy mediates NEMO sumoylation and NF-kappaB activation in response to genotoxic stress. *Nature cell biology*, **8**, 986–93.

304. Collins,J.L., Fivush,A.M., Watson,M.A., Galardi,C.M., Lewis,M.C., Moore,L.B., Parks,D.J., Wilson,J.G., Tippin,T.K., Binz,J.G., et al. (2002) Identification of a nonsteroidal liver X receptor agonist through parallel array synthesis of tertiary amines. *Journal of medicinal chemistry*, **45**, 1963–6.

305. Becker,L., Gharib,S.A., Irwin,A.D., Wijsman,E., Vaisar,T., Oram,J.F. and Heinecke,J.W. (2010) A macrophage sterol-responsive network linked to atherogenesis. *Cell Metab*, **11**, 125–135.

306. Shen,Y., Liu,J., Estiu,G., Isin,B., Ahn,Y.-Y., Lee,D.-S., Barabási,A.-L., Kapatral,V., Wiest,O. and Oltvai,Z.N. (2010) Blueprint for antimicrobial hit discovery targeting metabolic networks. *Proceedings of the National Academy of Sciences of the United States of America*, **107**, 1082–7.

8. Abbreviations

Abbreviation/ Symbol	**Full name/meaning**
ABC	ATP-binding cassette
ABCA1	ATP-binding cassette transporter subfamily A member 1
ABCG1	ATP-binding cassette transporter subfamily G member 1
ACAT1	Acyl coenzyme A:cholesterol acyltransferase 1
ADME	Absorption, distribution, metabolism and excretion
PARP1	Poly - ADP-ribose transferase
AF	Activation function
APOA1	Apolipoprotein A-1
APOE	Apolipoprotein E
ATCC	American Type Culture Collection
BCL3	B-cell lymphoma 3
CEAS	Cis-regulatory Element Annotation System
CEBP	CCAAT-enhancer-binding proteins
CETP	Cholesterol ester transfer protein
CHD	Coronary heart disease
CHD9	Chromodomain helicase DNA binding protein 9
ChIP	Chromatin immunoprecipitation
ChIP-qPCR	ChIP coupled with real-time polymerase chain reaction
ChIP-seq	Ultra-high-throughput parallel DNA sequencing
CITED2	Cbp/p300 interacting transactivator with Glu/Asp-rich carboxy-terminal domain 2

COL4A1	Collagen chain of basement membranes
CVD	Cardiovascular diseases
CXCR7	Chemokine orphan receptor 1
DAVID	Database for annotation, visualization, and integrated discovery
DBD	DNA binding domain
DMEM	Dulbecco's modified Eagle's medium medium
DMSO	Dimethylsulfoxide
DR4	Direct repeat separated by 4 nucleotides
ER	Endoplasmatic reticulum
FAIRE	Formaldehyde Assisted Isolation of Regulatory Elements
FAS	Fatty acid synthase
FBS	Fetal bovine serum
FDR	False discovery rate
GBP2	Interferon-induced guanylate-binding protein 2
GDM	Gene distance matrix
GEF 3	Rho guanine nucleotide exchange factor
GO	Gene ontology
GPS2	G-protein pathway suppressor 2
GSEA	Gene Set Enrichment Analysis
GWAS	Genome wide association studies
HDL	high-density lipoproteins
HRP	Horseredish peroxidase
IDL	Intermediate-density lipoproteins
IDOL	Inducible degrader of LDL receptor

IgG	Immunoglobulin G
IL10	Interleukin 10
iNOS	Nitric oxide synthases
IPA	Ingenuity Pathways Analysis
KEGG	Kyoto Encyclopedia of Genes and Genomes
LBD	Ligand binding domain
LD	Linkage disequilibrium
LDL	Low-density lipoproteins
LDLR	LDL receptors
LPL	Lipoprotein lipase
LPS	Lipopolysaccharid
LXR	Liver X receptor
MACS	Model based-analysis of ChIP-sequencing
M-CSF	Macrophage colony stimulating factor
ME1	Malic enzyme
MERTK1	Mer receptor tyrosine kinase 1
MPO	Myeloperoxidase
MYLIP	Myosin regulatory light chain interacting protein
NADP	Nicotinamide adenine dinucleotide phosphate
NCEH	Neutral cholesteryl ester hydrolase
N-CoR	Nuclear receptor co-repressor
NFκB	Nuclear factor kappa-light-chain-enhancer of activated B-cells
NGS	Next generation sequencing
NPC1, NPC2	Niemann-Pick 1 and 2

NPC1L1	Niemann-Pick C1-like protein 1
NR	Nuclear receptors
ORF	Open reading frames
oxLDL	Oxidized LDL
PBM	Human peripheral blood monocytes
PBMC	Peripheral blood mononuclear cells
PBS	Phosphate buffer
PIAS4	Protein inhibitor of activated STAT 4
PLA2G7	Phospholipase A2
PLTP	Phospholipid transfer protein
PMA	Phorbol 12-myristate 13-acetate
PPAR	Peroxisome proliferator-activated receptor
PPARα	Peroxisome proliferators activated receptor alpha
PRIC 285	peroxisomal proliferator activated receptor A interacting complex 285
PVRL2	Poliovirus receptor-related 2
PWMs	Position weight matrices
RCT	Reverse cholesterol transport
RE	Response elements
RELB	V-rel reticuloendotheliosis viral oncogene homolog B
RLU	Relative luciferase unit
RXR	Retinoid X receptor
SCD1	Sterol CoA desaturase 1
SEM	Standard error of mean
SNPs	Single nucleotide polymorphisms

SR	Scavenger receptors
SRC	Steroid receptor co-activator
SREBF1	Sterol regulatory element-binding transcription factor 1
STDEV	Standard deviation
TF	Transcription factor
TFBS	Transcription factor binding sites
TGFβ	transforming growth factor beta
TLR	Toll-like receptor
TNFα	Tumor necrosis factor alpha
TSS	Transcriptional start sites
UCP1	Uncoupling protein 1
UCSC	University of California Santa Cruz
UPR	Unfolded protein response
VLDL	Very-low-density lipoproteins
HDAC3	Histone deacetylases 3

9. Publications

Parts of this PhD thesis have been published in following journal publications:

Feldmann, R., Fischer, C., Kodelja, V., Behrens, S., Haas, S., Vingron, M.,Timmermann, B., Geikowski, A., Sauer, S. (2013) Genome-wide analysis of LXRα activation reveals new transcriptional networks in human atherosclerotic foam cells. *Nucleic Acids Res*., 10.1093/nar/gkt034.
http://dx.doi.org/10.1093/nar/gkt034

Feldmann, R., Geikowski, A., Weidner, C., Witzke, A., Kodelja, V., Schwarz, T., Gabriel, M., Erker, T., Sauer, S. (2013) Foam cell specific LXRα ligand. *PloS One*., 8, 10.1371/journal.pone.0057311.
http://dx.doi.org/10.1371/journal.pone.0057311

Submitted patent application on 01/29/2013 at European Patent Office with number: EP13153142.8

Title: Foam cell specific Liver X Receptor (LXR) alpha agonist, SIRT1 inhibitors as well as p300 inhibitors as pharmaceutically active agents

Further, parts of study data were also described in a Master's thesis with the title Genome-wide liver X receptor alpha binding and chromatin accessibility in different macrophage models by Cornelius Fischer tendered at the Freie Universität Berlin and in a Bachelor's thesis with the title "Molekularbiologische Charakterisierung neuer potentiell anti-arteriosklerotisch wirkender LXRα-Liganden" by Anne Geikowski tendered at the Beuth Hochschule für Technik Berlin.

10. Supplementary

10.1 Supplementary figures

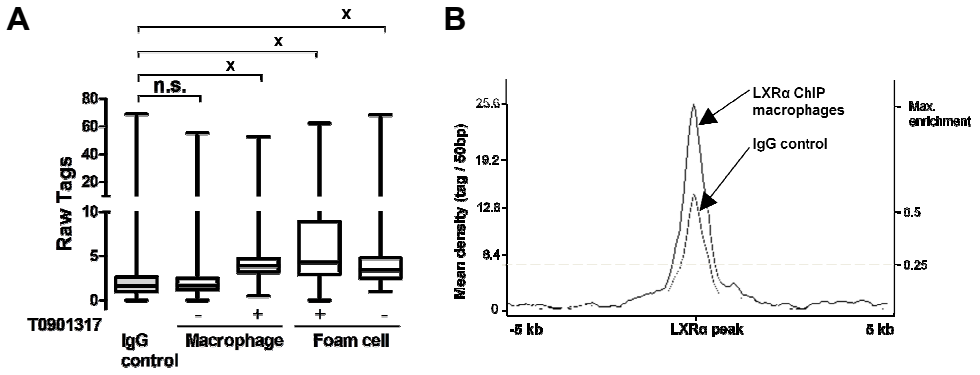

Figure S1: LXRα ChIP-seqencing validation and filtering. (A) Box plot of raw tags of each sequencing lane were plotted in Graphpad Prism 5. Significance was determined by multiple comparison of LXRα sequencing lanes and IgG control. x = $p < 0.05$. n.s.= not significant. (B) Excluded cluster with too high enrichment of IgG control. The mean density of LXRα and IgG ChIP enrichment are plotted at LXRα binding sites. IgG control enrichment is > 0.25 parts of maximal LXRα enrichment. Resolution is 50bp.

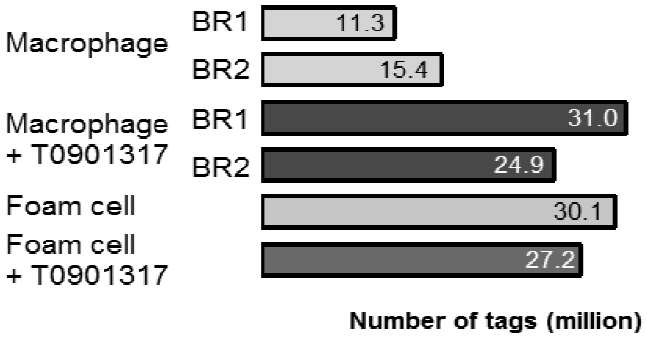

Figure S2: LXRα ChIP-seq sequence depth. Shown is the number of millions of tags for each biological replicate (BR) in macrophages, T0901317 treated macrophages, foam cells and T0901317 treated foam cells.

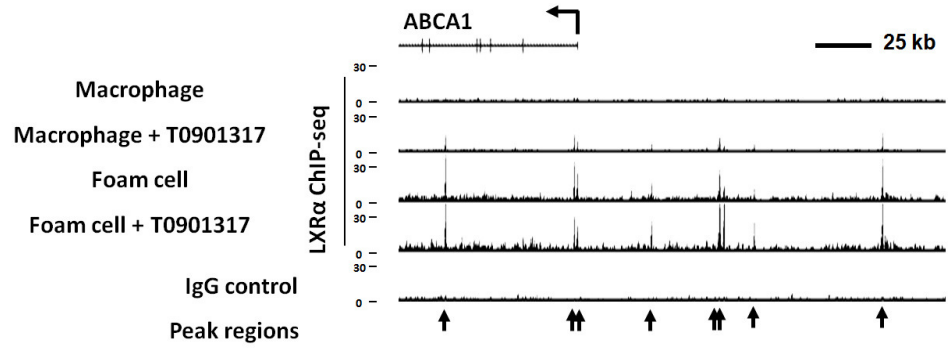

Figure S3: LXRα binding to ABCA1. Tag alignment tracks of LXRα ChIP-seq and IgG control at ABCA1 locus. Arrows indicate transcription start sites and orientation of transcription. Black arrows under tracks show sites of LXRα enriched binding.

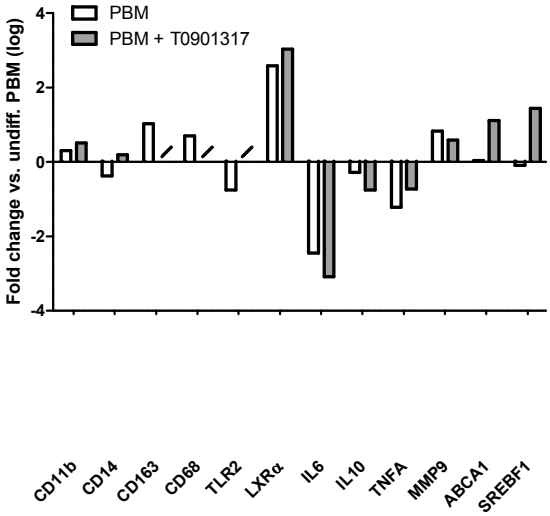

Figure S4: Validation of PBM maturation and T0901317 treatment. Bars represent the fold change against undifferentiated PBM. Shown is the mean fold change from technical triplicates.

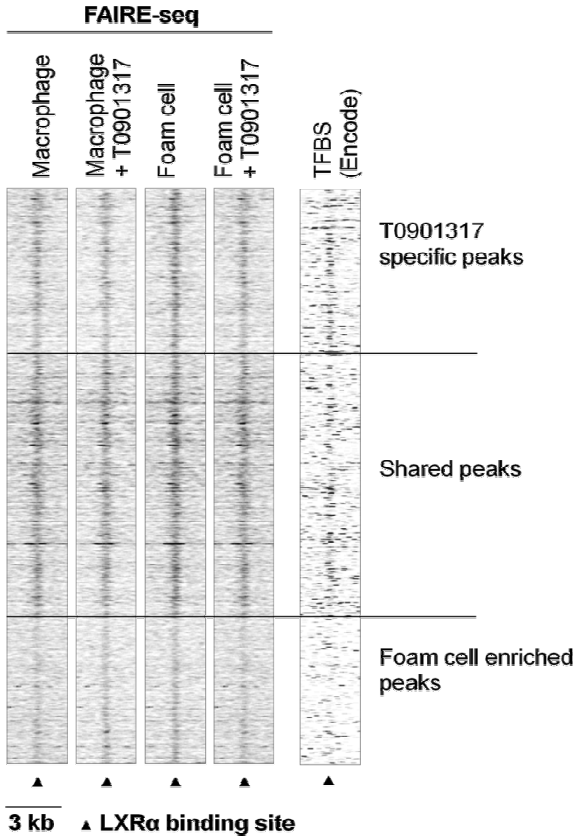

Figure S5: Chromatin openness. Shown is the FAIRE-seq heatmap of all cell models and the transcription factor binding site (TFBS) enrichment heatmap extracted from Encode data. Visualized region is +/- 1.5 kb from LXRα peak center. FAIRE-seq regions were sorted according to LXRα peak degree of variability.

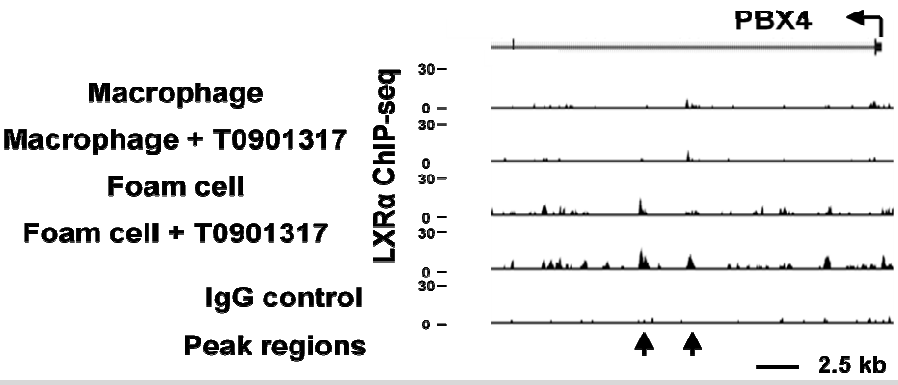

Figure S6: LXRα binding to PBX4. Shown are tag alignment tracks of LXRα ChIP-seq and IgG control at the PBX4 locus. Arrows indicate transcription start sites and orientation of transcription. Black arrows under tracks display sites of LXRα enriched binding.

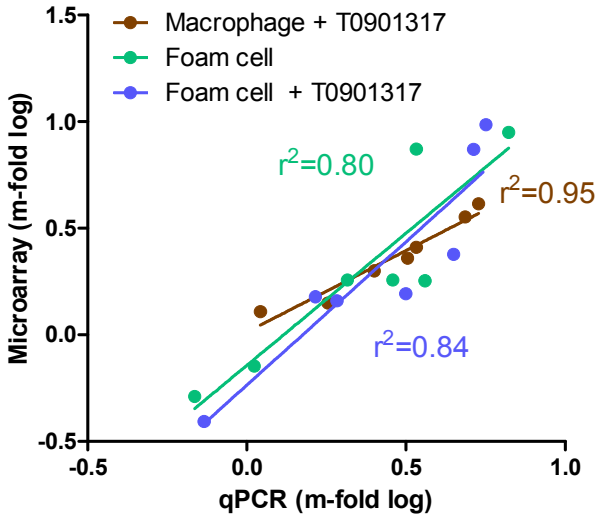

Figure S7: Robustness of whole-genome gene expression analysis. (B) Validation of Microarray analysis with qPCR of selected genes (*ABCA1, LXRα, PLTP, TLR4, CD36, PPARG, FASN*). Fold vs. ligand-free macropohages, n=4. Linear regression analysis shows high accordance.

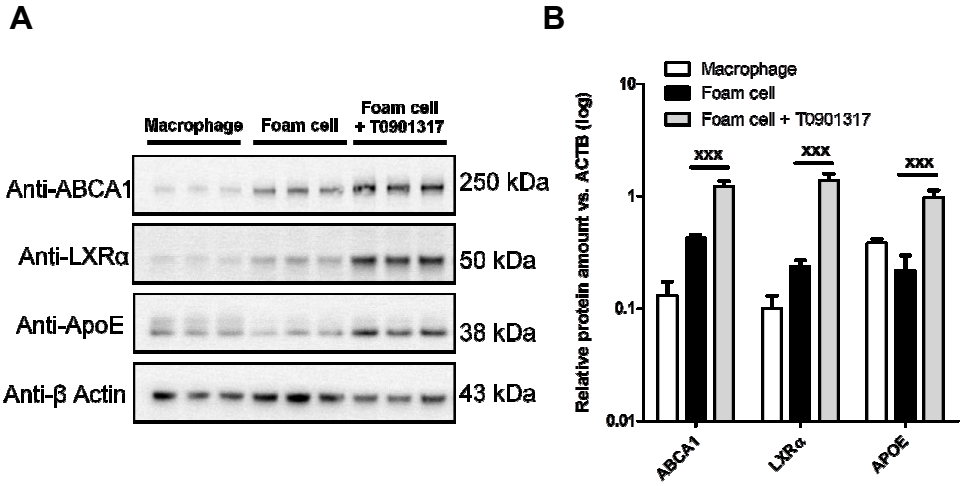

Figur S8: Protein content of LXRα target genes in macrophages, foam cells and T0901317 treated foam cells. (A) Western blot analysis of ABCA1, LXRα, APOE and β-Actin protein content in macrophages, foam cells and T0901317 treated foam cells. (n=3). (B) Densitometry data from western blot analysis. Data are presented as target protein amount vs. Anti-β-Actin (ACTB). (n=3, mean±SD) *** P<0.001 vs. foam cell.

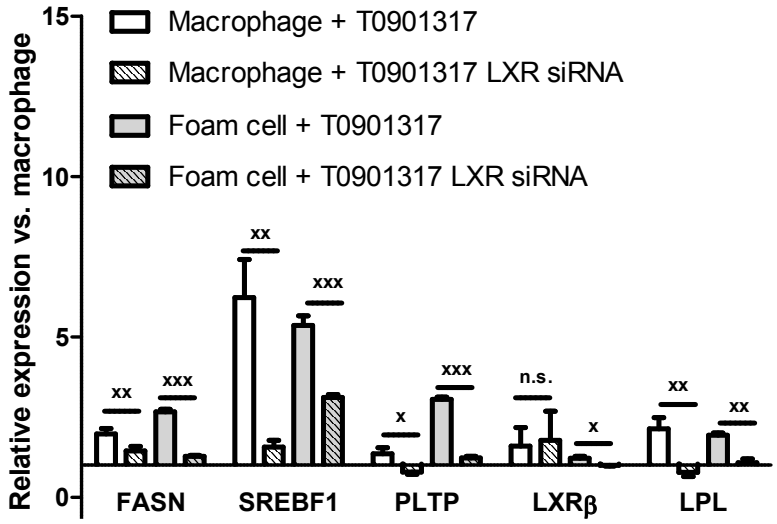

Figure S9: LXR knockdown. Ligand dependent gene expression in macrophages and foam cells after siRNA-mediated LXR knockdown. Analysed target genes are *FASN*, *SREBF1*, *PLTP*, *LXRβ* and *LPL*. Data is presented as relative expression vs. macrophage. (n=4, mean ±SD. * P<0.05, ** P<0.01, *** P<0.001, n.s.=not significant vs. neg. siRNA.

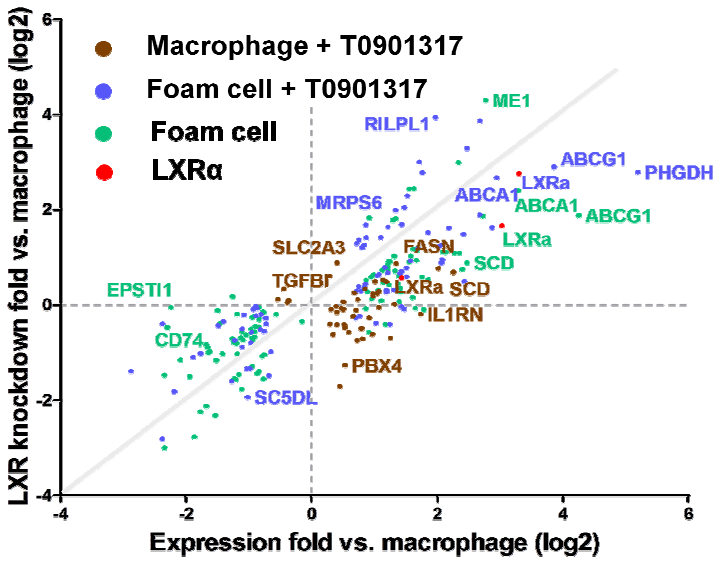

Figure S10: Influence of LXR knockdown. The differential gene expression of all cell models (fold vs. ligand-free macrophage, log2) is plotted against differential LXR knockdown gene expression of all cell models (fold vs. ligand-free macrophage, log2G. Gene names are visualized for selected target genes.

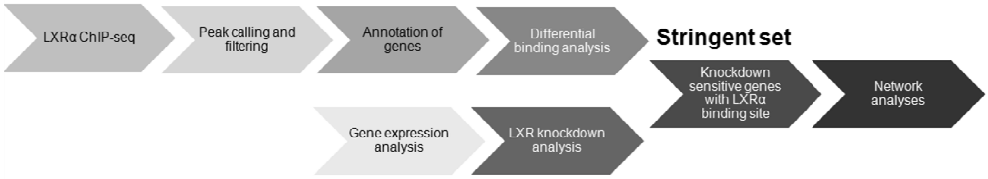

Figure S11: Project overview. For network analysis, peaks were filtered for maximal stringency.

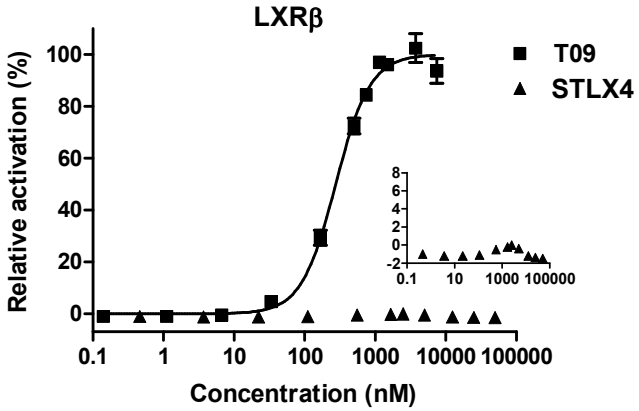

Figure S12: Transcriptional activation of LXRβ by T0901317 (T09) or STLX4 in a reporter gene assay. STLX4 does not activate the LXRβ subtype (mean ±SD, n=3).

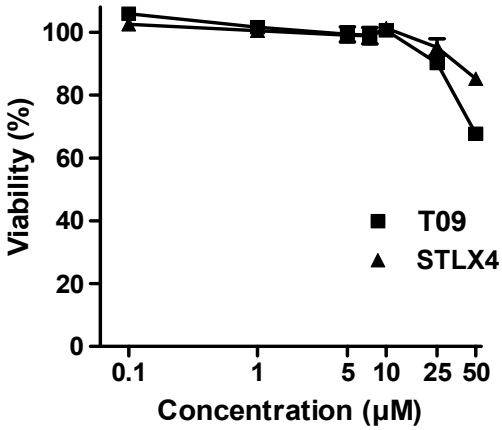

Figuren S13: Cytotoxicity of STLX4 in macrophages. STLX4 does not reduce cellular viability up to 25 µM. (mean ±SD, n=3).

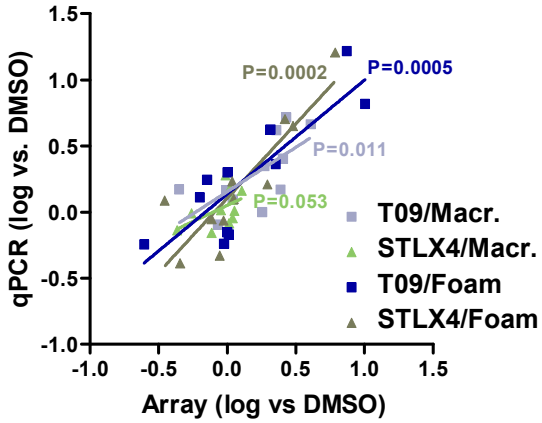

Figuren S14: Validation of gene expression microarray analysis by quantitative PCR. For all tested samples, array observations significantly correlated with qPCR results.

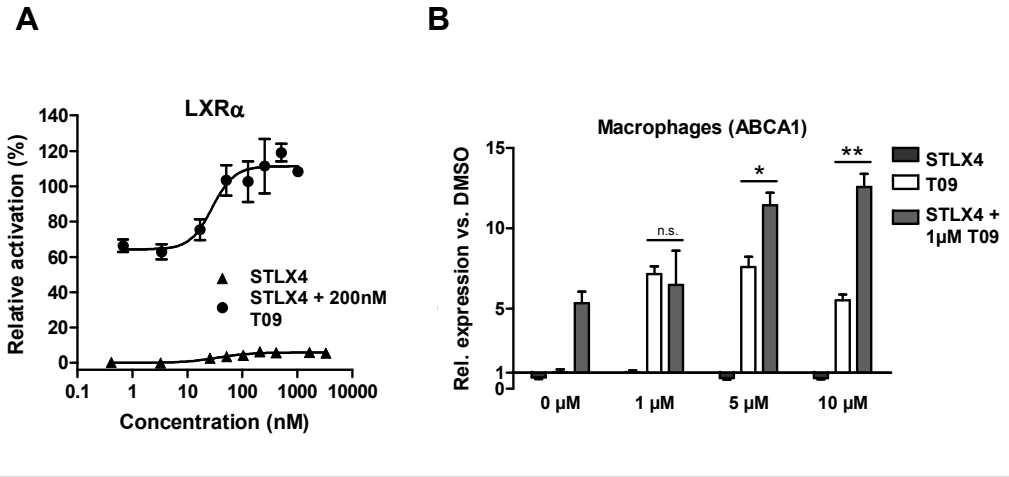

Figure S15: Additive activation mode of STLX4 (**A**) Transcriptional activation of LXRα by STLX4 in the presence or absence of 200 nM T0901317. Reporter gene assay data are expressed as mean ±SD (n=3). **(B)** Gene expression in THP-1 macrophages after treatment with different concentrations of T0901317 (T09) or STLX4 in the presence or absence of 1 µM T09. Data are expressed as mean ±SEM (n=2-3). * P<0.05, ** P<0.01, vs. DMSO; n.s,, not significant.

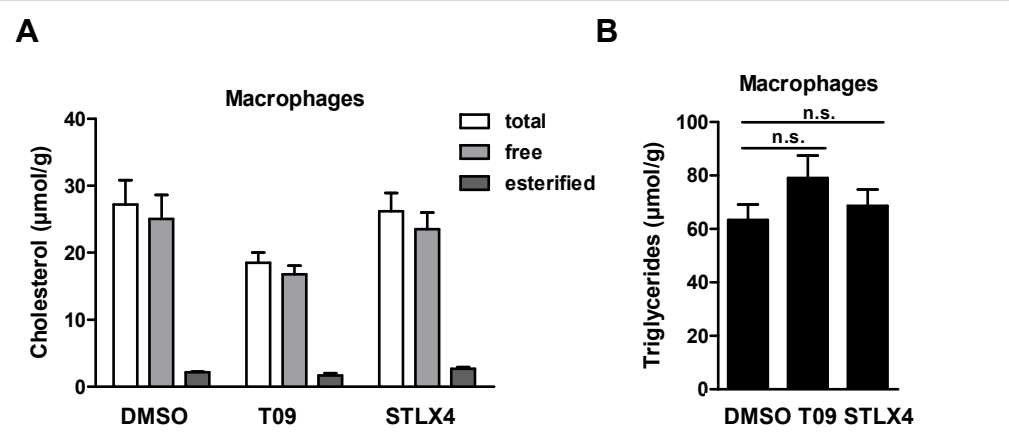

Figure S16: Physiological analyses of STLX4 treatment in macrophages. (**A)** Cholesterol content in macrophages after treatment with DMSO (0.1%), T0901317 (10 µM) or STLX4 (10 µM). Data are expressed as mean ±SEM (n=5-6). **(B)** Triglyceride content in macrophages after treatment with DMSO (0.1%), T0901317 (T09, 10 µM) or STLX4 (10 µM). * P<0.05, ** P<0.01, *** P<0.001 vs. DMSO; n.s., not significant.

10.2 Supplementary tables

Table S1: Western blot analysis

Densitometry (m-fold vs. ACTB)	Macrophage + T0901317	Macrophage	Foam cell + T0901317	Foam cell
Anti- LXRα	1.8	0.1	3.8	2.0
Anti-LXRβ	0.2	0.2	0.1	0.2
Anti-RXRα	1.2	0.9	1.4	1.3

Densitometry data from of main Figure 10. M-fold vs. Anti-β-Actin (ACTB) antibody data.

Table S2: MACS peak calling

MACS data	Macrophage + T0901317	Macrophage	Foam cell + T0901317	Foam cell
total tags in treatment	55884654	26744082	27247160	30161958
tags unique in treatment %	93.2	96.7	88.0	97.5
total tags in control	11918199	12664415	28025634	16020877
tags unique in control %	95.1	92.0	91.6	95.1
d shift [bp]	106	99	124	88
Peaks with MACS > 50	3780	6447	16014	2207 (471 manually validated)

Complete data output from MACS peak calling for each cell model.

Table S3: Peak filtering

Peaks after filtering	Macrophage + T0901317	Macrophage	Foam cell + T0901317	Foam cell
Tag/length >0,07	1342	287	1258	1025
k.Means linear enrichment cluster LXR vs. IgG < 4	1342	0	633	1025
Manually removed cluster after GB observation	1198	0	628	742

Derived peaks for each cell model after alternative filtering procedure.

Table S4: Functional analysis of LXRα target genes in peak sets

	Bioprocess	Count	%	P-value	FE	FDR
T0901317 specific peak set	Regulation of cholesterol esterification	3	1.4	4.9E-03	25.5	7.9
	Regulation of nervous system development	8	3.6	1.5E-03	4.6	2.5
	Phospholipid transport	4	1.8	1.2E-02	8.0	18.8
Shared peak set	Defense response	21	6.8	8.2E-04	2.3	1.4
	Fatty acid biosynthetic process	7	2.3	5.0E-03	4.3	8.1
	Response to inorganic substance	10	3.3	9.4E-03	2.8	14.8
	Regulation of foam cell differentiation	4	1.3	1.1E-02	8.2	17.0
Foam cell specific peak set	Skeletal system development	8	5.9	1.1E-03	4.9	1.7
	Glutamine family amino acid metabolic process	4	2.9	7.0E-03	9.9	10.7
	Glutamine family amino acid metabolic process	3	5.3	3.0E-02	10.7	36.4

DAVID functional annotation clustering analysis of gene ontology term bioprocess, for each peak set. All genes were LXR knockdown sensitive. Columns indicate the Category Bioprocess, the terms, its count and percentage in the target gene list, as well as the P-value, fold enrichment (FE) and false discovery rate (FDR).

Table S5: Correlation of LXRα binding data with GWAS

Disease/Trait	Pubmed ID	GWAS P-Value	SNP	Distance to SNP [kb]	LXRα target gene Symbol	Gene name	known LXRα target gene
	18193044	1.00E-80	rs4420638	5.7	APOC1	apolipoprotein C-I	BIOGRID
LDL cholesterol	20864672	2.00E-08	rs2142672	-52.1	MYLIP	myosin regulatory light chain interacting protein	BIOGRID
	19060906	2.00E-08	rs10401969	311.5	PBX4	pre-B-cell leukemia homeobox 4	New
Lipoprotein-associated phospholipase A2 activity and mass	20442857	6.00E-14	rs1805017	40.4	PLA2G7	phospholipase A2, group VII	New
	17463246	3.00E-13	rs4420638	5.7	APOC1	apolipoprotein C-I	BIOGRID
	19060906	4.00E-11	rs17216525	57.0	PBX4	pre-B-cell leukemia homeobox 4	New
Triglycerides	19060906	7.00E-11	rs7679	-33.3	PLTP	phospholipid transfer protein	NR-Resource
HDL cholesterol	19060906	4.00E-09	rs7679	-33.3	PLTP	phospholipid transfer protein	NR-Resource
Proinsulin levels	21873549	3.00E-09	rs4790333	33.4	SGSM2	small G protein signaling modulator 2	New
C-reactive protein	21300955	9.00E-139	rs4420638	5.7	APOC1	apolipoprotein C-I	BIOGRID
Mean platelet volume	19820697	6.00E-31	rs12485738	16.0	ARHGEF3	Rho guanine nucleotide exchange factor (GEF) 3	New
Crohn's disease	21102463	1.00E-20	rs12521868	117.7	SLC22A5	solute carrier family 22 (organic cation transporter), member 5	New
HIV-1 control	20411168	1.00E-08	rs7756521	-42.8	VARS2	valyl-tRNA synthetase 2, mitochondrial (putative)	New
	18794953	1.00E-07	rs3890745	-85.3	TNFRSF14	tumor necrosis factor receptor superfamily, member 14 (herpesvirus entry mediator)	New
Rheumatoid arthritis	21452313	2.00E-06	rs2062583	-84.4	ARHGEF3	Rho guanine nucleotide exchange factor (GEF) 3	New
Ulcerative colitis	21297633	3.00E-09	rs734999	-44.9	TNFRSF14	tumor necrosis factor receptor superfamily, member 14 (herpesvirus entry mediator)	New
Celiac disease	20190752	3.00E-09	rs3748816	-58.4	TNFRSF14	tumor necrosis factor receptor superfamily, member 14 (herpesvirus entry mediator)	New
Aortic root size	19584346	2.00E-11	rs10852932	152.6	SGSM2	small G protein signaling modulator 2	New
Myocardial infarction (early onset)	19198609	6.00E-11	rs9982601	17.2	MRPS6	mitochondrial ribosomal protein S6	New
Blood pressure	21909110	5.00E-09	rs13082711	-79.4	SLC4A7	solute carrier family 4, sodium bicarbonate cotransporter, member 7	(Pehkonen et al., 2012)
	21378990	4.00E-10	rs9982601	17.2	MRPS6	mitochondrial ribosomal protein S6	New
Coronary heart disease	21347282	3.00E-08	rs7801190	53.6	SLC12A9	solute carrier family 12 (potassium/chloride transporters), member 9	New
	19430483	1.00E-09	rs1530440	153.4	ARID5B	AT rich interactive domain 5B (MRF1-like)	New
	21909115	1.00E-09	rs2832538	-48.1	MOV10	Mov10, Moloney leukemia virus 10, homolog (mouse)	New
Diastolic blood pressure	21909115	4.00E-09	rs13082711	-79.4	SLC4A7	solute carrier family 4, sodium bicarbonate cotransporter, member 7	(Pehkonen et al., 2012)
	21909115	1.00E-09	rs2832538	-48.1	MOV10	Mov10, Moloney leukemia virus 10, homolog (mouse)	New
Systolic blood pressure	21909115	2.00E-06	rs13082711	-79.4	SLC4A7	solute carrier family 4, sodium bicarbonate cotransporter, member 7	(Pehkonen et al., 2012)
	21076409	6.00E-09	rs4587718	13.3	TKT	transketolase (Wernicke-Korsakoff syndrome)	New
Ventricular conduction	21076409	1.00E-06	rs9912468	11.3	PRKCA	protein kinase C, alpha	(Pehkonen et al., 2012)
Resting heart rate	20839382	6.00E-10	rs3114370	58.5	SLC12A9	solute carrier family 12 (potassium/chloride transporters), member 9	New
	20031577	1.00E-12	rs1016988	157.5	SLC22A5	solute carrier family 22 (organic cation transporter), member 5	New
Fibrinogen	20031577	8.00E-11	rs10512597	-135.3	CD300LF	CD300 molecule-like family member f	New
D-dimer levels	21502573	1.00E-06	rs2774920	164.3	ABCA4	ATP-binding cassette, sub-family A (ABC1), member 4	New
Alzheimer's disease	17998437	2.00E-44	rs4420638	5.7	APOC1	apolipoprotein C-I	BIOGRID
Amyloid A Levels	21124955	4.00E-22	rs2896528	92.5	LDHA	lactate dehydrogenase A	New
Cognitive performance	19734545	2.00E-06	rs17001239	179.4	JAM2	junctional adhesion molecule 2	New
Information processing speed	21130838	2.00E-07	rs6051520	-8.2	TRIB3	tribbles homolog 3 (Drosophila)	New
	21833068	1.00E-13	rs11154801	-105.7	AHI1	Abelson helper integration site 1	New
	20453840	2.00E-10	rs9857904	-167.2	CBLB	Cas-Br-M (murine) ecotropic retroviral transforming sequence b	New
Multiple sclerosis	21833083	1.00E-08	rs17174870	93.7	MERTK	c-mer proto-oncogene tyrosine kinase	(Pehkonen et al., 2012)
Neuroblastoma	21124317	5.00E-13	rs3768716	-27.3	BARD1	BRCA1 associated RING domain 1	New
Neuroblastoma (high-risk)	19412175	9.00E-18	rs6435862	-64.0	BARD1	BRCA1 associated RING domain 1	New
	20383146	5.00E-22	rs2453533	99.0	GATM	glycine amidinotransferase (L-arginine:glycine amidinotransferase)	New
Chronic kidney disease	20383146	1.00E-07	rs1933182	-19.9	SORT1	sortilin 1	(Pehkonen et al., 2012)
Renal function and chronic kidney disease	19430482	6.00E-14	rs2467853	41.4	GATM	glycine amidinotransferase (L-arginine:glycine amidinotransferase) mitochondrial protein	New
Bone mineral density	20966366	5.00E-08	rs2273061	52.0	JAG1	jagged 1 (Alagille syndrome)	New
Osteoporosis	20548944	1.00E-07	rs2278729	142.1	TBC1D8	TBC1 domain family, member 8 (with GRAM domain)	New
Serum phosphorus levels	20585539	1.00E-11	rs9469578	-65.8	LEMD2	LEM domain containing 2	New
Systemic lupus erythematosus	19838193	1.00E-17	rs2230926	36.6	TNFAIP3	tumor necrosis factor, alpha-induced protein 3	(Pehkonen et al., 2012)
Psoriasis	19169254	9.00E-12	rs6810604	33.2	TNFAIP3	tumor necrosis factor, alpha-induced protein 3	(Pehkonen et al., 2012)
Melanoma	21983785	9.00E-09	rs3219090	72.9	PARP1	poly (ADP-ribose) polymerase family, member 1	BIOGRID

Correlation of LXRα binding data with NHGRI GWAS catalogue, extended view. Columns indicate the associated diseases or traits, the Pubmed ID of the associated GWAS and the P-value of SNP-Disease association, SNP ID, the distance between LXRα binding sites and SNPs within the LD block is presented in kilobases (kb), LXRα target genes in proximity to the associated SNP and the status of LXRα target gene known from literature or unknown and new.

Table S6: Differential expression of LXRα target genes

LXRα target gene	Gene expression vs. Macrophage macrophage + T0901317	foam cell + T0901317	foam cell
APOC1	1,44	-	-
MYLIP	1.75*	6.63*	2.69*
PBX4	1.45*	6,78	6,02
PLA2G7	0,78	0.32*	0.43*
APOC1	1,44	-	-
PBX4	1.45*	6,78	6,02
PLTP	2.20*	2,47	-
SGSM2	-	-	1,95
APOC1	1,44	-	-
ARHGEF3	-	-	0.47*
SLC22A5	-	4,15	-
VARS2	-	1,96	2,19
TNFRSF14	-	-	1,76
ARHGEF3	-	-	0.47*
TNFRSF14	-	-	1,76
SGSM2	-	-	1,95
MRPS6	-	1,86	1.82*
SLC4A7	1,4	-	-
MRPS6	-	1,86	1.82*
SLC12A9	0,74	0.29*	0,45
ARID5B	-	0.46*	0,51
MOV10	-	1,82	-
SLC4A7	1,4	-	-
MOV10	-	1,82	-
SLC4A7	1,4	-	-
TKT	1,32	-	-
PRKCA	1,32	-	-
SLC12A9	0,74	0.29*	0,45
SLC22A5	-	4,15	-
CD300LF	-	3.45*	2.78*
ABCA4	-	-	2,45
APOC1	1,44	-	-
LDHA	1,29	0.32*	0,24
JAM2	-	3,54	-
TRIB3	-	3.62*	4,6
AHI1	-	2,8	2,06
CBLB	-	-	2,01
MERTK	1.32*	0.27*	0,31
BARD1	-	-	0,18
BARD1	-	-	0,18
TNFAIP3	-	0.47*	-
PARP1	-	0.52*	0.52*

* LXR knockdown sensitive

Target genes were derived from Correlation of LXRα binding data with NHGRI GWAS catalogue. M-fold expression vs. macrophage. *LXR knockdown sensitive, - not detected or not differentially expressed.

Table S7: Stringently validated LXRα target genes

SYMBOL	Gene name	T0901317 foam cell vs. foam cell	LXRα target gene
DUSP7	Dual specificity phosphatase 7	0.21	New
SIRT7	Sirtuin 7	0.31	New
SLC2A4RG	SLC2A4 regulator	0.33	New
MRPL12	Mitochondrial ribosomal protein L12	0.43	New
FGL2	Fibrinogen-like 2	0.44	New
CUEDC1	CUE domain containing 1	0.44	New
SPRYD3	SPRY domain containing 3	0.44	New
ZNF653	Zinc finger protein 653	0.48	New
PIAS4	Protein inhibitor of activated STAT, 4	0.51	New
MRPL20	Mitochondrial ribosomal protein L20	0.53	New
NENF	Neuron derived neurotrophic factor	0.53	New
ANPEP	Alanyl aminopeptidase	0.54	New
FAM20C	Family with sequence similarity 20, member C	0.62	New
CD151	CD151 molecule	1.11	New
COL4A1	Collagen, type IV, alpha 1	1.82	BIOGRID
MT1A	Metallothionein 1A	1.83	New
SDAD1	SDA1 domain containing 1	1.85	New
TEX2	Testis expressed 2	1.87	New
SCD	Stearoyl-CoA desaturase	2.03	NR-Resource
CXCR7	Chemokine receptor 7	2.08	(Pehkonen et al., 2012)
MT1F	Metallothionein 1F	2.09	(Pehkonen et al., 2012)
SCRN1	Secernin 1	2.12	New
MRPL2	Mitochondrial ribosomal protein L2	2.27	New
CITED4	Cbp/p300-interacting transactivator 4	2.29	New
SLC6A12	Solute carrier family 6 member 12	2.56	New
MGRN1	Mahogunin, ring finger 1	2.67	New
MYLIP	Myosin regulatory light chain interacting protein	2.70	BIOGRID
SSBP3	Single stranded DNA binding protein 3	2.70	New
GOLPH3L	Golgi phosphoprotein 3-like	2.73	New
FAM100A	Family with sequence similarity 100, member A	2.76	New
PAQR7	Progestin and adipoQ receptor family member VII	2.84	New
KLHDC8B	Kelch domain containing 8B	2.98	New
CDCA7L	Cell division cycle associated 7-like	3.04	New
JAM2	Junctional adhesion molecule 2	3.14	New
SLC22A5	Solute carrier family 22 member 5	3.29	New
IGFBP4	Insulin-like growth factor binding protein 4	3.60	New
TMEM135	Transmembrane protein 135	4.27	(Pehkonen et al., 2012)
GBP2	Guanylate binding protein 2	5.85	New

Stringently validated LXRα target genes differentially expressed upon T0901317 stimulation of foam cells compared to untreated foam cells. From left to right: gene symbol, gene name, m-fold expression and status of gene (known from literature and database analysis or so far unknown and therefore new).